Programme Area: Carbon Capture and Storage

Project: High Hydrogen

Title: Experimental results, detailed analysis, evaluation and recommendations

Abstract:

The report contains details for the complete project. This project commenced in 2011 and has completed works at the end of 2016. There have been three previous sections to this project, a literature review, laboratory scale experiments, a circular duct phase and this last phase incorporated a scale heat recovery steam generating boiler.

Context:

Hydrogen is likely to be an increasingly important fuel component in the future. This £3.5m project was designed to advance the safe design and operation of gas turbines, reciprocating engines and combined heat and power systems using hydrogen-based fuels. Through new modelling and large-scale experimental work the project sought to identify the bounds of safe design and operation of high efficiency combined cycle gas turbine and combined heat and power systems operating on a range of fuels with high and variable concentrations of hydrogen. The goal of the project was to increase the range of fuels that can be safely used in power and heat generating plant. The project involved the Health and Safety Laboratory, an agency of the Health and Safety Executive, in collaboration with Imperial Consultants, the consulting arm of Imperial College London.

Harpur Hill, Buxton
Derbyshire, SK17 9JN
T: +44 (0)1298 218000
F: +44 (0)1298 218986
W: www.hsl.gov.uk

HEALTH & SAFETY LABORATORY

ETI Project Report: Experimental results, detailed analysis, evaluation and recommendations.

MH/16/169

Report Approved for Issue By:	**J.T. Allen PhD, CChem MRSC.**
Date of Issue:	**08/02/2017**
Lead Authors:	**B.C.R Ewan PhD. K. Moodie MSc.**
Lead Author Technical Analysis:	**Hans. J. Michels, CEng, CPhys, FInstP, FIChemE, Professor of Safety Engineering.**
Contributing Author(s):	**W. Rattigan BSc. J.T.Allen PhD, CCHem MRSC. S. Hawksworth PhD. M. Christodolou PhD.**
Technical Reviewer(s):	**S. Hawksworth PhD.**
Editorial Reviewer:	**J.T. Allen PhD, CChem MRSC.**
HSL Project Number:	**PE02162**

This report and the work it describes were undertaken by the Health and Safety Laboratory under contract to the Energy Technology Institute. Its contents, including any opinions and/or conclusion expressed or recommendations made, do not necessarily reflect policy or views of the Health and Safety Executive.

DISTRIBUTION

P. Winstanley ETI

Andrzej.Pekalski Shell

Hans Michels Imperial College

Bruce Ewan Chementech

John Gummer HSL

Keith Moodie HSL

Wayne Rattigan HSL

John Allen HSL

Stuart Hawksworth HSL

Rosemary Gibson HSL

ACKNOWLEDGEMENTS

The authors wish to thank Paul Winstanley of the Energy Technologies Institute (ETI) together with their sponsors, in particular Colin Etheridge (Solar Turbines), and Dr. A Pekalski (Shell) for all the worthwhile contributions they made in both formulating the test programme and in contributing to the many technical discussion sessions held throughout its duration.

ACRONYMS

ETI	Energy Technology Institute
HSL	Health and Safety Laboratory
IC	Imperial College
CCGT	Combined Cycle Gas Turbine
CCGE	Combined Cycle Gas Engine
WP	Work Package
CHP	Combined Heat and Power
DDT	Deflagration to Detonation Transition
BoD	Basis of Design
FSO	Full Scale Output
ESTOPS	Emergency Stop Devices / Software
RPM	Revolutions per minute
CFD	Computational Fluid Dynamics
HRSG	Heat Recovery Steam Generator
P&ID	Pipe and Instrumentation Diagram
PID	Proportional Integral Derivative (Controller)
HAZOP	Hazard and Operability Study
EQR	Equivalence Ratio
TDMS	LabVIEW Test Data Exchange Stream
CSV	Comma Separated Values file

CONTENTS

EXECUTIVE SUMMARY

The report describes the design, construction, and operation of a reduced-scale model of a combined cycle gas turbine (CCGT) complete with a model heat recovery steam generator (HRSG). The report also presents the results and an analysis of tests carried out with this model in combination with the results obtained from previous laboratory and reduced scale tests using a cylindrical duct. The facility provides a means of measuring the consequences of ignitions of hydrogen and flammable gas mixtures, in this case binary mixtures consisting of hydrogen/methane or hydrogen/carbon monoxide when they are injected and spark ignited in the hot exhaust stream from a gas turbine.

The overall objective was to model at reduced scale, the consequences of a flameout in a full-size combined cycle gas turbine (CCGT) when running on high hydrogen fuel mixtures. In so doing the intention was to provide data sets that could be used to aid understanding of the physical processes involved as well as providing data that could be used for CFD modelling of the whole process. The test parameters varied were the fuel mixture composition and the equivalence ratio. The exhaust gas temperature and the engine mass flow rate were kept the same throughout the test programme. The heat recovery steam generator (HRSG) was modelled by a series of solid finned tubes giving a blockage ratio of 48% per tube row. The numbers of tube rows tested was 15 and the total number of tubes was 218.

The accuracy of the various types of sensors used was also examined in particular the performance of the pressure transducers used throughout the test programme. Detection of the flame was by flame ionisation and optical emission techniques, which provided complementary measurements in that the optical sensors observed a line of sight across the viewing plane, whilst the ionisation sensors were point measurement devices located just in from the side wall and detected flame that was present locally. Generally, the optical sensors captured the flame passage under most conditions whilst the ionisation sensors were less effective with weak flame events often being difficult to capture. High-speed videos of the tests were also made, which confirmed the variability in flame behaviour under different conditions of mixture and equivalence ratio. The pressure detection often showed complex behaviour arising from the different sensor locations and the changing flame speed behaviour within the model as a consequence of the combusting flows through the HRSG. In many cases the peak pressure was of short duration, followed by longer duration lower pressure components. This may have implications for the real impact of pressure pulses on the containing structures.

Mixtures of H_2/CH_4, pure H_2 and H_2/CO were investigated with equivalence ratios (EQR's) up to 0.65. Initially H_2/CH_4 mixtures were investigated with both an open end to the HRSG and a closed end combined with a vertical stack. This provided an end plate and a right-angled bend into the vertical stack at the end of the chamber.

The behaviours of these two geometries show both similarities and differences due to the presence of the end plate, with the pressures generated around the heat exchanger being similar in magnitude and duration but with clear indications of pressure wave reflections for those cases involving the end plate and stack geometry. The pressure and video records indicate that the peak pressure originates around the highly turbulent heat exchanger region, where combustion intensity is greatest and with pressure pulse widths

of around 5 msec. The propagation of this pressure pulse can be observed within the geometry and gives rise to an approximate and temporary doubling in the region of the end plate due to reflections. Amplitude changes due to geometry changes within the HRSG system are also observed and have an effect on the maximum peak pressures that can arise. The highest pressure observed was 1.79 barg, it occurred in a pure H_2 case using an EQR of 0.55, with the end plate present.

The peak pressures generated around the heat exchanger are of a similar magnitude to those observed originating around the obstacles in the circular duct tests of WP2.2, and although there is not an exact comparison, with HRSG peak pressures both above and below those for the duct tests, the similarity of the results suggests that the equal number and spacing of the tubular obstacles in both cases has had an influence despite the large difference in physical scale involved.

The reactivities of the various mixtures, based on peak pressures and flame speeds, indicated that dilution of pure hydrogen with methane had a greater reactivity reduction effect than dilution with carbon monoxide, which is consistent with WP2.1 and WP2.2 findings. Based on the limited number of tests carried out, preliminary estimates of the limiting EQR values for each mixture were made, based on two limiting peak pressures of 0.5 barg and 1.0 barg, which were agreed as indicative tolerable pressure limits in full scale industrial equipment.

Several lessons were learnt in respect of the data collection and processing system, such as dealing with noise issues, sensor dropouts, battery operation and automation of the data analysis. Suggestions are made as to how these may be improved in the future.

At the outset of the HRSG tests, little was known as to how the large scale system would behave and despite the small number of tests, the major uncertainties have been fully clarified enabling further tests to be carried out with some expectation of the outcome. Overall the tests carried out consolidate the knowledge gained from the circular duct tests and provide a correspondence between the two and a basis for further study.

It should be noted that around 67 tests were carried out for the circular duct work, while only 13 for the present HRSG work and this limited number of tests and the analysis of the data from this series have highlighted a number of additional tests, which are considered necessary to build confidence in the operational EQR values proposed for industrial applications, to further develop our understanding of the underlying physical processes involved, and to explore a means of mitigating the consequences of flameouts.

1 INTRODUCTION

1.1 CONTRACTUAL REQUIREMENTS

The report describes a reduced scale model of a combined cycle gas turbine (CCGT) complete with a solid heat recovery steam generator (HRSG), designed, built and operated by HSL and its collaborators on behalf of the ETI. As well as presenting, evaluating and commenting upon the results obtained, the report also presents the results and an analysis of tests carried out with this model in combination with the results obtained from previous laboratory and reduced scale tests using a cylindrical duct (WP 2.2). The experimental work formed Work Package 2, Task 3 (WP 2.3) of the ETI sponsored high hydrogen project.

The work was done as part of the requirements listed under the terms and conditions of the ETI Contract Number PE02162, Section 6: Work Packages. It is reported in accordance with the requirements of milestone 10 of the 4th contract amendment 2015.

1.1.1 Project value objectives

The overall project value objectives are to provide a more detailed evidence base for, and advance the state-of-the-art in, the safe and efficient operation of high hydrogen gas mixtures for energy production in order to enable the following outcomes:

- Identify the bounds of safe design and operation of proposed high hydrogen systems to avoid unpredicted hazardous outcomes (limits of flammability, ignition and significant overpressure potential [including DDT] in exhaust systems for a range of CHP/CCGT applications);
- Operate existing systems with more confidence within their bounds of safety in order to increase energy production and avoid unnecessary trips (for example, enabling gas engines to run at higher fuel/air ratios, or operating CCGT systems with higher trip set-points); and
- Outline the applicability of the results by extrapolation to larger duct dimensions and geometries, identifying specific limitations on validity, plus any further work required to increase confidence in the extrapolation process.

1.1.2 Critical success factors

The Parties agree that the Project is intended to meet the following critical success factors, which shall characterise or are required to facilitate a successful Project outcome:

- The Project should make a significant step forward in developing the evidence base and tools for the safe and more economical design and operation of gas engines and gas turbines using high hydrogen fuels.

- The Project must provide sufficient information and present it in such a manner as to enable the ETI to make informed decisions at the end of the Project regarding any follow-on work that may be required.

1.2 BACKGROUND

Prior to commencing this part of the test programme a literature review was completed to aid definition of the overall objectives. In addition a series of small scale laboratory tests were completed in support and as part of the overall programme of work.

Those aspects of the project described herein initially required the design, manufacture, commissioning and operation of a test rig comprising a Rolls-Royce Viper jet engine, and a nominal 600 mm diameter tube that was some 12 metres long as shown in Figure 1. This work formed the work package (WP 2.2) of the overall test programme.

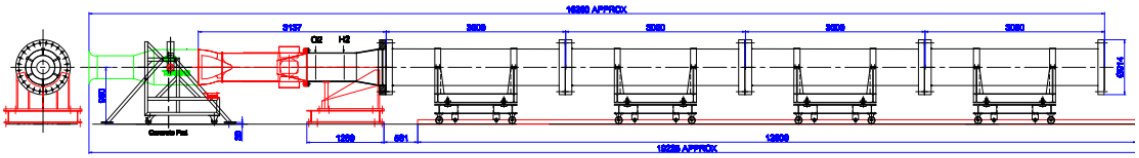

Figure 1: WP2.2 Circular duct rig

For the later stage (WP 2.3 the subject of the rest of the report)), a scaled model of a Heat Recovery Steam Generator (HRSG) including an expansion section, a tube bank and an exhaust stack was attached to the end of the tube as shown in Figure 2. The engine exhaust provided a hot vitiated air flow that travelled along the tube and in the case of WP 2.3 through the HRSG. Flammable high hydrogen gas mixtures were added to the exhaust stream and ignited. The second rig thus provided a reduced-scale model of an actual CCGT, in which the behaviour of representative fuel/air mixtures could be measured as the ignited mixtures passed through the tube bank of the HRSG. Consequently its effect on flame acceleration and possible lead-up to detonation could be examined in some detail.

ga

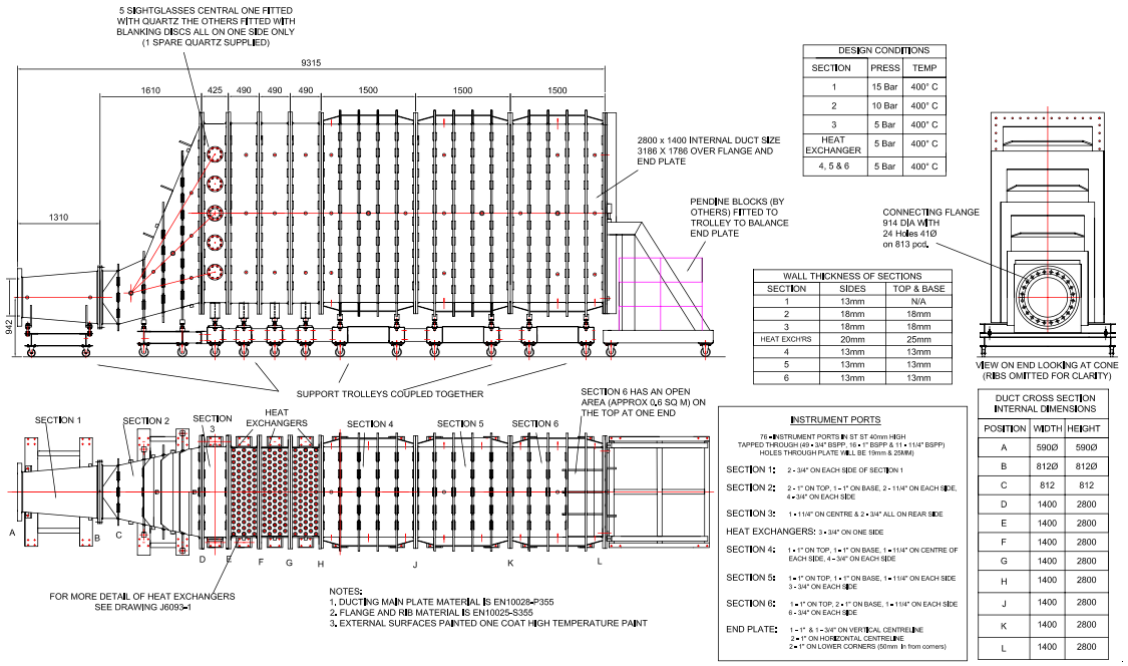

Figure 2: WP2.3 HRSG extension.

The basis of design, manufacture and installation, the commissioning and operating procedures used for both rigs are presented in separate documents for WP 2.2, see Refs [1, 2] and for WP 2.3, see Refs [3, 4].

The rigs provided two experimental facilities to investigate engine flameouts in CCGT/CCGE systems and the consequences of unburnt fuel passing through the turbine (in the CCGT case) and into the exhaust system and igniting. In such circumstances the maximum 100% hydrogen concentrations in the downstream mixtures were not expected to exceed an EQR[1] of 0.5 when fuelled with pure hydrogen. For CCGE applications the hydrogen concentration may be higher by up to a factor of two. However gas engine systems run at much lower mass flow rates and with lower exhaust velocities than do gas turbine driven systems. If ignition in the exhaust system is assumed to occur, the project seeks to assess the potential consequences, particularly in respect of the flame acceleration and the detonation propensity of the combusting air/fuel mixtures as they travel through the rig and exit via the exhaust stack.

The complete WP 2.3 rig and the housing containing it are shown below in the isometric cutaway drawing as Figure 3. Note the end plate and stack are not present in this Figure.

[1] *The Equivalence Ratio (EQR) is defined as the ratio of the actual fuel/air ratio to the stoichiometric fuel/air ratio. Stoichiometric combustion occurring when all the oxygen is consumed in the reaction and there is no molecular oxygen in the combustion products.*

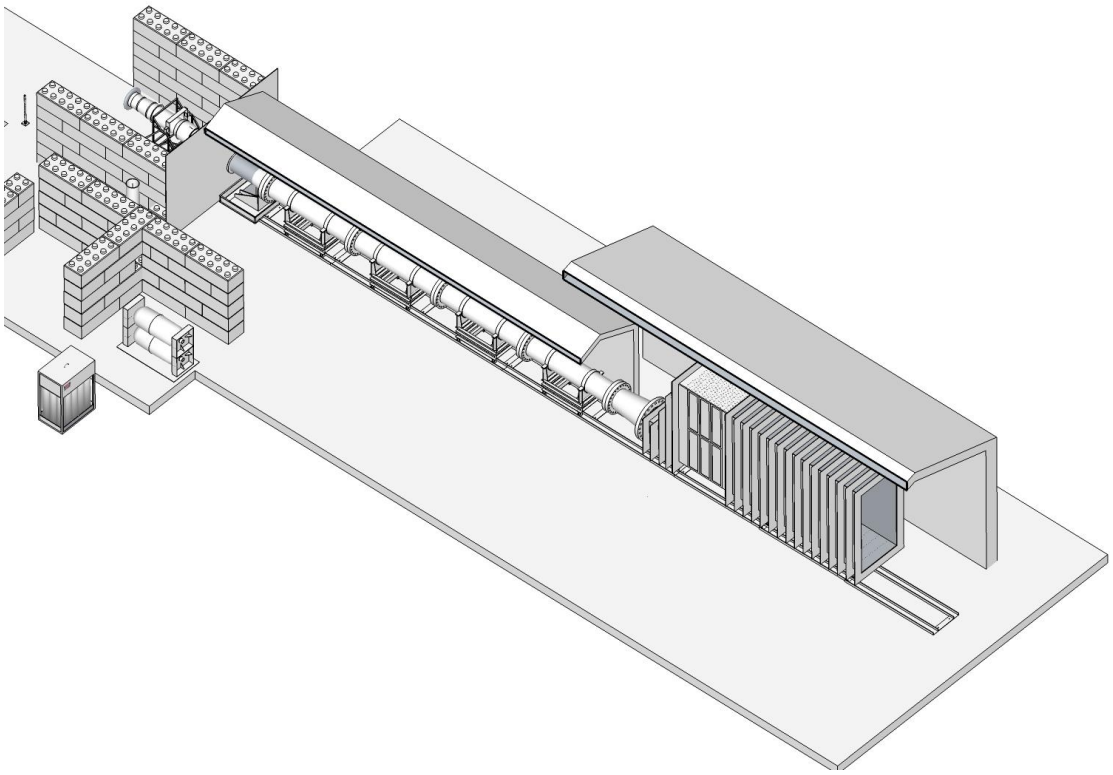

Figure 3: Isometric (cutaway) drawing of complete rig.

The two rigs combined as shown in Figure 3, provide a reduced-scale model of an actual CCGT/CCGE exhaust system including the heat exchanger (HRSG). As such it was designed to enable predictions to be made of the hazards at full scale. The tests also quantified the combustion behaviour, as measured by the flame speeds and over-pressures observed for the fuel mixtures being tested. The data gathered was used to assess the influence of the HRSG on combustion intensity, as measured by generated pressures and flame speeds, which could lead to a better understanding of the propensity of the mixtures to detonate as they passed through the model heat exchanger. This allowed safe concentration limits to be identified for the mixtures being tested. Safe in this context was taken to mean the maximum EQR's that could be used without risk of generating pressures likely to exceed the maximum working pressures of the rigs. The WP 2.2 and 2.3 experiments used a hot vitiated airflow at two constant, but relevant flow rates.

The facility has also provided a better appreciation of the technology required to safely control and operate gas turbine engines running with hydrogen-enriched fuels, in particular where and when a combustible gas mixture exists in the exhaust gas stream immediately downstream of the turbine.

1.3 EXPECTATIONS

The HSL based test programmes undertaken using both of the test rigs, collectively totalled almost 90 ignition tests, for which representative sets of data were obtained. These tests were carried out on releases of flammable gas mixtures made up of various combinations of hydrogen, methane and carbon monoxide. The information generated

by these tests, which comprised over-pressure, flame and wave speed measurements, is documented in this report. HSL, Chementech and Imperial College staff for the overall analysis of the various mixtures tested used this data. The primary objective of the analysis was to understand how such mixtures would behave in full-size industrial CCGT systems. There was also an understanding that the data acquired would be suitable for validating CFD models of CCGT systems.

The information generated from the analysis is currently being used by industry to help define the safe working envelope for industrial systems in the event of accidental releases and the subsequent ignition of flammable gas mixtures as a consequence of a flame-out in gas turbines or gas engines when operating on high hydrogen fuel mixtures in the future.

The sheer volume of the data obtained is substantial and it is now being used in industrial modelling studies to support the development of effective CFD/combustion predictive methods for comparable geometries. The data will continue to be analysed by others and Imperial College in student based work for many years to come. It is expected that this may yield further insights in the future in respect to the safe operation of CCGT/CCGE systems on high hydrogen based fuels. The data obtained is complex and difficult to analyse due firstly to the complex interactions arising within the combustion processes being examined, and secondly to the difficulties, such as noise generation and harsh environmental conditions experienced in making measurements on industrial scale plant in the field.

2 PROJECT OBJECTIVES

2.1 OVERALL OBJECTIVES

The overall objective of this part of the programme of work (WP 2.2 and 2.3) was to design and manufacture two experimental test rigs that, together, provided a reduced-scale model of a typical industrial CCGT system. The rigs to then be used for an experimental testing programme as defined and discussed later in this report.

The first rig comprised a Rolls-Royce Viper gas turbine whose exhaust flowed through a 600 mm diameter duct and, for the second rig, into a scaled HRSG that contained a geometrically representative tube bank. Flammable gas mixtures and make-up oxygen could be added to the exhaust stream in a controlled manner. The test rigs thus reproduced at a reduced scale the conditions likely to occur in the event of a flame out in an industrial CCGT in which high hydrogen flammable gas mixtures enter the turbine exhaust and ignite subsequently. As a consequence the combusting gas mixture may produce unacceptably high overpressures in the exhaust system, especially as the flame front passes through the HRSG where the high turbulence levels increase the risk of high overpressures occurring possibly leading to a detonation.

The supporting experimental programme therefore sought to quantify the flame speeds and over-pressures that occurred for a range of representative high hydrogen gas mixtures. The design of the test programme drew upon the literature review and the laboratory work already completed the latter as WPs 2.1 and 2.2. The commissioning programme for WP 2.3 was undertaken with the HRSG being open-ended initially in order to assess the influence of the tube bank on pressure development and flame speed when compared with the open duct test programme carried out as part of WP 2.2. The bulk of the test programme utilised the HRSG tube bank with the end plate and exhaust stack in place, such that their influence on the combustion intensity could be fully examined with a view to identifying the operational limits necessary to avoid any excessive overpressures.

The agreed test programme for WP 2.3 is shown in Appendix 12.1.

2.2 CONTRACTUAL OBLIGATIONS: DELIVERABLES

The deliverable contractual obligations in respect of milestone 10 are the provision of a comprehensive final report that meets the original requirements listed in Appendix 12.2.

2.3 ACCEPTANCE CRITERIA

The original acceptance criteria in respect of milestone 10 are also listed in Appendix 12.2.

During the course of the programme of work modifications and/or changes in emphasis to both the deliverables and the acceptance criteria were made to ensure that they reflected better the outcomes of specific parts of the work programme.

3 BASIS OF DESIGN (BOD) FOR WP 2.3 TEST RIG

3.1 DESIGN PHILOSOPHY

The design philosophy followed was to provide a versatile rig that would enable a wide range of test parameters to be examined together with a large range of flammable gas mixtures, representative of the operational envelope expected to be used in practice. In addition, safe operation of the rigs was to be paramount, which was to be implemented through the safe working pressure that the rigs were designed to withstand, the use of high temperature stainless steel or carbon steel for the key structural elements of the rig and through a comprehensive HAZOP study of the whole of the rig's design and its operating procedures. The latter resulted in strict operating procedures [Appendix12.6] and control measures, which were intended to mitigate the consequences of the major accident scenarios.

The rig was designed, manufactured, installed and operated in compliance with the relevant CDM, DSEAR and Pressure Systems Regulations.

3.2 DESIGN SPECIFICATION FOR WP 2.3

The specification for the WP 2.3 rig was given originally in the BoD and commissioning documents [3, 4]. However as a consequence of commissioning the rig and its subsequent operation when undertaking the test programme, development changes were made to the design specification as work progressed. The final specification and current capabilities of the rig are listed for completeness in Appendix 12.3.

4 SUMMARY DESCRIPTION OF THE TEST RIG

4.1 INTRODUCTION

This section of the report gives a high level overview of the WP 2.3 test rig, its instrumentation, the data collection system and the operational procedures used for the test programme. A more detailed description of both rigs can be found in the Basis of Design and Commissioning documents [1-4].

The test rig was designed to investigate the potential consequences associated with the ignition of mixtures of flammable gases as may occur in CCGT or CCGE installations when the prime mover fails, allowing a flammable gas mixture to enter the exhaust system and ignite. A flame front and associated pressure wave will then travel through the exhaust system and enter the HRSG where the pressures generated may cause structural failure with potentially serious consequences. The design objective is achieved by the provision of the following elements:

- A gas turbine engine with its associated fuel supply that provides hot exhaust gas to a circular tube of 600 mm diameter and at a temperature comparable to the full-scale installation;
- An engine control system that can be operated remotely;
- A means of restoring the oxygen level in the tube to the normal air level;
- A means of injecting a controlled amount of test fuel into the tube to simulate flame-out conditions;
- An extension to the tube that replicates an actual HRSG comprising fifteen rows of finned tubes together with an expansion section and a vertical exit stack;
- An ignition system for the hot flammable gases in the tube, which is linked to the data acquisition event;
- A range of sensors with both medium and fast responses to enable the monitoring of the operating conditions and the capture of the flame and pressure signatures during an ignition event; and
- A data logging and processing system.

4.2 BASIC LAYOUT OF THE ENGINE, DUCT AND HRSG

The test rig consisted of a Rolls-Royce Viper, type 301, gas turbine, whose exhaust fed into a 600 mm diameter circular tube. This was 12 metres in overall length and consisted of four 3m long insulated sections, flanged and bolted together (see Figure 1 for the complete layout of the WP 2.2 rig). There was a scaled model of an actual HRSG bolted to the tube exit as shown in Figure 2, which was a 1/8th reduced-scale replica of a GE 350 MW design, except that the section downstream of the tube bank was extended on the model. This was done in order to allow space for the flow to become established downstream of the tube bank for measurement purposes. The tube bank itself consisted of 218 vertical tubes of 38 mm diameter solid finned heat exchanger tubing as shown in

Figure 4. These gave a blockage ratio of 48% across the section when the cross-sectional areas of the tube fins were included. The HRSG section had either a vertical stack attached at the end of it or it could be left completely open depending on the test conditions required.

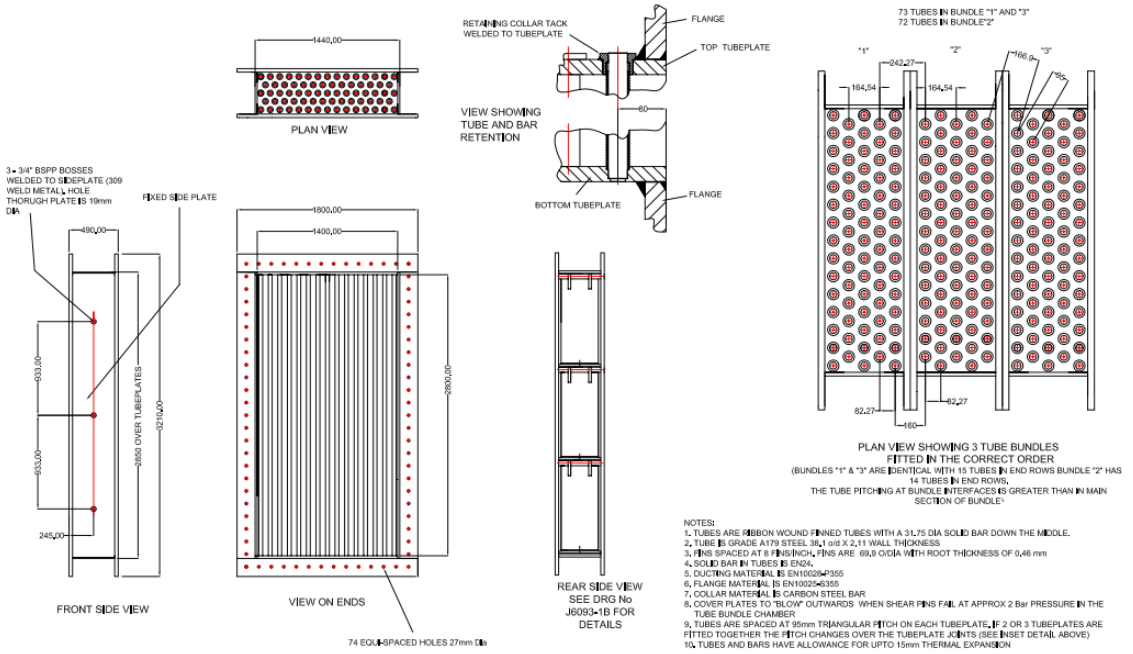

Figure 4: Tube bank in the HRSG

4.3 CHANGES IN THE RIG SETUP FROM WP 2.2 TO WP 2.3

Descriptions of the WP 2.3 rig's key features, together with details of the changes from WP 2.2 are given in Appendix 12.4 and in the commissioning report [4]. The following is a summary of these to aid an understanding of the remaining sections of the report.

4.3.1 Gas turbine

The engine exhaust gas temperatures immediately after the turbine varied up to a maximum of 650^{0}C depending on the operating conditions being used. The maximum power used for these tests corresponded to a mass flow rate of around 9.2 kg/s. Consequently the engine exhaust temperature increased in line with increasing mass flow rate up to approximately 600 °C over the operating range used for the test programme.

4.3.2 Diverter and transition sections

The flow rate into the duct was controlled by an orifice plate in combination with the diverter as was the case for the WP 2.2 tests. However, the orifice plate used for these tests is shown in Appendix 12.4.2 (Figure 33). Depending on engine speed, this allowed velocities along the duct of between 60-90 m/s, but typically 85 m/s to be achieved, this range being representative of the exit velocities occurring in actual CCGT systems immediately after the turbine.

4.3.3 Injection and mixture systems

The means of injecting the oxygen and gas mixtures was the same flow-through system used previously. Thus the gases were injected directly into the exhaust stream and relied on the injection process to ensure that the gases were fully mixed with the exhaust stream. However the gas storage capacity was doubled for both the fuel gases and the oxygen giving a capacity of 450 litres and a maximum working pressure (MWP) of 200 barg. This was necessary because of the increased rates of injection required.

4.3.4 Turbulence generator and igniter

The turbulence generator at the entrance to the first section of the duct remained the same as in WP 2.2; however, the spark igniter was now located 250 mm downstream from the beginning of the second duct section, but remained attached centrally through the top instrument port.

4.3.5 Velocity profile measurements

A pitot-static probe was used to obtain the pressure profiles across the duct. It traversed right across the duct and was located through the optical viewing port on the fourth section of duct.

4.3.6 Building housing the rig

The complete test facility comprising the jet engine, duct, and HRSG all with their associated components was housed in the original 15 metre long by 3 metre wide by 3.5 metre high cross-section ventilated agricultural style building. However, the HRSG part of the rig was housed in a 5 metre high by 6 metre wide extension to the original building, as shown in Figure 3.

4.3.7 Engine control system

The engine control system remained the same as used previously for WP 2.2, making use of a National Instruments cRIO system which is effectively a PLC device that records engine parameters and also has the ability to operate valves and to switch pumps on/off using relays and pneumatic valves.

Failsafe hardware was installed, which in the event of a power failure, gas leakage, engine over-speed or over-temperature would automatically shut down the engine as well as the gas delivery system.

4.3.8 Gas delivery control system

The fuel/oxygen injection systems were both controlled from the control room situated approximately 90 metres from the test rig, and remained essentially the same as used previously. However, during commissioning several updates were made to allow tuning of the PID parameters for the control valves so that their response times were optimised for fast response with only a small amount of overshoot. Also, from experience gained running the oxygen and mixed gas systems it proved necessary, in order to improve the efficiency of the injection process, to modify the logic of how the software triggered operation of the two systems and how the valves and dome loaders were operated.

An important aspect of the fuel and oxygen injection protocol was to ensure that sufficient time was allowed after the target injection levels were reached for downstream purging by the new mixture to be achieved. Some CFD analysis had previously been carried out in the region of the expansion duct, indicating that around 3 seconds was required for the recirculation zone to be purged, and in addition, pre-combustion tests indicated that the HRSG main chamber had fairly uniform flow of around 6 m/s. This latter figure suggests that transit times for flow in the HRSG are around 0.7 seconds. For the closed HRSG geometry, there will be additional recirculation zones around the chimney and also around the bottom corner of the end plate region, which will require more time to purge this zone.

Table 1: Purging times after mixture conditions are reached before ignition for HRSG tests.

HRSG Test No.	O_2 target reached (sec)	Fuel mixture target reached (sec)	Ignition (sec)	Purging time before ignition (sec)
3	7.583	10.883	17.019	6.136
4	7.338	9.966	16.743	6.777
5	6.640	10.645	18.214	7.569
6	3.593	11.119	19.064	7.945
7	7.269	11.871	21.483	9.612
8	5.770	9.149	16.516	7.367
9	5.041	20.594	25.732	5.138
10	6.000	9.261	20.167	10.906
12	7.613	10.414	18.852	8.438
13	O_2 and fuel data collected just prior to ignition			
15	0	9.869	15.066	5.197
16	O_2 and fuel data collected just prior to ignition			
17	3.450	9.213	16.210	6.997

The data files also capture gas delivery data and this can be combined with the time for ignition to provide an indication of the time available for total purging of the mixed gas. This is presented in Table 1, Taking the initiation of gas injection as time-zero then the second column shows the time point in seconds at which the O_2 injection target mass flow rate was reached, the third column the time when the fuel injection target was reached and the fourth column the time when the ignition was activated. The fuel mixture target was always achieved later that that of O_2 and therefore the time difference between ignition and the achievement of fuel target is the time period during which the full O_2/fuel mixture was available for purging the system before ignition. It can be seen that generally more than 6 seconds is provided for this operation. (Note that for two

cases the gas delivery data was initiated later than intended and started just before ignition, meaning this time interval is not available from the collected data. However the injection procedures were the same for these cases.)

4.3.9 High speed data acquisition system

SCITEK designed and installed the data acquisition system on the rig, using hardware from National Instruments. The original data logging system used for WP 2.2 before the HRSG was installed had a limited number of channels and could not accommodate the additional inputs identified as necessary for the WP 2.3 work programme. Consequently, an extra thirty-two data acquisition channels were added to acquire the additional data from the instrumentation added to the HRSG rig. As part of this upgrade, choosing cards that could share the same clock pulse and thus were able to record data synchronously by default eliminated synchronisation issues between the individual data acquisition cards. For the high-speed data channels, this improvement made real-time comparisons between channels easier as well as more accurate. The data collection software ensured that all critical data was displayed in numerical and graphical form and stored for more detailed analysis in due course in TDMS file format. The software for data acquisition and control was written in LabVIEW.

The inclusion of additional sensors and instrumentation required additional cabling, power and amplification for the signals. For the pressure transducers a 16-channel Fylde amplifier was acquired which also helped reduce signal noise levels and was compatible with all the types of strain gauge sensors used. It also had the added benefit of being able to zero sensor outputs before starting an experiment, thus removing any drift in the DC offset of the sensors. This made comparisons of pressure signals that much easier to follow.

During re-commissioning of the rig to operate at the increased velocity required for the WP 2.3 test programme, several further updates to the software became necessary to overcome a number of safety related issues and also to improve the operation of the control systems. These included modifications to the software of the engine control PLC system so that when the signal was given to the PLC (from the engine user interface software) it was on condition for an ignition test and would immediately start monitoring the rpm, fuel flow and fuel supply pressure to the engine. The PLC then recorded the current parameters and took a five second running average. If any one of these three parameters dropped by a pre-defined percentage, the PLC would initiate a software activated E-Stop. The predefined percentage values were read from an initialisation file so that they could be altered without needing to carry out changes to the software. A software initiated ESTOP was also transmitted to the gas delivery system PLC, which shut down the fuel and oxygen flow to the rig. When the engine user interface signalled to the engine PLC that the test had been completed it stopped monitoring the three parameters and the system then operated as before.

The engine user interface was also modified to include a button that was activated by the operator to signal to the PLC that the test condition had been reached; this notified the PLC system to start monitoring the parameters mentioned above. When this button was deactivated a signal was transmitted to the engine PLC to stop monitoring these parameters, consequently it did not activate the software ESTOP if any of the parameters

dropped below the defined limits. The reason that necessitated this feature was that if the engine shut down (because of an event that was not caused by an ESTOP e.g. fuel blockage or compressor stall) during an ignition test there was a risk of a potentially damaging pressure rise occurring in the rig due to the engine mass flow rate being significantly lower and as a consequence the EQR of the test mixture increasing. With this feature in place if the engine shut down the software ESTOP would also shut down the GDS system thus preventing a release of the test gas mixture.

4.3.10 Instrumentation

Table 2 below lists the types and numbers of sensors used during the WP 2.3 test programme, a full description of their operation can be found in Appendix 12.5.

Table 2: Sensors in use on HRSG rig

Sensor Type	Quantity	Range	Sample Rate	Response
Ionisation Probe	24	0 to -5V	100 kHz	0.1 μs
Ionisation Rakes	4 x 3 sensors	0 to -5 V	100 kHz	0.1 μs
Optical Probes	12	0 to 5V	100 kHz	3 μs
Kulite Pressure Transducer	10	0 to 7 barg	100 kHz	10 μs
Thermocouple	24	-200 to 1250 °C	1 kHz	1-2 s

For Tests 3 - 12, a number of ionisation probes (IPs) and optical probes (OPs) were located towards the exit of the cylindrical duct in order to characterise the exhaust velocity entering the expansion section of the HRSG and the remaining sensors were distributed in such a way as to cover the expansion, heat exchanger and HRSG downstream regions adequately, which were also aimed at providing pairs of similar types which could be used for velocity estimation. For Tests 13 - 17, the IP and OP sensors were arranged slightly differently in that only OP10 and 11 were dedicated to duct exit velocity monitoring and the remaining sensors were clustered around particular axial 'stations' in HRSG sections 2, 4, 5 and 6, with the intention of identifying flame as it passed these particular stations and/or even particular 'channels' within these station positions. For example, two OP sensors arranged at a particular axial station might be 'observing' at right angles to one another, hence resolving flame at the centre or edge of the HRSG.

4.3.11 Operating procedures

See appendix 12.6 for a description of the rig operating procedures etc. Section 11.6.9 in particular covers safety related issues encountered during the commissioning and operation of the system.

5 PRESENTATION OF RESULTS FROM WP 2.3

5.1 INTRODUCTION

The rationale for the test programme is discussed in the Imperial College report [5] noting that it is based upon the need to identify conditions for unacceptable overpressure generation for the chosen test gas mixtures with increasing EQR and decreasing gas temperature. A brief summary of the IC work consists of the following:-

Experimental configurations were aimed at providing a comprehensive assessment of the relative influence of chemistry and flow, and involved ignition delay times measured by Stanford University using a shock tube, auto-ignition in a turbulent shear layer formed between a fuel jet and a stream of hot combustion products, turbulent burning velocities using fractal grid generated turbulence in an opposed jet configuration in order to determine the strength of turbulent deflagrations, and the DDT potential in a turbulent flow using an obstructed shock tube configuration and related to the fuel reactivity. The results consistently show a notable difference between dilution of H_2 fuel with CO and CH_4. Comparatively small amounts of added CH_4 causes a noticeable decline in mixture reactivity while a CO content of up to 50% shows only a modest impact. The results obtained from the shock tube and auto-ignition studies suggest that under the current condition, the reactivity of CH_4/H_2 blends becomes increasingly reduced by the CH_4 component beyond the 50/50 mixture. By contrast, CO mixtures remain much more reactive over the entire range of conditions.

The three gases used in the present test programme and the various mixture combinations used were based on the requirements of the project as identified in the original proposal and subsequently updated in the light of discussions with all the interested parties. The test programme, see Appendix 12.1, was also updated as the tests proceeded and results became available.

The results reported here focus on the combustion outcomes from the WP 2.3 test programme and include summary data for these tests which also includes the injected fuel composition, equivalence ratio of the fuel in the exhaust, fuel and oxygen mass flow rates, flame speeds and the peak pressure observed following ignition of the fuel mixture.

5.2 PRESENTATION OF RESULTS

There were a total of 13 tests successfully completed for the WP 2.3 programme and these are numbered HRSG3 - 17 in all of the reporting procedures. The main test parameters for the tests are shown in Table 3 below. HRSG tests 1-2 were unsuccessful, HRSG11 was not analysed although some data was collected, and HRSG 14 was classed as a failed test because of excessive noise on key instrumentation channels. Immediately after a test was completed all of the data from a valid test was stored and backed-up on the system computers and individual storage devices. The high-speed data from the HRSG rig was stored in TDMS format so that it could be analysed using the National Instruments Diadem software package. The engine data and the control and gas supply data were stored in CSV format. There was an additional pitot-static probe data file also stored in CSV format. This data when plotted showed the velocity profiles

across the 600 mm duct section and was used to demonstrate the repeatability of the flow conditions generated by the gas turbine.

There was also a large body of data collected for each test that was related to the supporting hardware. This included engine running conditions (rpm, internal temperatures, internal pressures, vibration etc.) and control system operation (valve positions, injected fuel and oxygen mass flow rates, exhaust oxygen concentration). All of this data is available to the project for analysis.

Table 3: List of the main test parameters.

Mixture	Test Number	Eq. Ratio	CH_4 (vol%)	CO (vol%)	H_2 (vol%)	Fuel gas flow rate (kg/s)	Oxygen flow rate (kg/s)	End plate condition
CH_4/H_2	3	0.55	40	0	60	0.252	0.498	OFF
CH_4/H_2	4	0.62	40	0	60	0.286	0.512	OFF
CH_4/H_2	5	0.65	40	0	60	0.296	0.517	OFF
CH_4/H_2	6	0.55	40	0	60	0.248	0.515	ON
CH_4/H_2	7	0.62	40	0	60	0.281	0.496	ON
CH_4/H_2	8	0.65	40	0	60	0.300	0.520	ON
H_2	9	0.47	0	0	100	0.107	0.480	ON
H_2	10	0.51	0	0	100	0.121	0.505	ON
H_2	12	0.55	0	0	100	0.132	0.520	ON
CO/H_2	13	0.51	0	60	40	1.058	0.547	ON
CO/H_2	15	0.56	0	60	40	1.185	0.519	ON
CO/H_2	16	0.59	0	60	40	1.272	0.506	ON
CO/H_2	17	0.62	0	60	40	1.345	0.503	ON

The positions of the instruments actually used for each test are shown in Table 4 below.

The data was used initially to generate a set of data templates or summary sheets. The first of these showed the positions of the sensors used for a particular test; following sheets summarised the test set-up, the test conditions and the actual test parameters used, such as the mixture ratio and it's EQR. Further sheets summarised the test results, such as the maximum flame speeds and pressures, an example of a set of data sheets is shown in Appendix 12.7.

All of the tests were undertaken at the same engine operating conditions (11,800 rpm) and with the tube bank consisting of fifteen rows of tubes. The sensor locations were changed in the course of the test programme to reflect the need to gather additional data downstream of the tube bank once the end wall was fitted. There was also an additional PCB supplied pressure sensor located in the end wall from test number HRSG6 onwards.

Table 4 Sensor port positions for HRSG tests. Rakes (highlighted in red) occupy 2 ports.

Sensor positions for tests 2 to 12		Sensor positions for tests 13 to 17	
Sensor	Port Number	Sensor	Port Number
TC0	7	TC0	7
TC2	9	TC2	9
TC3	11	TC3	11
TC4	13	TC4	13
TC5	19	TC5	19
TC7	33	TC7	33
KU6	39	KU6	39
TC9	41	TC9	41
IP5	45	KU7	47
IP4	46	OP11	50
KU7	47	OP10	51
OP11	50	OP0	57
OP10	51	TC12	59
IP3	53	TC24	60
IP2	54	**RA1**	61
IP1	55	**RA1**	62
IP0	56	TC13	63
OP0	57	TC25	64
IP6	59	**RA2**	66
RA1	61	**RA2**	67
RA1	62	KU8	69
IP7	63	TC16	70
TC24	64	IP9	71
OP1	65	OP2	72
RA2	66	IP8	73
RA2	67	IP11	75
KU8	69	KU9	76
TC16	70	TC26	77
TC25	71	IP7	78
IP8	72	KU0	81
OP2	73	TC20	83
KU9	76	IP10	84
TC26	77	TC17	85
TC27	78	KU1	87
KU0	81	OP3	82
TC20	83	OP4	90
IP10	84	OP6	91

Sensor positions for tests 2 to 12		Sensor positions for tests 13 to 17	
Sensor	Port Number	Sensor	Port Number
TC17	85	KU4	93
KU1	87	IP4	94
OP3	82	OP1	95
OP4	90	IP2	96
OP6	91	IP12	97
OP5	93	IP13	98
IP13	94	**RA3**	99
IP12	95	**RA3**	100
TC28	96	IP14	101
KU2	97	IP21	102
RA3	99	OP7	103
RA3	100	KU3	105
IP14	101	IP16	106
OP7	103	OP5	107
KU3	105	IP0	108
IP16	106	IP15	109
IP15	107	IP1	110
KU4	108	**RA4**	111
TC29	110	**RA4**	112
RA4	111	IP5	113
RA4	112	IP3	114
IP17	113	OP8	115
OP8	115	KU2	117
TC18	117	IP19	118
IP19	118	OP9	119
TC30	122	IP23	120
TC23	124	IP18	121
IP20	125	IP22	122
IP18	126	TC18	124
KU5	127	KU5	125
OP9	128	IP6	127
TC31	129	IP17	128
PCB	133	IP20	129
		PCB	133

5.3 COMBUSTION TEST SUMMARY DATA

A summary of the test result peak pressures is presented in Table 5 below. The peak pressures shown (in bold) were taken from any of the ten Kulite pressure transducers

used in these tests. In some cases, the peak pressures were observed towards the exit of the circular duct, in others within the HRSG section downstream of the tube bank. It should be noted that, due to the fact that the pressure traces were generally complex, including multiple peaks, it was considered misleading to associate the recorded peak pressure in the Table 5 below with particular times in the event train, particularly since a secondary peak may be close in amplitude to the main one. For this reason, the occurrence times of these peak pressures have not been included in the table.

Table 5: Summary of test result pressures

Mixture	Test No.	Eq. Ratio	CH_4 (vol%)	CO (vol%)	H_2 (vol%)	Ku0 - Ku4 highest pressure (barg)	Ku5 peak pressure (barg)	Ku6 - Ku7 highest pressure (barg)	End plate
CH_4/H_2	3	0.55	40	0	60	0.38_{Ku0}	0.22	0.58	OFF
CH_4/H_2	4	0.62	40	0	60	0.66_{Ku2}	0.33	0.74	OFF
CH_4/H_2	5	0.65	40	0	60	1.41_{Ku2}	0.90	1.13	OFF
CH_4/H_2	6	0.55	40	0	60	0.50_{Ku3}	0.65	0.76	ON
CH_4/H_2	7	0.62	40	0	60	0.59_{Ku2}	0.96	1.12	ON
CH_4/H_2	8	0.65	40	0	60	1.30_{Ku2}	1.63	1.31	ON
H_2	9	0.47	0	0	100	0.41_{Ku0}	0.52	0.60	ON
H_2	10	0.51	0	0	100	0.98_{Ku4}	1.03	0.96	ON
H_2	12	0.55	0	0	100	1.78_{Ku2}	1.79	1.21	ON
CO/H_2	13	0.51	0	60	40	0.60_{Ku2}	0.64	0.76	ON
CO/H_2	15	0.56	0	60	40	0.52_{Ku2}	0.55	0.82	ON
CO/H_2	16	0.59	0	60	40	0.59_{Ku2}	0.60	0.81	ON
CO/H_2	17	0.62	0	60	40	1.21_{Ku2}	1.35	1.31	ON

It is noted that EQR in Table 5 is the fraction of the stoichiometric fuel mixture used in the injection. The stoichiometric fuel fraction is the minimum fraction of fuel in the fuel/air mixture which consumes all of the available oxygen. For the various fuel gas mixtures used, the following values in Table 6 apply.

Table 6 Stoichiometric fuel values for gas mixtures used.

Fuel mixture	Stoichiometric fraction in fuel/air mixture
CH_4	0.095
60%H_2 / 40%CH_4	0.1603
40%H_2 / 60%CH_4	0.1304
CO	0.2957
40%H_2 / 60%CO	0.2957
60%H_2 / 40%CO	0.2957
H_2	0.2957
40%H_2 / 25%CH_4 / 35%CO	0.1935

If Y is the stoichiometric fraction of fuel for a particular fuel gas being used and X is the actual fuel fraction used in the fuel/air mixture, then the EQR in Table 5 is defined as EQR = X/Y.

It can be seen from Table 5 that the recorded peak pressure is represented by three columns, one relating to Kulite sensors K0 - K4 (highest pressure sensor indicated with the sensor subscript), one relating to K5 in the region of the HRSG end plate and one covering the end region of the circular duct (i.e. Ku6 and Ku7). There is a second pressure sensor around the end plate region, which is the PCB sensor. Due to the fact that this sensor normally showed some ringing in its pressure trace, it was preferred to report the end plate pressure using Ku5. The discussion below indicates that this latter peak pressure is related to the source pressure originating in the vicinity of the heat exchanger. The HRSG pressures (i.e. Ku0 - Ku5) are of particular interest in the context of pressure sensitivity in this structure, and the K6/K7 pressures may be relevant depending on the robustness of the circular duct region in a real industrial system.

An indication of the variation of peak pressure within the overall system is shown in Table 5, where it is combined with the rig layout geometry to show the pressure, section by section. Also included in Table 7 are the ‘near horizontal or x-direction’ velocities associated with these sections, where it is possible to make a reasonable judgement of these. In essence and ideally this requires signals from two optical sensors positioned not only at appropriate lengthwise separation distances, but also at the same vertical heights and depths. The sensor pairs may also need to be of the same type. The same reasoning may also apply to both the y-directions and z-directions, as it is apparent from the high-speed videos of the tests that the velocity vector in the region after the tube bank (Sections 4-6, see Table 7) is two-dimensional and possibly three-dimensional. Thus in order to provide a meaningful interpretation of the flow in these regions it is necessary to have an appropriate three-dimensional grid of sensors. However, it needs to be borne in mind that the x-direction velocity dominates the flow field.

5.4 HRSG TEST HIGHLIGHTS

Identifying the peak pressures is straight forward, however as indicated above the same cannot be said for flame velocities. As an example of this, it is noted that a number of flame sensors are located near the exit of the cylindrical duct section and, since the flame propagation within this duct is relatively simple (1-D), one can have confidence in the extraction of a near horizontal velocity for this part of the system. However, even for this part of the geometry, the flame front did not always appear to be normal to the axis of the duct, based on arrival times at different sensors, thus showing that underlying factors, e.g. flame kernel growth or geometrical layout, may give rise to subsequent asymmetries. The velocities shown in Table 7 have been estimated using information from the ionisation sensors, optical sensors and also the video records where necessary and, due to the complexity downstream of the heat exchanger, must therefore be interpreted and used with care. The velocities in the table carry subscripts indicating the sensors from which they have been derived.

Table 7: Distribution of peak pressures and flame velocity estimates through duct and HRSG system

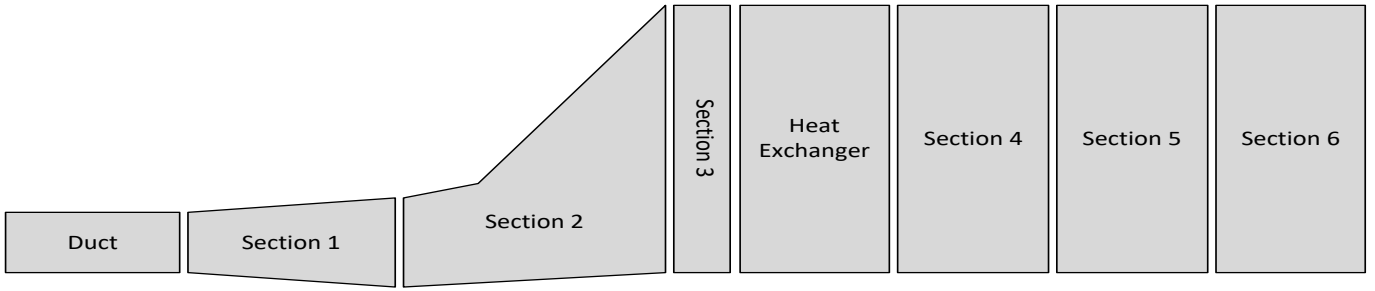

HRSG Tests	Test No.		Duct	Section 1	Section 2	Section 3	Heat Exchanger	Section 4	Section 5	Section 6
$40CH_4/60H_2$ EQR = 0.55	3 (end open)	Vel m/s	$292_{OP10,OP11}$	$189_{OP0,OP10}$	$94_{IP7,IP8}$		$88_{OP2,OP3}$	$104_{IP12,IP14}$	$81_{IP12,IP14}$	-
		P bar	0.57		0.39	0.51	0.38	0.33	0.30	0.22
$40CH_4/60H_2$ EQR = 0.62	4 (end open)	Vel m/s	$314_{OP10,OP11}$	$247_{OP0,OP10}$	$125_{IP7,IP8}$		$146_{OP3,OP4}$	$176_{IP12,IP14}$	$185_{OP6,OP7}$	$35_{IP20,IP19}$
		P bar	0.75		0.57	0.40	0.49	0.65	0.44	0.33
$40CH_4/60H_2$ EQR = 0.65	5 (end open)	Vel m/s	$278_{OP10,OP11}$	$277_{OP0,OP10}$	$103_{IP7,IP8}$		$32_{5OP1,OP3}$	$219_{IP12,IP14}$	$179_{OP5,OP7}$	-
		P bar	0.99		0.98	0.68	0.94	1.41	1.16	0.90
$40CH_4/60H_2$ EQR = 0.55	6 (end closed)	Vel m/s	$307_{OP10,OP11}$	$328_{OP0,OP10}$	$147_{OP0,OP1}$		$71_{IP8,IP12}$	$291_{OP3,OP5}$	$114_{IP13,IP16}$	-
		P bar	0.78		0.46	0.4	0.47	0.39	0.50	0.65
$40CH_4/60H_2$ EQR = 0.62	7 (end closed)	Vel m/s	$306_{OP10,OP11}$	$334_{OP0,OP10}$	$146_{OP0,OP1}$		$132_{OP3,OP4}$	$201_{OP6,OP7}$	$61_{IP12,IP15}$	$18_{OP8,OP9}$
		P bar	1.13		0.64	0.49	0.59	0.59	0.59	0.96
$40CH_4/60H_2$ EQR = 0.65	8 (end closed)	Vel m/s	$333_{OP10,OP11}$	$246_{OP0,OP10}$	$205_{OP2,OP0}$		$165_{OP2,OP3}$	$314_{OP4,OP5}$	$205_{OP6,OP7}$	-
		P bar	1.24		1.26	0.64	1.12	1.30	1.15	1.63

Table 7 (cont): Distribution of peak pressures and flame velocity estimates through duct and HRSG system

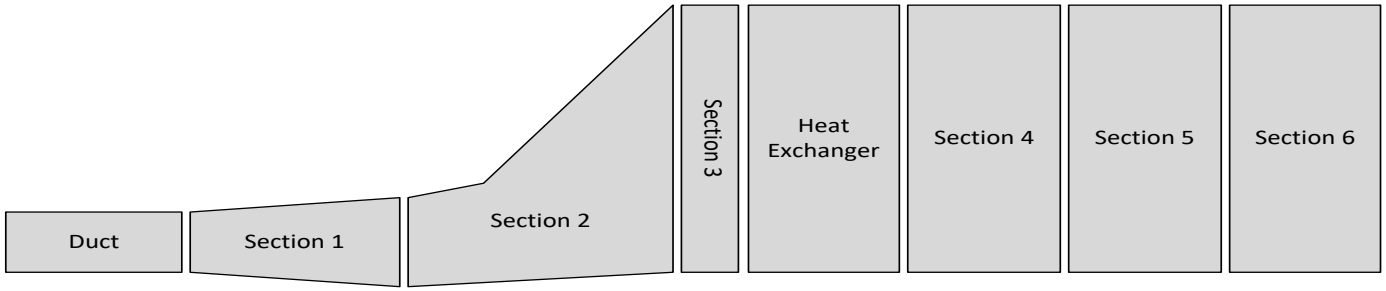

HRSG Tests	Test No.									
$100H_2$ EQR = 0.47	9 (end closed)	Vel m/s	$250_{OP10,OP11}$	$227_{OP0,OP10}$	$149_{OP2,OP0}$		$84_{OP3,OP4}$	$213_{IP12,IP14}$	$145_{IP19,IP16}$	$18_{OP9,OP7}$
		P bar	0.57		0.4	0.31	0.41	0.39	0.37	0.52
$100H_2$ EQR = 0.51	10 (end closed)	Vel m/s	$333_{OP10,OP11}$	$273_{OP0,OP10}$	$134_{OP1,OP0}$		$106_{IP12,IP10}$	$331_{IP13,IP16}$	$68_{OP7,OP6}$	$2_{OP9,OP7}$
		P bar	0.86		0.88	0.56	0.75	0.92	0.98	1.03
$100H_2$ EQR = 0.55	12 (end closed)	Vel m/s	$362_{OP10,OP11}$	$276_{OP0,OP10}$	$158_{OP2,OP0}$		$342_{OP3,OP2}$	$431_{OP5,OP3}$	$168_{OP7,OP6}$	$23_{OP9,OP7}$
		P bar	1.21		1.87	0.64	1.12	1.79	1.50	1.79
$60CO/40H_2$ EQR = 0.51	13 (end closed)	Vel m/s	$312_{OP10,OP11}$	$227_{OP0,OP10}$	$150_{OP2,OP0}$		$126_{OP4,OP3}$	$88_{IP7,IP13}$	22	-
		P bar	0.77		0.45	0.38	0.46	0.42	0.40	0.65
$60CO/40H_2$ EQR = 0.59	16 (end closed)	Vel m/s	$260_{OP10,OP11}$	$273_{OP0,OP10}$	$151_{OP2,OP0}$		$268_{OP1,OP3}$	$107_{IP21,IP12}$	56_{video}	-
		P bar	0.82		0.51	0.36	0.42	0.42	0.42	0.59
$60CO/40H_2$ EQR = 0.62	17 (end closed)	Vel m/s	$378_{OP10,OP11}$	$363_{OP0,OP10}$	$165_{OP3,OP0}$		$208_{IP12,IP10}$	$153_{IP4,IP16}$	58_{video}	-
		P bar	0.65		1.22	0.39	0.65	0.68	0.65	1.35

Significant complexity is further introduced to the flame propagation behaviour as it propagates through the expansion section and then the heat exchanger. This is due to the introduction of strong fluid dynamic features and large scale turbulent structures. This means that, whilst the flame sensors are arranged progressively downstream from the entrance region, flame arrival at the sensors may not follow a corresponding chronological order. This gives rise to difficulties in extracting a flame velocity and requires great care in selecting those pairs of sensors used for this purpose. The nature of the signal generated by the flame sensors is also influenced by the nature of the flame front. Figure 5 shows two contrasting cases, which reflect the general view regarding the width and nature of laminar and turbulent flames.

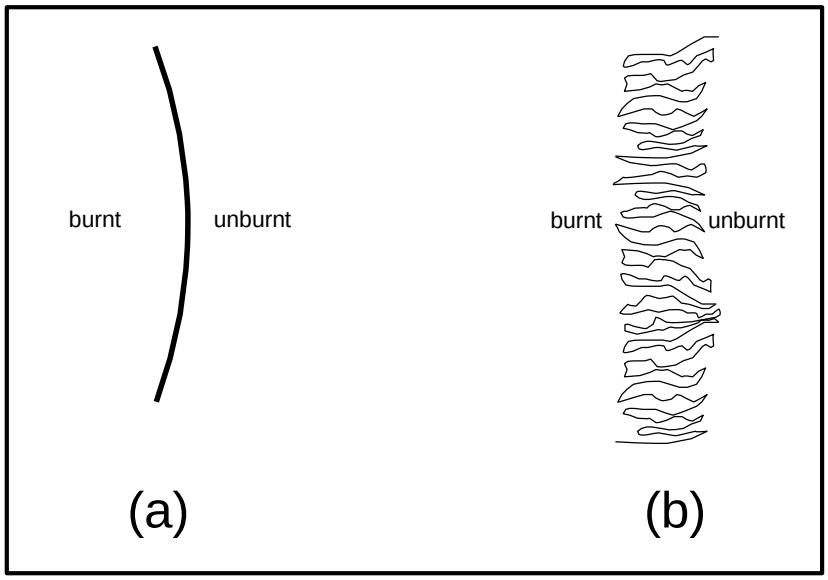

Figure 5: Flame front shapes for two sample cases, (a) low turbulence (b) high turbulence.

Case (a) is typical of a flame passing through a low turbulence environment and shows a sharp transition between the unburnt and burnt gases behind the flame. For such a flame passing over the flame sensor, the signal transition is correspondingly sharp on the time axis enabling the flame arrival time to be identified with good resolution. In case (b), where flame is passing through a turbulent environment, it gives rise to a 'flame brush', the transition from unburnt to burnt gases is less sharp and the corresponding transition time for the sensor response may be longer, reflecting the longer time of flame passage. In this case the resolution on the time axis will be poorer giving rise to greater uncertainty in estimates of the local velocity.

CFD analysis of the expanding entrance region to the heat exchanger has shown recirculation behaviour around the upper surface of this expansion and this is likely to add complexity to the propagating flame as it enters the heat exchanger. Any asymmetry across the reflection plane of the HRSG in this entrance region will also add to this and may show itself in the behaviour of the flame emerging from the heat exchanger. Aspects of this nature have provided a challenge in reporting flame velocities throughout the HRSG section and this contrasts with an ideal test geometry where a plane flame front propagates normally, and where the measurement on any part of the flame front at two axial positions can be considered representative of the general propagation of that front

for the purposes of velocity estimation. The video evidence indicates that flame propagation within the HRSG is not of this ideal nature and velocity estimates based on two sensors are more likely to be representative of the 'mid-position velocity' when these points are closer rather than well separated. The spatial resolution within the HRSG is of the order of 1m and care needs to be exercised in the choice of flame sensors being used for velocity estimates if flow asymmetries on this scale are present. There are for example several instances within the data where the flame arrival at a downstream point occurs before flame arrival at some point further upstream. In these cases, it is prudent to avoid assigning a flame velocity based on these particular data points, as it is preferable to use this data to try to inform the flame development behaviour within the system.

It is useful in this context to refer to the high speed video data in order to complement that from the rig sensors and to extract velocity data where sensors do not provide a satisfactory signal. Working in this way can resolve uncertainties in any sensor data and provide a rational account of the flame behaviour. An example of this is given here for Test 17(40% H_2/60% CO, EQR of 0.62). The location of particular sensors or other landmarks within the HRSG are identified along with the arrival time of flame at these positions and these are given in Table 8.

Table 8: Observation of flame arrival events for Test 17 using IP, OP and video data

Location	Position	Flame arrival		Flame speed
		Sensor	Video	
	(mm)	(sec)	(msec)	(m/s)
HE exit	16580		297.237	198 (sect 4, video)
IP21 (HR4)	18165		305.236	
OP6 (HR4 top)	16985	16.2775	297.903	
OP1 (HR4 R1M)	16985	16.2775	↓	
IP4 (HR4 L1L)	16985	16.2762		
IP2 (HR4 L1M)	16985	16.2770		
IP12 (HR4 R1U)	16985	16.2811		
IP13 (HR4 L1U)	16985	16.2794	301.903	
RA3 (HR4 R3M)	17575	16.2791		
IP14 (HR4 R5M)	18165	16.2852	306.236	
IP21 (HR4 L5M)	18165	16.2838	305.236	173 (sect 4, IPs)
IP2 (HR4 L1M)	16985	16.2770	298.903	186 (sect 4, video)
OP7 (HR5 top)	18775		324.236	
End of HR4	18315		309.236	26.5 (sect 5, video)
Middle of HR5	19375		349.901	

IP and OP signal times are taken from the TDMS files, whilst for the video record only the msec part of the time record is used. This latter has a resolution of 0.333 msec.

The region immediately downstream of the heat exchanger is of particular interest since the combustion intensity is greatest here, and the table identifies event timings in this region (HR4) and also the following region (HR5), where signals can be identified.

There are a number of IP and OP sensors within panel 1 of HR4 and these are grouped together. It can be seen for example that OP6 and OP1 show coincident signal peaks since they are looking across the same axial view, although arranged at right angles. The group IP4, 2 12 and 13 are arranged on the right and left sides at low, medium and high positions. The indicated flame arrival times for these 16.2762 to 16.2811 sec. It can be seen for example that the signals at IP4 (16.2762 sec) and IP13 (16.2794 sec), showing a delay of 3.2 msec are consistent with the delay in flame arrival at the bottom and top of the HRSG. Inspection of the video record indicates that a similar 3 msec delay from bottom to top is evident at this axial location and this is indicated in the table with flame arrivals being approximately from 297.9 - 301.9 msec. The signals from OP1 and OP6 also fall within the same time band as the other sensors at this axial station as would be expected since the flame front is fairly well defined at this early position.

Also shown in Table 8 are flame velocity estimates from both the IP and video records. These are indicated in the 5th column. For the HR4 section these range from 173 - 198 m/s depending on the measurement basis. Recalling that the normal exhaust velocity is around 6 m/s for the HRSG, this velocity confirms that this is a region of high combustion intensity, producing a corresponding high flame speed. The discussion in other sections of the report will suggest that this is the main region for transient pressure generation within the system and that the decay of turbulence beyond the heat exchanger results in a consequent rapid drop in flame speed. This is confirmed from estimated flame speeds in the next section (HR5), where the video record shows an average flame speed of around 26 m/s.

The video record also shows that the flame front progress is interrupted around the boundary of HR4 and HR5 and this will be examined in relation to pressure wave reflections later in this report. It can also be seen that the nature of the flame during its subsequent progress is of a much more diffuse form, with no evidence of a sharp flame front as can be seen around the heat exchanger exit. This may explain the absence of strong flame signatures on the IP and OP sensors in the downstream region of the HRSG and is a feature of most of the closed end HRSG tests. It is noted that the issue of fuel/air purging times has already been highlighted in Section 4.3.8 and the possibility that poor flame indication in the downstream sections is due to this possibility appears unlikely since purging times are around 9 times the residence time. This statement is based on the preliminary flow tests carried out with the open ended HRSG under engine running conditions where uniform velocity distributions were observed. The main effect of introducing a vertical chimney is to turn the flow by 90^{o} upwards and this is expected to introduce a recirculation zone in the lower corner opposite the chimney. This however is unlikely to have a significant effect on the purging of gas in section 5 or the upstream half of section 6, where limited flame data is achieved.

5.5 LDA TEST RESULTS

The LDA measurements were made by SCITEK using the system and methodology described in Appendix 12.9. A total of five traverses were successfully completed at the five vertical locations shown in Figure 2, i.e. at the entry region to the heat exchanger. The objective of these measurements were two fold; firstly to measure the horizontal and vertical velocities simultaneously, and secondly to use these results to obtain both the velocity vectors and the turbulence intensities. The test results are shown in Appendix

12.8. These data sets provide the horizontal and vertical velocities together with the relevant turbulence intensities as measured by the LDA system. Velocity vectors have then been derived from the data and are also shown in Appendix 12.8.

The HRSG results confirm expectations and predictions of CFD, and show the presence of a re-circulation zone in the upper regions, originating from the separation occurring in the expansion section and raised axial velocities in the lower region of up to 35 m/s due to flow convergence there. The results are discussed more fully in Section 6.6.A further set of LDA measurements were made to assess the velocity but in particular the turbulence levels across the 600 mm diameter duct. These were requested following a change in the design of the orifice plate controlling the gas flow into the duct, and which gave a much more uniform flow distribution across the duct. The results from these measurements are shown in Appendix 12.9.

It should be noted that these LDA results were of course obtained for exhaust-flow only and that, in turn, this limits their value. While the horizontal and vertical velocity components in the expansion section confirm first instance understanding and predictions of the CFD modelling, they will inevitably need to be significantly modified when the “base flow” becomes dominated by expanding combustion, progressing at different velocities through the centre and in the diverging boundary flows, of which especially the one along the bottom appears understandably and from limited results to be highly turbulent.

6 DISCUSSION OF RESULTS FROM WP 2.3

This section provides an assessment of the results obtained, in particular the clarity of the data, and its interpretation from the different sensor types and locations. Given the scale and complexity of these tests some anomalies were observed and are highlighted and discussed. The key sensors employed were the pressure measuring sensors, the absolute values of which were important in judging the deflagration/detonation behaviour of the different gas mixtures and EQR ranges being tested.

Interpretation of the optical and ionisation sensors was in most respects more straight forward as they were essentially on/off devices. Similarly for the thermocouples, as these were calibrated at source there was far less likelihood of their outputs being variable.

6.1 CONSISTENCY OF DATA

As always, a limited number of prioritised combustion tests were undertaken to cover the required conditions spanning mixture and EQR values. These were selected to match identified operational boundaries of mixture ratio and exhaust EQR that represented safe limits with regard to peak pressures following ignition. It was also of interest to confirm that changes in these parameters produced results that followed a logical and simple trend, namely that the combustion event became more powerful with increasing EQR other parameters remaining constant.

In general, three exhaust EQR values were tested for each fuel mixture combination, and these were chosen to span mixtures that produced peak pressures just above and just below the expected operational limit of 1-2 barg, in all cases, as shown in Table 3, Table 5 and Table 7. Increasing EQR values for each mixture composition studied generally resulted in increased maximum observed pressures, together with increased horizontal flame speeds either side of the tube bank.

6.2 VALIDITY OF PRESSURE SENSOR DATA

Two types of pressure sensors were used to measure the transient overpressures produced during a test. These were ten Kulite high temperature piezo-resistive pressure transducers (XTEH - 7L-190) with a maximum pressure measurement range of 7 - 10 barg and full scale output of 100 mV. These were positioned along the walls of the duct and HRSG at locations identified as key to the phenomena of interest. The signals from the Kulites were amplified using Fylde high frequency amplifiers. A single piezoelectric transducer was also deployed in the end wall of the HRSG, which was a PCB Piezotronics sensor, type 113B24.

The calibration of the Kulite sensors was carried out at prescribed intervals using a Drück calibrator; see Appendix 12.6.3 for the procedure employed. The Kulite sensors were found to hold their calibration well over periods of several weeks. The frequency response of these sensors was important for following the dynamic behaviour and the performance of these has been discussed in the commissioning document [4].

A key aspect of the pressure measurements was to identify mixture and exhaust concentration which were safe or unsafe in respect of the over pressures generated, and the confidence that can be placed on the absolute values obtained. This could be judged

by the variability of the pressure behaviour from shot-to-shot for the same conditions. The programme of tests did not allow this variable to be investigated in detail, but where repeats were carried out the peak pressures did show some variability in measured values as might be expected. It is suggested that the underlying stochastic nature of the combustion process can introduce differences which have not been quantified in this work. Table 9 gives selected comparisons of the HRSG pressures generated for particular sensors under similar operating conditions or incrementally changing conditions. Although the peak pressures in Table 3 show an increase with EQR, there are some apparent inconsistencies among tests for particular sensors.

Table 9: Observed variability of pressures for similar conditions.

Test case	EQR	K0 peak (barg)	K1 peak (barg)	K2 peak (barg)	K3 peak (barg)	K5 peak (barg)
11 (100% H2)	0.54	1.01	1.03	2.34	1.2	1.74
12 (100% H2)	0.55	0.754	1.12	1.79	1.25	1.79
13 (60% CO / 40% H_2)	0.51	0.46	0.45	0.60	0.40	0.65

From the pressure sensor data we are able to identify the finely defined boundaries between moderate pressure development and higher pressure development. For the previous circular duct tests, this was shown to arise over quite small changes in EQR of as little as 0.05. For the circular duct tests it was possible to explore this sensitivity to EQR and allow high pressures to develop. This was more difficult with the HRSG rig, since the duct was designed to tolerate much higher pressures than was the case with the HRSG design. Despite this however, there is some evidence from the tests that a similar sensitivity exists and this is suggested in the graphs in Figure 6 below for three fuel mixtures, which plots the Kulite 0 sensor pressure versus EQR for the three mixtures.

Ku0 is located at the heat exchanger and the discussion in Section 6.5 below explains the significance of this particular sensor in gauging the combustion behaviour around the exchanger. Although the 100% H_2 case appears linear for the EQRs used, there is evidence of non-linear behaviour for the 60%H_2 / 40%CH_4 mixtures, suggesting it could be operated at a higher EQR value. The behaviour of the four points representing the 40%H_2 / 60%CO mixture is not easily explicable as the first three mixtures indicate unexpectedly flat pressure behaviour and may be an indication of shot-to-shot variability already discussed.

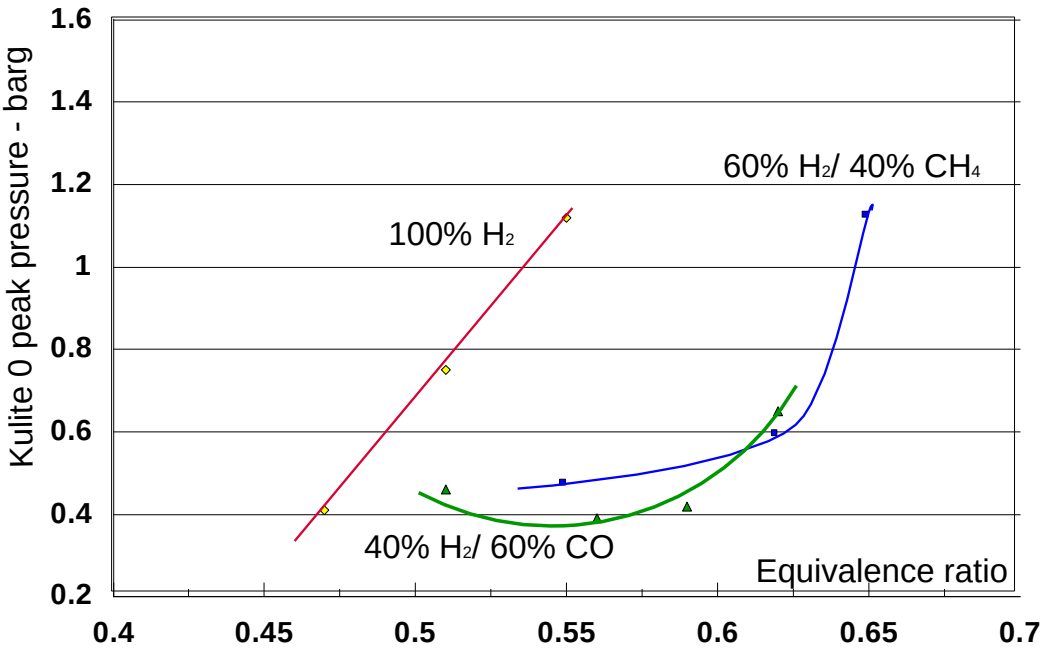

Figure 6: Variation of Ku 0 peak pressure with EQR for three different fuel mixtures including 100% hydrogen.

6.3 OBSERVATIONS REGARDING THE USE OF FLAME SENSORS

IP and OP data has been recorded in order to support the interpretation of observed pressure data and provide an insight into the development of pressures, through the observation of flame progression through the system. For the first nine HRSG tests, 21 surface ionisation flame sensors (IPs), 12 bulk flow ionisation flame sensors located within four pipe shaped rake devices, and 12 optical sensors have been deployed. These have been described previously. The IP devices and rakes provide typical output voltages of around -0.5V and the OPs around +1V. The IPs and rakes will only provide a signal if the flame passes over the sensitive twin electrode tip, which is around 10mm in overall dimension. The identification of flames passing over the IPs and rakes was made by assessing when the sensor output deviated from its baseline (ground) level. Ideally this is a sharp transition, reflecting a well behaved and narrow flame front traversing a region.

The optical sensor collects light from within a collimated column of around 15mm in diameter and in principle will detect a flame if it exists anywhere within this columnar region, noting that normal square law applies to intensity received and signal generated. The OPs are based on the detection by a PbSe photoconductive chip, which has wavelength sensitivity corresponding to CO_2 and H_2O, thus making it suitable for both carbon and hydrogen based fuel combustion detection. The signal normally carries a ~ 15V offset and for this reason the output is AC coupled, which in turn means that the signal is the derivative of the received intensity. This is useful since the maximum of the signal corresponds to the maximum rate of change of the received intensity. This would normally be expected to occur when the flame front passes the centre of the observed 'detection column'. The IPs, rakes and OPs share a common ground level and considerable effort was expended to ensure that this level was as free as possible from

electrical noise when the engine was running at full rpm. This effort had variable success and it is noted that any residual random noise had a greater effect on IP and rake signal interpretation than on the OP signal interpretation. The reason for this was that the detection point for the IPs and rakes was that point where the signal initially lifted away from the baseline. The identification of this point would sometimes be influenced by the baseline noise level, particularly if the signal strength was weak, e.g. with weak flame mixtures. For the OPs, the detection point was the maximum of the signal, which was generally well separated from the baseline noise level.

The performance of the IP sensors and rakes depended on the EQR value being tested. In general, with higher EQRs, a stronger, better-defined flame front occurred leading to a greater degree of flame detection. This is illustrated by the tests with the 60%H2/40%CH4 mixture where for an EQR of 0.55 (Test 3), 14 of 21 IPs and 5 of 12 rake sensors produce a signal, compared to an EQR of 0.65 (Test 5) these rise to 16 of 21 IPs and 10 of 12 rakes.

Differences in flame arrival times between wall mounted and centrally located IPs are frequently observed, which may be attributed to differences in the flame dynamics at the wall compared to the body of the duct and/or the HRSG. For lower EQR values, approaching the combustion limit for a mixture, IP signals were frequently poor or not seen. This may have been due to the poorly defined nature of the flame front or flame brush, or the lower flame temperature associated with the weaker mixture. It was also noted that the high speed video records taken for all of these cases confirmed that, for the weaker mixtures, flames may have weakened after exiting from the HRSG.

The OP signals were generally more secure, being an average measure across the duct diameter and these usually provided flame arrival signals after they had been lost on the IPs with reducing EQR values. The OPs are principally used for flame speed estimation and using OPs as a group rather than combining OP signals with those of the IPs most reliably achieves this. This is stipulated due to the difference in the measuring nature of the OPs, i.e. line of sight across the duct rather than a point measurement. Since the sensor and circuit provide an output proportional to the rate of change of received intensity, the maximum of this signal is taken to be representative of flame passage and therefore the maximum of the OP signal has been used as a consistent measure of the flame arrival for all tests. It should also be noted that baseline noise levels have, in a number of cases, made it difficult to judge the transition point for flame passage at IPs and this has reduced the number of flame sensors from the maximum, which could be used in most cases.

6.4 REVIEW AND ANALYSIS OF IP AND OP DATA

Whilst the primary function of the flame sensors was to detect when a flame passed a particular location, combinations of sensors would often be used to calculate a local flame speed. Experience showed that care needed to be exercised in this endeavour. Figure 7 shows the IP traces for IP0 - IP5, these are arranged in opposing pairs near the exit of the circular duct (0/1, 2/3 and 4/5). This is the simplest part of the overall geometry and it can be seen that the flame passage recorded for each member of the pair occurs at a slightly different time, with around 1.5 msec separating the signals. This implies that the flame front is not normal to the duct axis and for a flame speed to be calculated, it becomes important to choose the correct adjacent pair of IPs, i.e. those on the same

side of the duct such as IP0 and IP2 or IP3 and IP5. If this is done, then a consistent flame speed is calculated for each pair of sensors, in this case a value of 391 m/s at the duct exit. Two of the ports on the circular duct near the exit carry optical sensors and the traces for these are shown in Figure 8 for Test 3. The exit velocity derived from these signals.

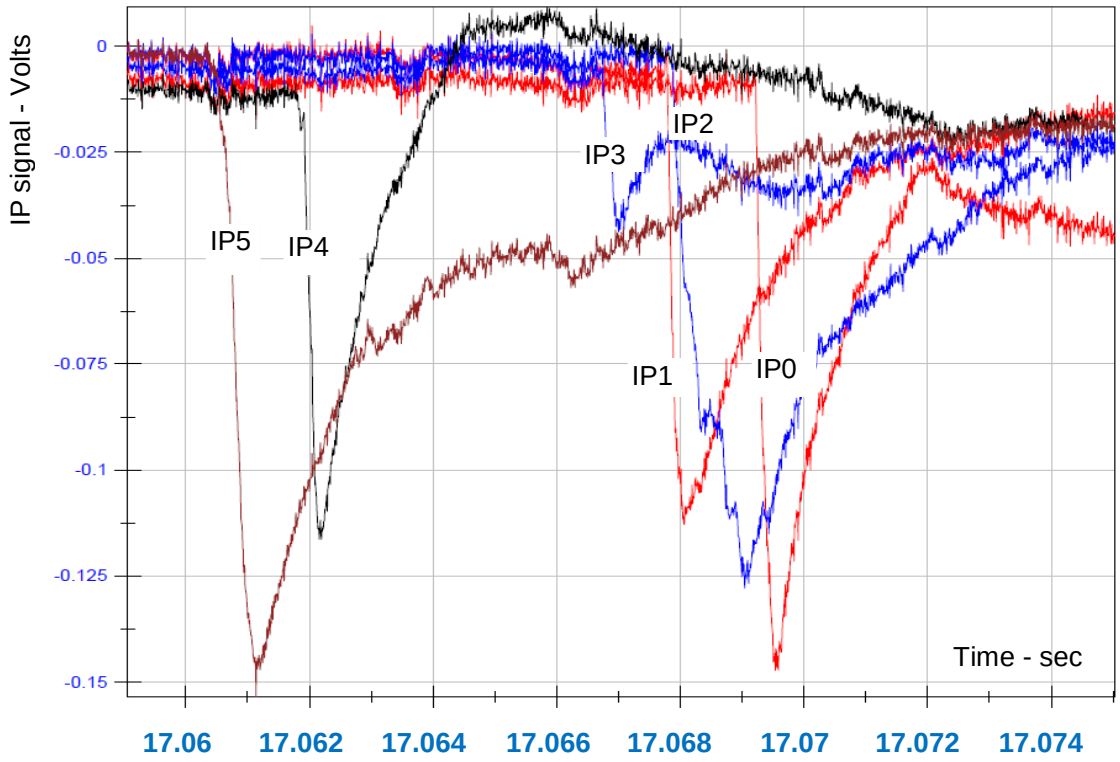

Figure 7: Test 3, comparison of IP traces for opposing pairs close to the end of the circular duct. Pairs are IP0/1, IP2/3 and IP4/5. Each pair is located at the same axial distance on the surface of the duct.

It can be seen that the nature of the signals is very different. For the OPs, any flame front within the line of sight is likely to contribute to an output signal. This means that for flame, which may cross at an angle to the line of sight, there is a progressive rise in the signal to a maximum, and a judgement needs to be made carefully as to when a flame passes any particular point. In general also, it is not advised to mix IP and OP signals when estimating a local flame speed.

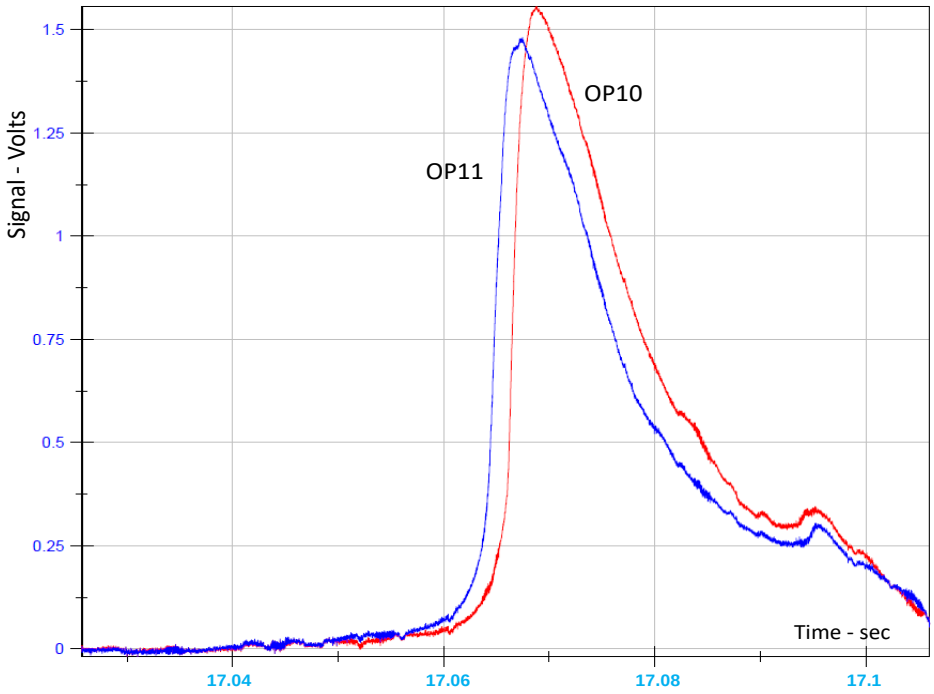

Figure 8: Test 3, comparison of adjacent OP traces near exit of duct.

The set of data involving the OPs has generally been more complete than for the IPs and rakes, which is likely related to the factors discussed above. OP's 10 and 11 are near the exit of the circular duct and in all cases, clear signals are provided by these. OP's 8 and 9 are near the end of the HRSG and in the majority of cases signals are missing from these sensors. These represent two extremes of the geometry, in the first case the flame is strong and confined, whilst in the latter, a well-defined flame may be absent or may bypass the sensor detection window. (It should be noted that all flame sensors were regularly checked in situ for correct operation). OP sensors at intermediate positions have mostly provided useful signals and these have usually been of a form that allowed a measurement to be made of flame passage in the relevant region. Figure 9 shows the collection of traces for the OPs within the HRSG for Test 3.

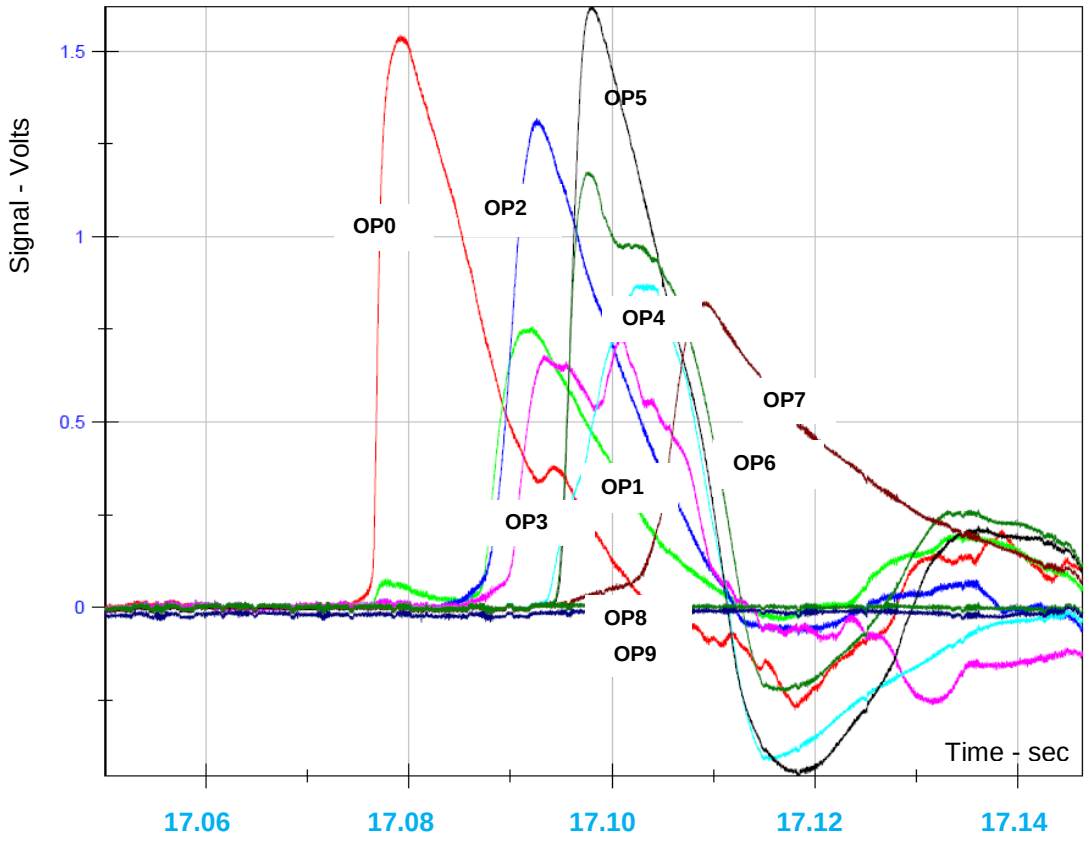

Figure 9: Test 3, collection of OP signal within HRSG. Axial positions within test rig are in mm, OP0(12152), OP1(14215), OP2(14745), OP3(15600), OP4(16580), OP5(16985), OP6(16985), OP7(18775), OP8(20575), OP9(21165).

It can be seen for Test 3 that all but OP8 and OP9 at the end of the HRSG provide useful signals and that the maxima of the traces occur in chronological order according to their axial position, with the exception of OP4 which is slightly later than OP5 and OP6. This shows that it cannot be assumed that the flame progression through the system is a simple one. It can also be seen that a double peak occurs on OP3, which is within the heat exchanger array, which may imply multiple flame passage events.

The OP signals in Figure 9 are typical of those seen for all of the tests, which also include the time ordering of signal peaks. For the traces around the expansion and heat exchanger peak half widths tend to be around 10 msec and these increase to 20 msec in moving further down the HRSG, e.g. for OP7. Only in one case, namely Test 12, was a signal observed on OP9 near the HRSG end plate.

6.5 REVIEW AND ANALYSIS OF PRESSURE DATA

The pressure data within the system reflects the features of both the geometry and flame velocity behaviour during a combustion event. Total pressure is the result of cumulative pressure losses through the system due to fluid flow, and changing pressure is a reflection of changes in fluid flow rates arising from changing volume generation rates during flame passage.

Concerning the three combustion tests with an open HRSG, this feature is shown in Figure 10 in a simple way for Test 3. The ignition time for this case is at 17.02 sec and the figure shows the pressure on Ku7 near the end of the circular duct section (distance = 9758 mm). This pressure sensor shows the highest pressure within the system. Due to an increasing volume generation rate as flame travels down the duct, the pressure rises over a 25 msec period to a maximum at point (a). This corresponds to the exit of the flame from the circular duct into the expanding sections 1 and 2. A drop in Ku7 pressure as the flame passes through this section indicates a reduction in volume generation rate. Also shown in the figure is the flame sensor signal on IP10, which is located on the surface of the central panel of the heat exchanger.

It is expected that flame arrival at this point will result in strong flame acceleration due to the turbulence generated giving rise to a high rate of volume generation. This will give rise to a further steep pressure rise locally, which is experienced at Ku7 some time later, shown as peak (b). The time interval between the flame signal on IP10 and this second peak at Ku7 is 7.7 msec and is the transit time of the pressure wave back to Ku7 over a distance of 6.33 m. This corresponds to a sound speed through the hot exhaust of 820 m/s, consistent with a burnt gas temperature around 1200 °C. The final maximum on Ku7 of around 0.5 barg at 17.18 sec occurs after the flame has been recorded at the end of the HRSG and may correspond to the reaction effect of an external explosion as the external combustible gas is ignited by the flame emergence. These features are also shown on the other open end tests, Tests 4 and 5.

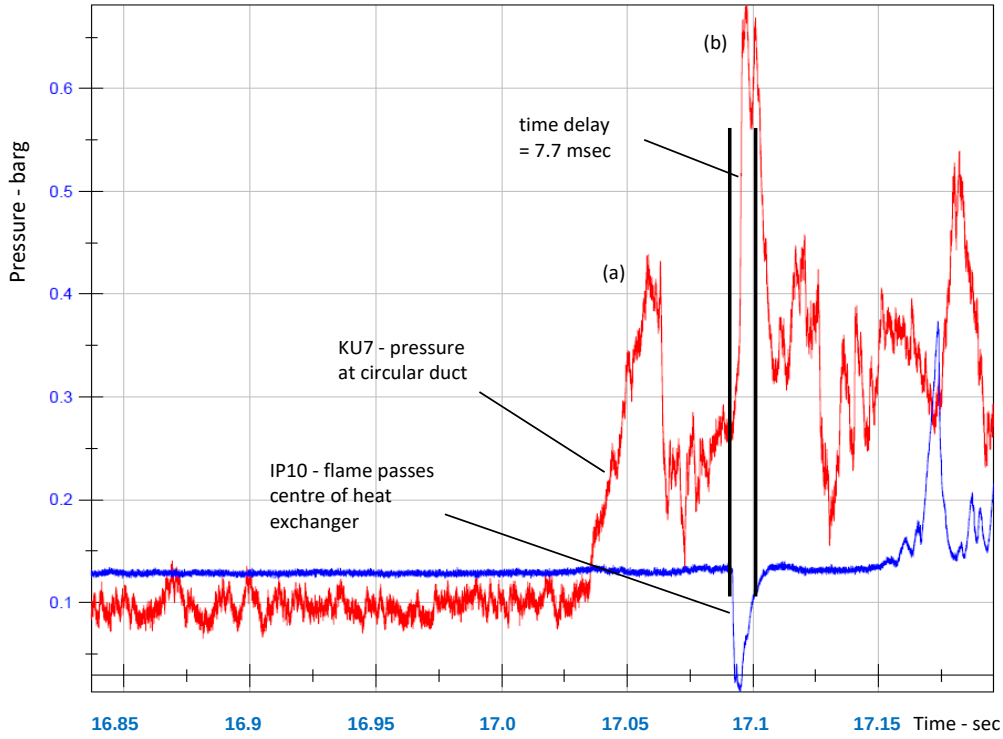

Figure 10: Traces of pressure at Ku7 near exit of the circular duct and flame arrival on IP10 located on central panel of heat exchanger.

The behaviour of the pressure sensors from the position of the heat exchanger and downstream toward the exit gives a clue as to the development of the combustion in this

extended region. Figure 11 shows the time traces for five sensors for the same Test 3 as discussed above. Ku0 is located at the heat exchanger and it can be seen that the peak pressure here is 0.375 barg. As discussed above, this pressure pulse is experienced at the Ku7 position upstream in the circular duct a few msec later, where the second peak on Ku7 has a value of 0.580 barg. The compression associated with the reducing diameter apparently gives rise to this increase in amplitude by a factor of 1.

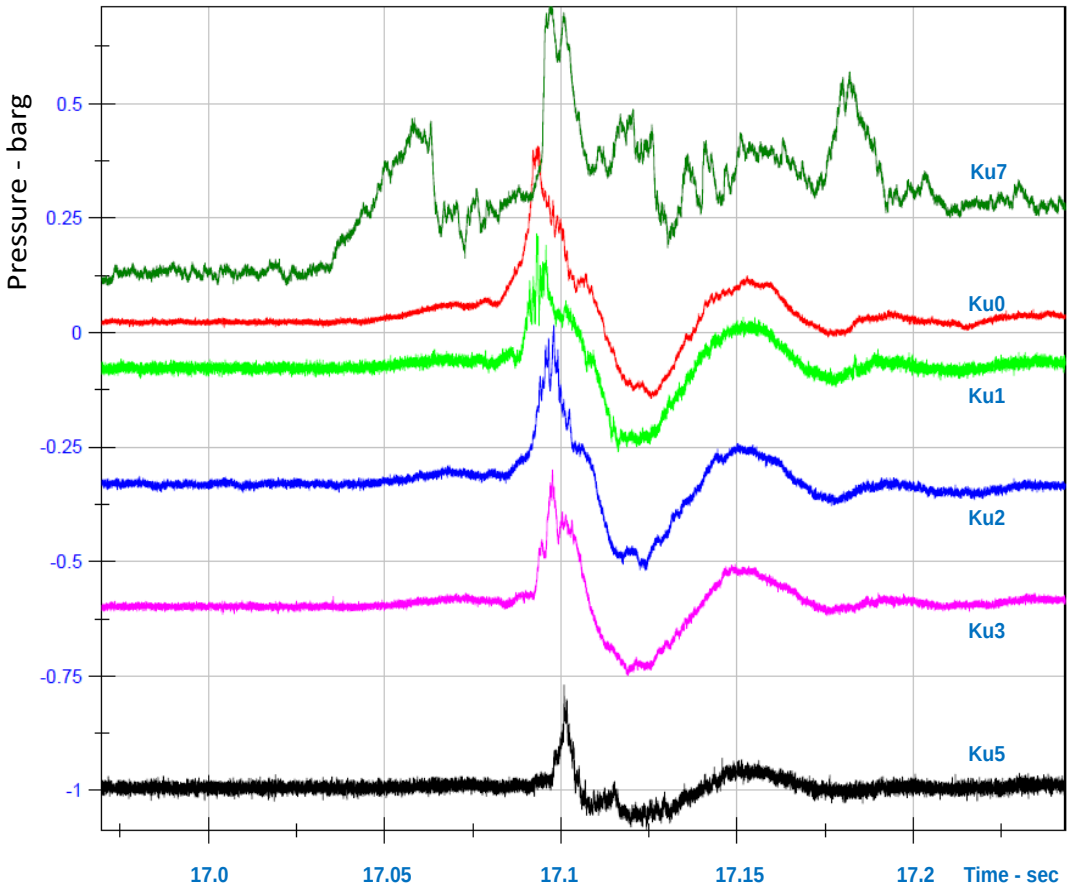

Figure 11: Pressure versus time at five pressure sensor positions for Test 3. Ku7 (within circular duct, 9.758m), Ku0 at heat exchanger (15.6m), Ku0 (16.58m), Ku2 (16.985m), Ku3 (18.775m) and Ku5 at HRSG exit (21.165m). ***Note - traces are offset in vertical direction for better clarity***

In moving downstream from the heat exchanger, Figure 11 shows that the subsequent sensors have pressure amplitudes of 0.316 barg (Ku2), 0.290 barg (Ku3) and 0.221 barg (Ku5). The timescale between the peak on Ku0 and Ku5 at the HRSG exit is around 8 msec corresponding to the sound transit time of the pulse created around the heat exchanger. This transit distance is 5.7m and since the flame speed is around 150m/s downstream of the heat exchanger, the flame will have travelled around 1.2 m in this time. It can be seen from the width of the pressure trace for Ku0 that the pressure has dropped to around half of its peak value in this time interval, which in turn suggests that most of the combustion intensity has arisen close to the heat exchanger and that this level of intensity cannot be maintained as the flame moves into less turbulent gas. The

decrease in pressure amplitude of the sensors moving downstream is consistent with pressure loss effects due to gas being driven along the HRSG. As with most vented gas explosions, the gas momentum continues to take gas out of the HRSG exit even when the pressure is at atmospheric, leading to a negative pressure in the chamber. This can be seen on all four of the sensors Ku0 - Ku5 and also that the pressure returns to a value close to atmospheric due to the small frictional pressure losses downstream associated with the steady combustion flow following the ignition event. For the upstream location at Ku7, the final steady pressure is above the initial value due to the pressure drop through the heat exchanger for this same steady flow.

The pressure behaviour for tests with the end plate of the HRSG in place and with the exhaust being directed through a vertical chimney can be examined in a similar way as for the open case. Test 7 is used as an example, in a similar way to Test 3 and Figure 10. Thus Figure 12 below shows the pressure recorded on Ku7 in the circular duct as well as the IP10 flame sensor at the heat exchanger. The behaviour is very similar for this case as before and the discussion is the same as for the open Test 3 case. In this case the time interval between IP10 and the middle of the second maximum on Ku7 is 8.2 msec as shown.

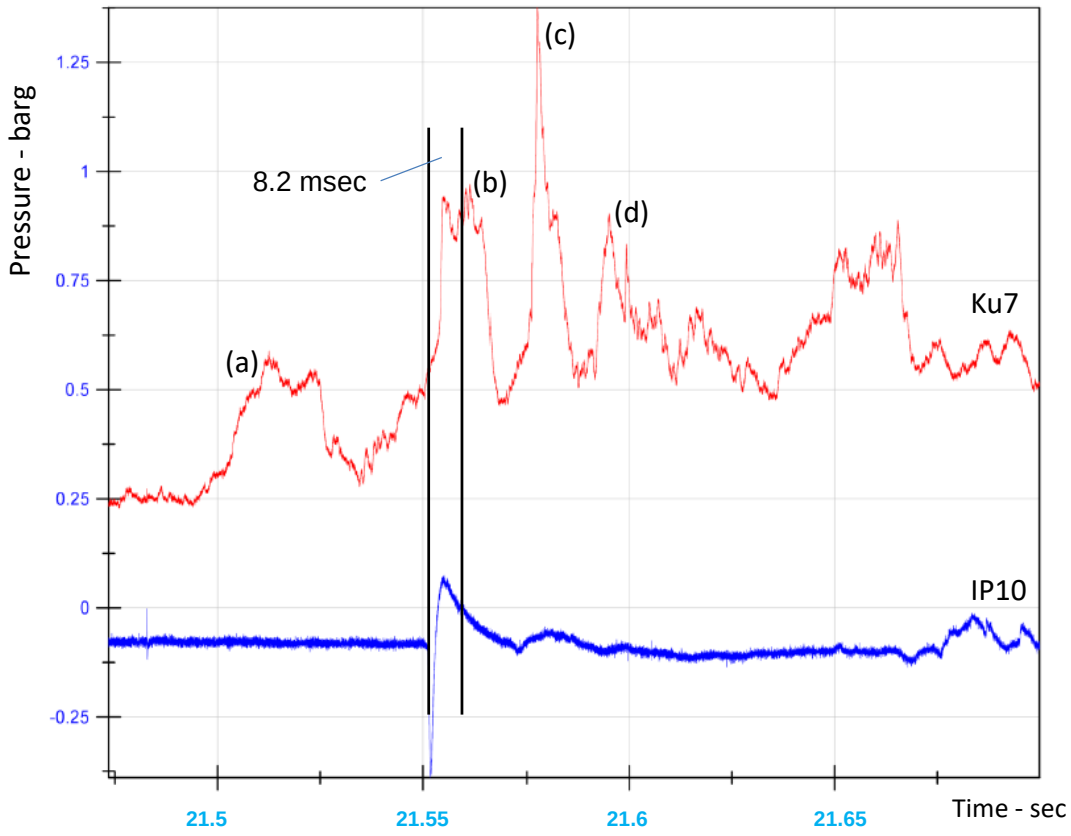

Figure 12: Traces of pressure at Ku7 near exit of the circular duct and flame arrival on IP10 located on central panel of heat exchanger.

Again, looking at the pressure sensors around the heat exchanger and downstream toward the end plate, these can be seen in Figure 13. Ku0 is the pressure at the heat exchanger and this shows two peaks, with a time separation of 20 msec. The first peak has an amplitude of 0.5 barg. This can be interpreted as the source pressure wave due

to vigorous combustion around the heat exchanger, whilst the second peak is the reflection of this wave from the end plate, arriving back 20 msec later. The round trip distance is 11.46 m providing an average sound speed of 573 m/s. This is consistent with an exhaust temperature of close to 500^{o}C, which is known to be the exit gas temperature from the gas turbine engine. Looking at the peaks associated with the other downstream pressure sensors (0.6 barg (Ku2), 0.4 barg (Ku3) and 0.8 barg (Ku5)), it can be seen that the separation between the incident and reflected pulses reduces as the round trip distance decreases. Due to the finite width of the pressure pulse, the reflected wave in the vicinity of Ku5 close to the end plate arises while the pressure here is still high, with the result that Ku5 shows a doubling of the local pressure. The finite width of the pressure pulse has been discussed in connection with Test 3 and therefore the doubling of pressure locally is only likely to arise in the region close to the end plate wall as a consequence. It is for this reason that a separate column has been allocated to Ku5 in Table 5.

Referring back to Figure 12, it can be seen that in addition to peaks (a) and (b), where (b) is due to the pressure wave originating at the heat exchanger and propagating back up to Ku7, there is also a peak (c), occurring 17.5 msec later. The most likely explanation for this peak is due to the end plate reflected wave returning to Ku7. This reflected wave adds a further 11.46 m to the round trip distance, and based on an average gas temperature of 725 ^{o}C, since some gas is turbine exhaust and some is burnt gas, this leads to an additional time delay of 17.1 msec. An additional peak (d) can be seen on the trace, which occurs a further 17.2 msec after peak (c). This may be due to a further partial reflection from the heat exchanger array of the returning wave, which then undergoes a second round trip off the end plate.

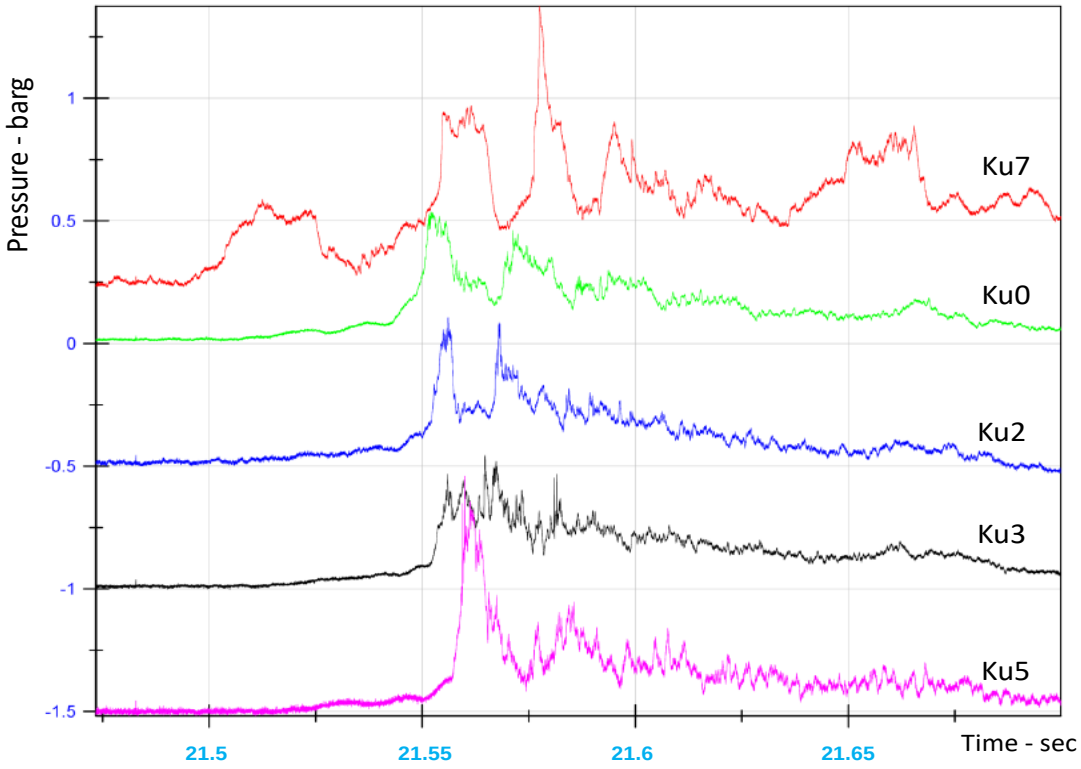

Figure 13: Pressure versus time at five pressure sensor positions for Test 7. Ku7 (within circular duct, 9.758m), Ku0 at heat exchanger (15.6m), Ku2 (16.985m), Ku3 (18.775m) and Ku5 at HRSG exit (21.165m). *[Note: traces are offset in vertical direction for better clarity].*

The behaviour of the further ignition tests up to Test 8 involving H_2/CH_4 mixtures, with regard to pressure development, was found to be closely similar to the two tests discussed above. The first two tests involving pure hydrogen also followed a similar behaviour but it was found that for Test 12, using pure hydrogen with an EQR of 0.55, the behaviour was slightly different. Figure 14 below shows the traces for Ku7, Ku0 and OP4 in a similar way as the graphs above. The main difference to observe is that peak (a) for Ku7 does not show a drop when the flame passes out of the circular duct, as was discussed for Test 3. The interpretation here is that the flame intensity is maintained as the flame passes into the expansion section.

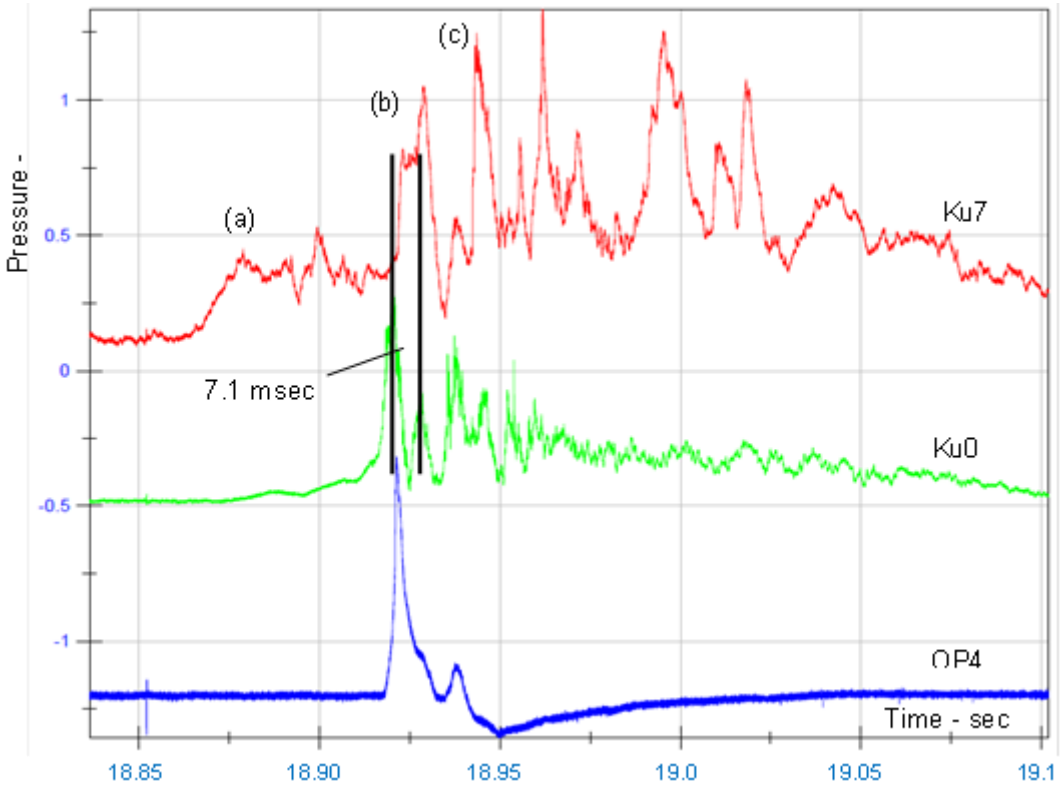

Figure 14: For Test 12, traces of pressure at Ku7 near exit of the circular duct, Ku0 around the heat exchanger and flame arrival on OP4 located on central panel of heat exchanger.

The subsequent pressure peaks (b&c) on Ku7 behave in a similar way as previously discussed and their timings are consistent with the reasoning previously provided.

It should also be noted that the video record for this test, which resolves frames with 0.33 msec resolution, shows that the flame development has more than a single phase in the vicinity of the heat exchanger, and the additional intermediate pressure peaks, for example on Ku0 at 18.925 sec, may be the result of a surge in the combustion at this time point.

Tests 13 - 17 relate to those with H_2/CO mixtures. The main features described for Test 7 above can also be seen for these later tests. For example, Test 13 (EQR 0.51) shows the typical rise in pressure to ~ 0.3 barg within the circular duct (Ku7) and on this occasion this pressure again decreases as the flame enters the expansion section, where previously for pure H_2 this pressure was maintained. As with other cases, the peak at the heat exchanger shown on Ku0 (0.46 barg), coincides with the peak on optical sensor OP3 within the heat exchanger, and appears as a second peak on Ku7 ~ 7 msec later. A second peak on Ku0 arrives ~20 msec later following end wall reflection and this interval is closely similar to that found in the other cases referred to above. The sensor Ku3 (18775 mm) has a round trip distance to the end plate of 5110 mm and this corresponds to 8.8 msec, based on sound speed calculated from the Ku0 peaks. Since the pulse half width for Ku0 is around 9.5 msec, the pressure trace on Ku3 shows only a single broad peak since the reflection arrives on the decaying side of the outgoing Ku3 pressure wave. For Ku2 (20575 mm) the reflected wave is well within the pulse width and a single larger amplitude wave (0.6 barg) can be seen at this sensor position with a

width similar to that of the source pressure wave at Ku0. Ku5, being at the end plate, shows similar doubling and pulse width behaviour.

Test 16 (EQR 0.59) shows closely similar behaviour to that of Test 13 and a similar description would apply in this case.

Test 17 has the largest EQR (0.62) and the pulse timings are found to be very similar to those discussed above. An important difference exists with this case however, in that the combustion in the heat exchanger region exhibits a twin surge in intensity. This is firstly evident in the optical sensor trace from OP3 within the heat exchanger, which shows a double peak with separation of around 4 msec. This double peak is not evident on the pressure trace of Ku0 within the heat exchanger but is clearly resolved at Ku3 (18775 mm) where the peak time separation is the same as for OP3. The pressure doubling behaviour discussed above for Ku2 (20575 mm) and Ku5 (21165 mm) is also present for this case, but now appears as a double peak due to the twin incident pulses.

6.6 REVIEW AND ANALYSIS OF EXHAUST FLOW VELOCITY DATA

Two sets of velocity measurements were made as part of the test programme. In one case pitot-static probe measurements were made across the full width of the 600 mm diameter duct at a distance of 250 mm from the beginning of the fourth section of duct. These profiles were measured in the main after or during each test. In the second case LDA measurements were made of the velocity profiles and turbulence intensities across the rectangular approach section to the tube bank. These measurements were made at five different vertical heights. A further set of LDA measurements were also made across the duct in the fourth duct section.

6.6.1 Duct velocity profiles using P-S probe

The duct velocity profiles differed from those made previously during the WP 2.2 test phase in that they covered the full width of the duct; a new traversing mechanism having being obtained specifically for this purpose. The profiles were measured after a new pepper-pot type orifice plate had been installed. This appeared to have improved the symmetry of the profiles significantly as can be seen from a typical profile shown in Figure 15 below, and taken from the commissioning report (4). As explained previously the velocity and temperature profiles obtained from these traverses were used to calculate the exhaust mass flow rate for each test, and hence the required fuel and oxygen injection rates for the tests.

Due to the relative simplicity of the confinement the impact of combustion on the flow patterns is unlikely to significantly affect the qualitative character of these results.

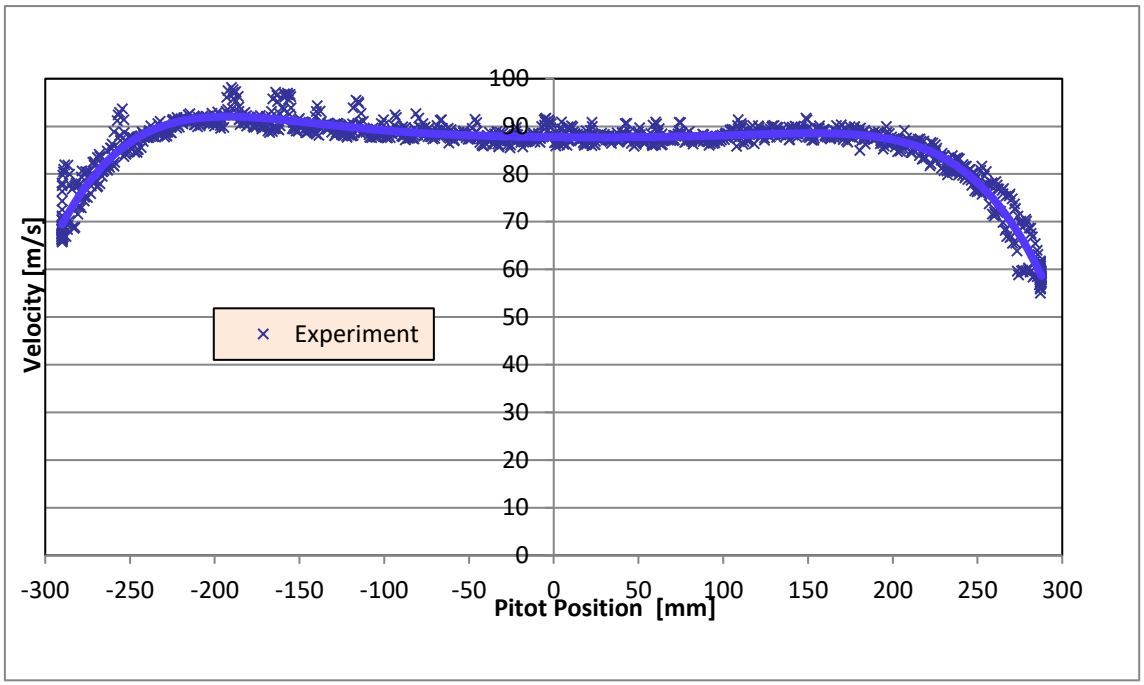

Figure 15: Velocity traverse across section four of the duct after HRSG was installed.

6.6.2 Velocity profiles across HRSG entrance using LDA

A set of five horizontal LDA traverses were made across the entry section to the tube bank, using the system described in Appendix 12.5.8, the results from which are shown in Appendices 12.8, including a set of velocity vectors derived from the original results 12.8.1 to 12.8.10. It should be noted that the LDA system was only able to traverse about one metre across from one side of the rig instead of across the full 1.4 metre width of the rig. The reason for this is given in Appendix 12.5.8.

There was evidence of highly unstable and turbulent flow regions near the beginning of the traverses, but which were not apparent once the flow had settled down away from the wall region. In an effort to establish if there was anything unusual occurring in those regions not traversed by the LDA system, a series of pitot traverses were made using a two metre long pitot-static probe supplied by Kimo UK. Although these measurements could only be regarded as indicative due to the difficulty of aligning the probe in the flow direction, they did show that there was nothing unusual in the flow patterns existing in these regions, when compared with the LDA results. Thus indicating some degree of symmetry about the flow if somewhat skewed from the centreline. The velocity results (represented by position 15 on the accompanying data sheets) show that low down the horizontal velocity component dominates the flow but at progressively higher positions the vertical component dominates. The peak centreline horizontal velocity at the first measuring position is around 32 m/s dropping to around -2 to -6 m/s at the third and fourth measuring positions before picking up slightly too around 6 m/s at the uppermost position. Whilst the centreline vertical component varies from 11 m/s at the lowest position to -9 m/s at the top position dropping to around 3 m/s in the central positions. This is interpreted as showing the existence of a recirculation flow zone or zones towards the middle and top of the duct expansion zone and which is in broad agreement with the

CFD predictions shown in the commissioning report (4). The derived velocity vectors also support this conclusion, where the centreline velocities vary from 35, 5, 3, 6, and 11 m/s, as measured from the bottom to the top, with the vector angle varying from 20 degrees to -55 degrees when measured on the centreline from bottom to top.

The measured centreline turbulence intensities are more difficult to interpret as they vary from 35, 200, -280, -100 to 80% in the horizontal direction when measured from the bottom to the top, whilst the vertical measurements vary from 56, 100, 220, 240 to -70% bottom to top. These are consistent with the general flow pattern in this region where the flow is changing from jet type behaviour near the base of the heat exchanger entrance to one of a recirculation flow regime towards the middle and top of the heat exchanger entry. It should also be noted that obtaining mathematically meaningful turbulence levels in what is a separated flow region in the upper section of the HRSG entry region is difficult due to the near zero velocities together with the flow reversals that are occurring in this region. Consequently very high values should be discarded as meaningless or not representative. In addition the flow structure is likely to be significantly modified when the flow becomes dominated by the expanding combustion flow progressing at different velocities through this section of the HRSG.

6.6.3 Velocity profile across 600 mm diameter duct using LDA

These measurements were made to re-measure the turbulence levels in particular as a consequence of a change in the design of the orifice plate used for the WP 2.3 test programme. The measurements were made over three different days due to engine fuel pump problems; this in itself was not a problem as the turbulence measurements were consistent across the duct, although there was some small variation in the velocity profile due to small changes in the engine running conditions. The three sets of data were amalgamated into a full set by post processing.

The tabulated results from the horizontal LDA traverses across the fourth section of the duct, some 250 mm from the beginning of the section are shown in Appendix 12.9, together with a description of the LDA equipment. This equipment was virtually the same as that used previously for the HRSG entrance measurements except for using a different focal length lens. The full set of data consists of a series of measurements at discreet locations across the diameter of the duct from -290 mm to +290 mm, with higher spatial density at the two radial extents near the boundary layers.

The measured velocity profile is shown in Figure 16 and the RMS profile in Figure 17 below and a direct comparison with the Pitot traverse results in Figure 18.

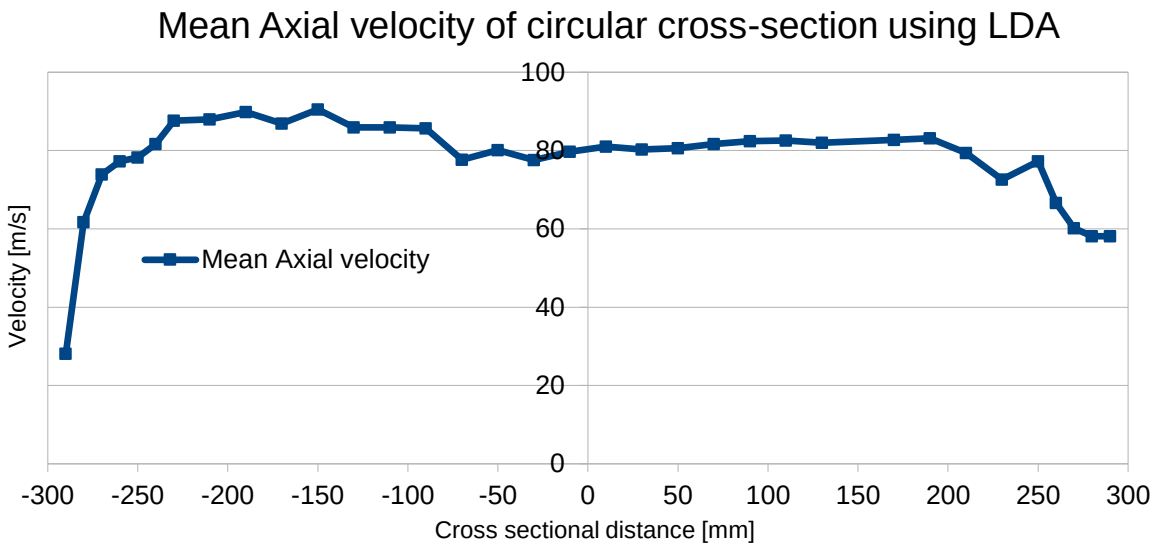

Figure 16: Amalgamated Mean Axial Velocity data of circular cross-section

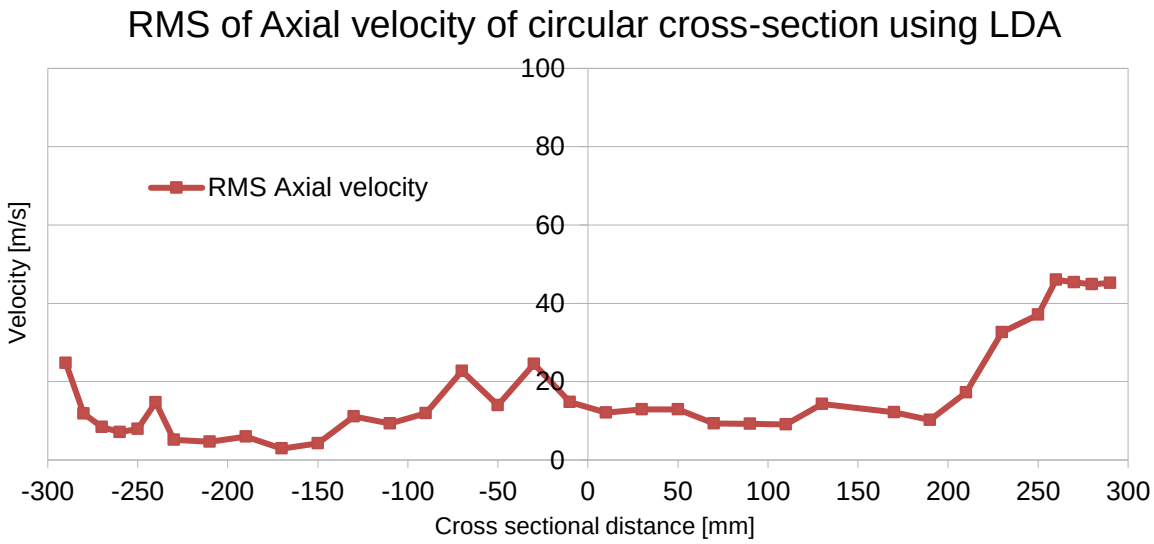

Figure 17: Amalgamated RMS velocity data of circular cross-section

The mean velocity is around 80 m/s deviating to between 30 to 60 m/s in the boundary layers and is in very good agreement with the velocity profile measured previously by pitot tube as illustrated below. Both the LDA and the Pitot measurements show the velocity being slightly higher along the negative radius which is the side close to the measurement window.

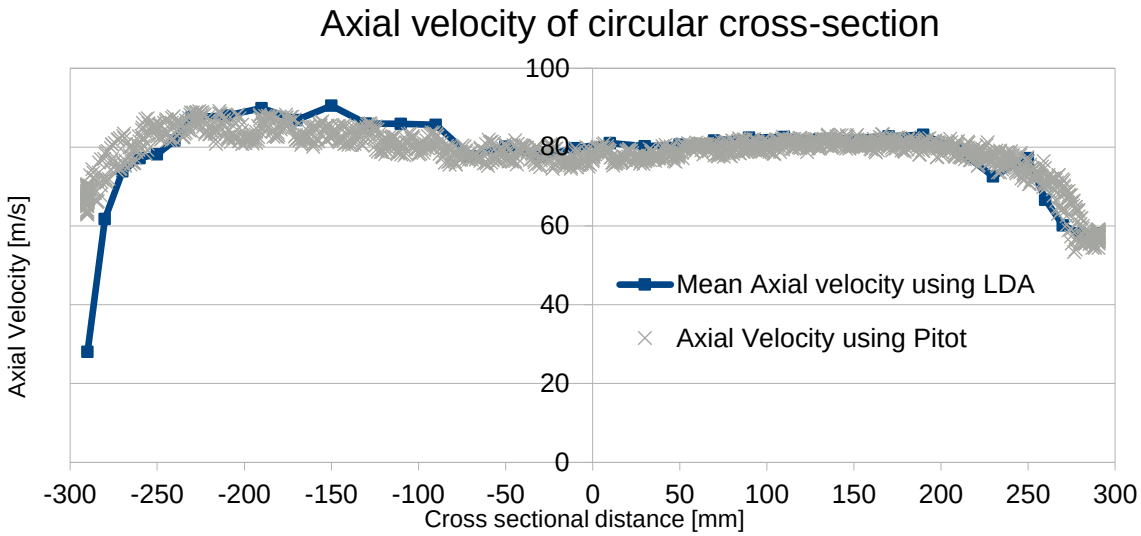

Figure 18: LDA measurements vs pitot tube measurements

The parameter of most interest is the ratio of the RMS to mean velocity or turbulence intensity which is shown below and this can be seen to be in the region of approximately 10-15% and as expected it increases to around 80 to 90% in the boundary layers.

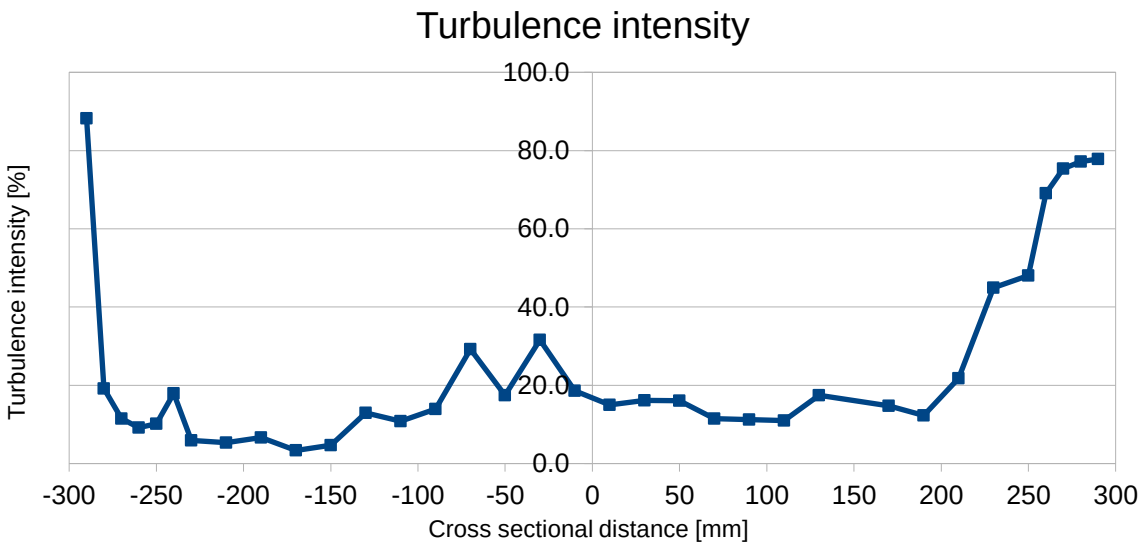

Figure 19: Turbulence intensity using LDA data across circular cross-section

The values themselves are very similar to those measured previously in WP 2.2 for the same velocity. It was therefore concluded that the change in orifice plate design made little or no difference to the turbulence levels in the flow, and by inference the turbulence generating grid downstream of the orifice plate would appear to be the main component governing the turbulence levels.

6.7 REVIEW AND ANALYSIS OF HIGH SPEED VIDEO DATA

Video records were produced for all of the successfully completed tests. In all cases the high-speed video camera was positioned to view the flame front emerging from the

HRSG tube bundle using a framing rate of 3000 fps. A 150 mm diameter quartz glass viewing port positioned on the centreline of the HRSG was used to view the tests when the end plate was in position. Those tests when the end plate was not in position were viewed with the camera mounted on the centreline of the end plate but with the end plate fixed some six metres downstream from the end of the HRSG. For the majority of the tests, which had the end plate attached to the HRSG, a wide angled lens was used in an effort to capture the flame front movement from the tube bundle up to the end wall and out through the exit stack. All of the video recordings were taken using colour.

Copies of all of the video records are included in the data package provided to the ETI as part of milestone 10.

The emission intensity for the different gas mixtures was different due both to mixture content and EQR used. In all cases the emergence of the flame front from the tube bank could be seen as it illuminated the exit of the tube bundle array. Against this emission could also be seen a degree of chaotic flow on the downstream side of the tube bundle due to the turbulence generated and the subsequent dispersion in the void downstream of the tube bundle. The apparent energy of the flame propagation event was qualitatively consistent with the peak pressures observed in each case. For example, the CH_4/H_2 mixture at an EQR of 0.60 produced the fastest flame event and also the greatest emission level. The colour video indicated clearly that the flame emission was not uniform across the rectangular cross-section of the HRSG, and also that the flame emerged from the congestion in an asymmetrical manner, with the lower region of the tube bundle showing the body of the flame front emerging from there first.

This is likely to be due to the flame path length from the circular duct exit being shorter to the bottom of the heat exchanger than to the top. The flame emergence from the heat exchanger then progressively moves toward the top of the tube bundle and the overall flame can then be seen moving toward the exit, whilst maintaining the original angled profile. This can be expected to generate a progressive rise on the optical sensor signals looking downwards rather that a sudden transition due to a flame normal to the HRSG axis. Flame speed downstream of the congestion could also be deduced semi-quantitatively from the video record.

There was also a good indication from the video that the flame weakened and slowed down considerably before it reached the exit of the HRSG be that the open end or through the vertical stack. This may be consistent with the turbulence decaying soon after the heat exchanger. It is noted that the main mechanism for flame acceleration through the heat exchanger is flame- area enhancement associated with 'flame folding' caused by the presence of the tubes. Once the flame leaves the tube section this mechanism is no longer available and the only mechanism available to sustain the flame intensity is turbulence, which decays with axial distance.

For the weaker tests it was likely that the decay of the flame towards the exit resulted in a loss of signal strength from the OPs and IPs as was usually found to be the case for these types of sensors. Overall the video records have a value in confirming the other parameters measured in the tests, as well as having the ability to reveal any anomalous behaviour in flame development and propagation.

The main purpose of the high speed video record was to support the interpretation of the combustion wave as it progressed through the system, and to provide some correlation

between flame behaviour as seen on the flame and pressure sensors with any physical observations within the HRSG, noting that this may also include the apparent absence of a strong flame signature.

A number of examples of such correlations are provided below covering the main mixture groups and the open/closed end conditions.

6.7.1 HRSG with open end

Test 5 provides a useful example for comparing the high speed data with some of the features of the high speed video record. The video is recorded at 3000 fps and features of interest include the first emergence of flame from the tube bundle and its arrival at various internal landmarks, such as the section boundaries, which can be visually identified from the video.

Table 10 below picks out a few of these features. Times on the sensor data files are in seconds, whilst those from the video files, the millisecond part of the clock timer are to one decimal place. These timings are evident within their respective data files. The time points for flame emergence from the tube bundle and its arrival at the end of sections 4 and 5 are identified from the video record, which allows an approximate flame velocity to be estimated for these. Table 7 has already calculated these values from the data files and these are included for comparison, which can be seen to be reasonable/good. Another interesting feature of the video files, when they are examined closely is the progress of a 'wave' along the HRSG walls. This can eventually be identified as steam condensation when the wave finally emerges at the exit. The time for this in the video file is noted in

Table 10. Closer inspection reveals that a second wave follows the first and this exits a short time later, and is shown to be 1.6 msec. This is shown in a snapshot picture in Figure 20.

Table 10: Some event timings from data and video files for HRSG Test 5

Sensor data	sec	msec	Velocity (m/s)
IP10 transition (centre of heat exchanger)	18.276		
Time for 1st peak on Ku5 (HRSG exit)	18.2849		
Time for 2nd peak on Ku5	18.2866		
Time interval between Ku5 peaks		1.7	
Section 4 average flame velocity (Table 7)			219
Section 5 average flame velocity (Table 7)			179
Video data			
First flame emerges at floor of lower half		392.7	
Flame arrives at end of 4th section		399.4	
Approx. flame velocity across section 4			224
First wave of steam appears at exit		398.4	
Second wave of steam appears at exit		401.0	
Time interval between 1st - 2nd steam wave exits		1.6	
Flame arrives at end of 4th section		399.4	
Flame arrives at end of 5th section		409.4	
Approx. flame velocity across sections 5			150
Flame emerges from HRSG exit		425.0	

The wall temperatures of the HRSG remain cool during a typical test, and by inspection after the test, these are around 40 °C in the sections after the heat exchanger, which runs much hotter due to the turbulent heat transfer in this region. Previous analysis of the exhaust gas composition indicates that the water vapour content of the exhaust is around 40 mbar at an overall ambient pressure. Steam tables indicate that condensation at a temperature of 40 °C requires absolute vapour pressures of around 80 mbar, i.e. around twice the exhaust vapour pressure at overall atmospheric pressure. This indicates that overall pressures of around 1 bar gauge (2 bara) are required to produce condensation at these steam compositions and wall temperatures. Referring to the pressure data for this case shows that Ku5 at the end of the HRSG records two pressure peaks arising from the combustion around the HRSG and these are around 0.9 barg. The peaks also show a time separation of 1.7 msec as

Table 10 shows, which is consistent with the wave separation from the video and implies that the propagation of these pressure waves are followed soon after by corresponding condensation waves.

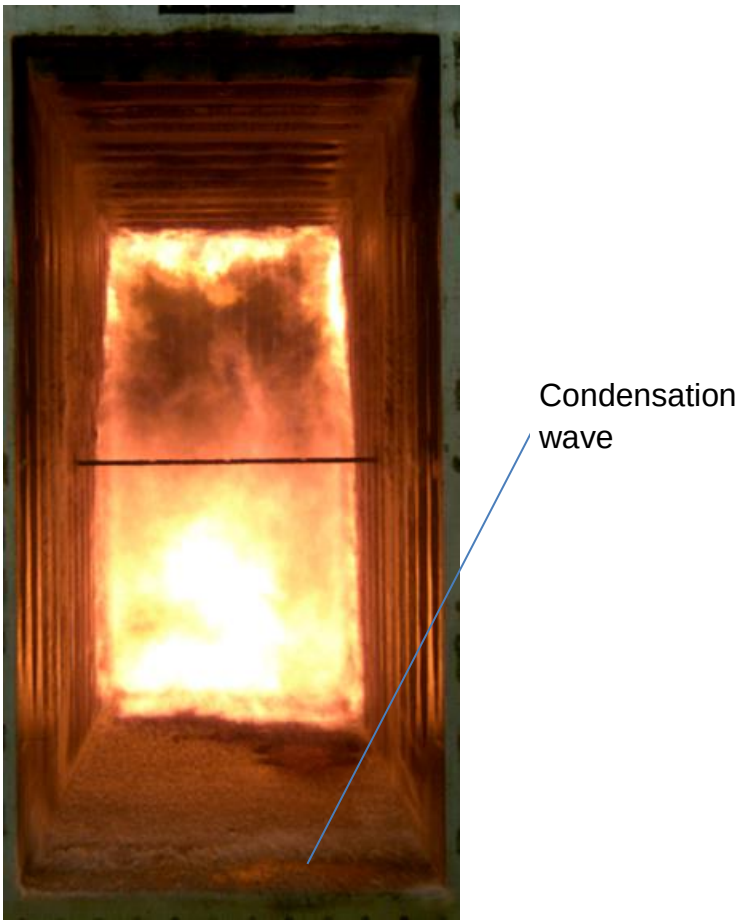

Figure 20: HRSG Test 5 - indication of condensation wave following propagation of pressure wave at 401.0 msec.

It should be noted that for the lower EQR cases using an open ended HRSG, the peak pressures are lower and the same condensation wave behaviour is not shown in the video records. The video record shows that after around 33 msec, there is evidence of flame emerging from the exit of the HRSG and this provides an overall average velocity from the heat exchanger to the exit of ~ 45 m/s.

6.7.2 HRSG with closed end

The video record for the closed end tests shows a number of important differences from the open-end cases. The pressure behaviour has already been discussed in Section 8.5 and this plays a key part in the appearance of the flame development during the time after emergence of the flame from the heat exchanger.

In general, the behaviour of the flame following its emergence from the heat exchanger shows a similar pattern for all of the closed end cases. Initially the flame can be seen appearing around the lower half of the exchanger. This grows in radiation intensity whilst the flame progresses upwards and outwards and normally fills the full height of the exchanger by the time the lower part of the flame has progressed to around 1m from the

exit point. Around this time the flame will have reached its maximum radiation intensity and may progress steadily towards the end of Section 4 of the HRSG. However, before this point is reached there is a noticeable faltering in the forward progress of the flame. This point is usually around 15 msec after flame emergence and, combined with the decreasing radiation emission, gives the appearance of a reversal in progress. Close examination of the video record shows that forward flame progress resumes soon after this reversal and faint flame traces appear to progress toward the exit plane, but at a much slower rate. The video record also shows that the flow downstream of the heat exchanger shows chaotic features, with random components of velocity in horizontal and vertical directions. Reference has been made to the difficulty of obtaining simple flame speeds in this downstream region due to this 'disturbed' flow behaviour and the video record has provided semi-quantitative information to aid this process. The discussion below shows how this record can be used to inform the pressure and flame progress events.

Table 11: Some event timings from data and video files for HRSG Test 8

Sensor data	sec	msec
IP10 transition (heat exchanger)	16.581	
Time for peak on Ku0 (Heat exchanger)	16.583	
Time for peak on Ku5 (end plate)	16.591	
Time interval between Ku0 and Ku5 peaks		7.9
Time for reflected peak on Ku3 (Section 4)	16.597	
Time interval between Ku5 and Ku3 reflected peaks		6.3
Video data		
First flame emerges at floor of lower half		45.5
Flame limiting position in section 4 (~ 1m)		~ 60
Condensation first appears at end plate		53.5
Time interval between flame appearance and first steam appearance at end plate		8
Width of reflected pressure wave		~ 2

Of particular interest are the pressure peaks on Ku0 (at the heat exchanger), Ku5 (end plate) and the reflected peak on Ku3 (Section 4). The times for these from the data file (in seconds) are shown in Table 11. It is noted that the interval between the peak pressure on Ku0 and the arrival of the associated pressure pulse at Ku5 is 7.9 msec, whilst the time for this reflected pulse to reappear on Ku3 is 6.9 msec. The video file gives an idea of the time point at which the maximum pressure arises around the heat exchanger region, which is taken to be 45.5 msec (from video time record) and a careful study of the record shows the sudden appearance of steam around the end plate at 53.5 msec. Therefore similar condensation behaviour is present in this case as for the higher pressure case of Test 5 discussed above. The peak pressure at Ku5 due to reflection in the end plate region is 1.63 barg, which is sufficient to produce condensation at the wall temperatures prevailing as discussed previously. It is noted that this condensation occurs 8 msec after the approximate peak pressure frame of the video record which is exactly consistent with the pressure pulse interval of 7.9 msec obtained from the data file for Ku0 and Ku5. A snapshot frame from the video record of this condensation event is shown in Figure 21.

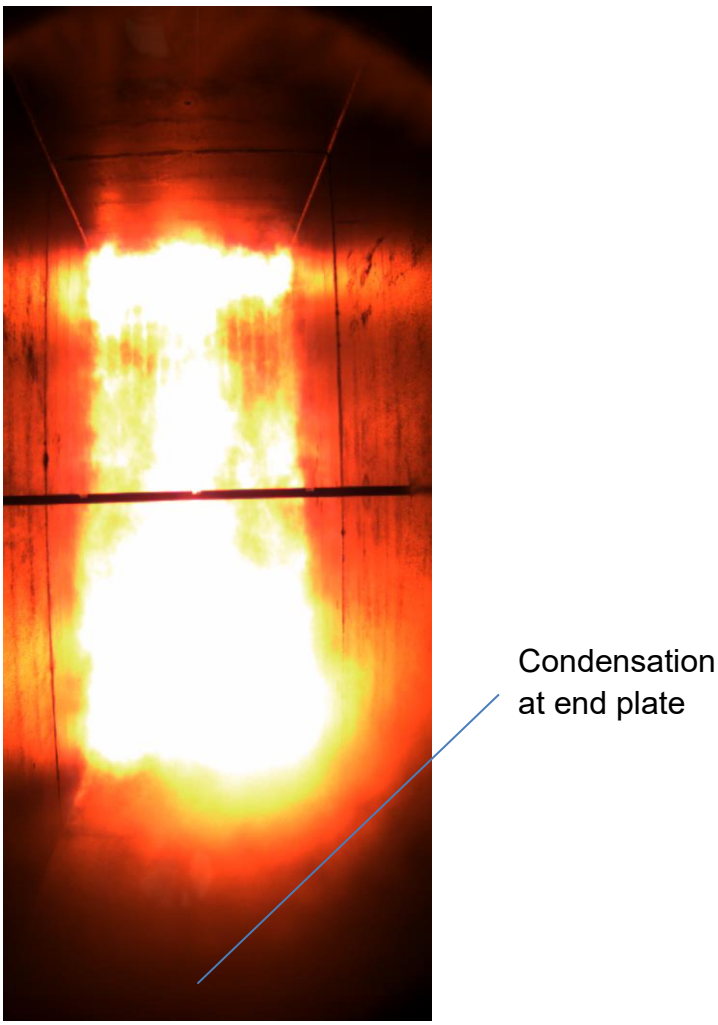

Figure 21: HRSG Test 8 - indication of condensation wave around end plate at 53.5 msec following propagation of pressure wave.

The behaviour of the flame progress for this case is different from that of the open cases and careful observation shows that, following emergence from the heat exchanger (45.5 msec) the visible flame progresses to a point within Section 4, which is around 1 m from the heat exchanger, at which point it falters and then retreats back upstream, at the same time losing its intensity. Unlike the open case, there is no visual evidence that the flame progresses as far as the end plate. Ku3 is the nearest pressure sensor to this limiting position and the time interval for the reflected pulse peak arriving back at Ku3 is indicated in Table 11 (6.3 msec). Also from the video file, there is a corresponding time interval between the end plate condensation appearance and the limit of progress of the flame front in Section 4 (60 - 53.5 msec), i.e. 6.5 msec. The reasonable conclusion would be that the reflected pressure pulse has had a significant effect in limiting the progress of the flame front along the HRSG.

The reflected pressure on Ku3 has a pulse width of around 3 msec. This wave will also have an associated shock velocity and gas flow velocity behind the shock directed upstream. The peak Ku3 reflected pulse pressure is between 1.7 - 2.2 bara and since this represents a pressure ratio of around 2 between the pressure ahead of the shock to

that behind the shock, from normal shock relations, this implies a shock Mach number of 1.37. Figure 22 captures the features of this dynamic event.

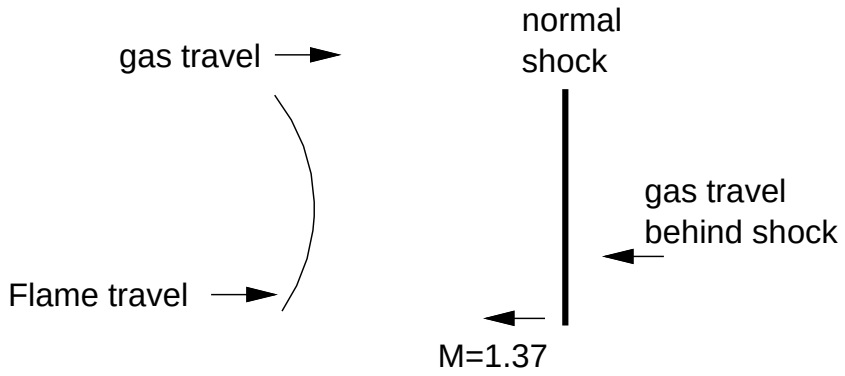

Figure 22: Configuration of flame, shock and post shock gas motions during shock/flame interaction.

Normal shock tables indicate that the post shock gas has a relative velocity of around 1.37 M- 0.75 M =~ 0.6 M. Since the sound speed in the exhaust gas is close to 600 m/s, this implies a relative gas velocity of 360 m/s, i.e. relative to the upstream gas velocity. Within a frame of reference where the HRSG is stationary and the exhaust gas is moving downstream at around 50 m/s, this implies that the gas behind the reflected pressure wave is moving upstream with a velocity of around 300 m/s for the duration of the pulse. This is suggestive of a 'blow out' scenario since the fuel rich gas in the downstream region is moving counter to the flame front during the wave transit and may be the reason behind the apparent flame suppression seen on the video files.

There is much literature on the effect of the reflected shock wave interacting with the flame. The global effect is to slow it down and this is usually followed by a re-acceleration when the reflected wave returns from reflection off the ignition end, or in this case the tube array. The velocity oscillation continues for a period of time . Each time the shock interacts with the flame it can lead to Rayleigh Taylor (RT) instabilities that can result in an increase in the local burning rate. For an open end the compression wave reaching the end of the channel will result in an expansion wave interacting with the flame that results in a global acceleration of the flame. This also results in the onset of RT instabilities on the flame and is well known from vented explosions (see FM Global recent publications, ref [Q])

The discussion below and the supporting sensor traces will show that there is a strong coupling between the pressure wave generation around the heat exchanger region and the arrival of the flame front at the same position due to increase in combustion intensity. The subsequent evolution of flame progress and pressure wave progress is then divergent, since flame speeds beyond the heat exchanger are much lower than those of pressure waves.

Table 12: Some event timings from data and video files for HRSG Test 12

Sensor data	sec	msec
OP4 transition (heat exchanger)	18.921	
Time for peak on Ku0 (Heat exchanger)	18.920	
Time for peak on Ku5 (end plate)	18.927	
Time interval between Ku0 and Ku5 peaks		7
Time for reflected peak on Ku3 (Section 4)	18.932	
Time interval between Ku5 and Ku3 reflected peaks		4.9
Video data		
First flame emerges at floor of lower half		926.7
Flame limiting position in section 4 (~ 1m)		939.4
Condensation first appears at end plate		934.7
Time interval between flame appearance and first steam appearance at end plate		8
Width of reflected pressure wave		~ 2.5

A second closed end case, Test 12 with 100% H2 and EQR of 0.55, has been reviewed in a similar way, see

Table 12. The behaviour is very similar to that of Test 8 for which the timing parameters are shown in Table 11. Once again, the video shows steam condensation around the end plate at a certain time interval after flame emergence from the heat exchanger (8 msec) and this corresponds with the interval between the Ku0 and Ku5 pressure peaks from the data file (7 msec). As for Test 8, the video shows a limiting extent of the flame travel from the heat exchanger exit of around 1m and this is around 4.7 msec after condensation appears at the end plate (939.4 - 934.7 msec). This time interval again coincides with that between the pressure peak at the end plate (Ku5) and the arrival of the reflected peak at Ku3, shown to be 4.9 msec. The pulse width of this peak is around 2.5 msec. Examination of the other pure hydrogen test cases shows similar behaviour and the reasoning discussed above for Test 12 can also be applied to these.

6.8 THE INFLUENCE OF THE HEAT EXCHANGER ON THE COMBUSTING FLOW

The heat exchanger initially acts as a partial blockage to flow from upstream. This means that as the combustion wave progresses downstream of the spark source, gas volume is generated through combustion temperature rise and the expulsion of this additional gas volume through the HRSG system requires upstream pressure. This pressure rises as the volume generation rate rises but will tend to fall again as the proportion of hot exhaust gas versus very hot combustion gas upstream of the heat exchanger tends to reduce due to exhaust expulsion through the heat exchanger. This can be seen in Figure 23 which shows the pressure on Ku7 near the end of the circular duct. The ionisation sensor IP0 at the end of the duct is also shown indicating when the flame exits the duct.

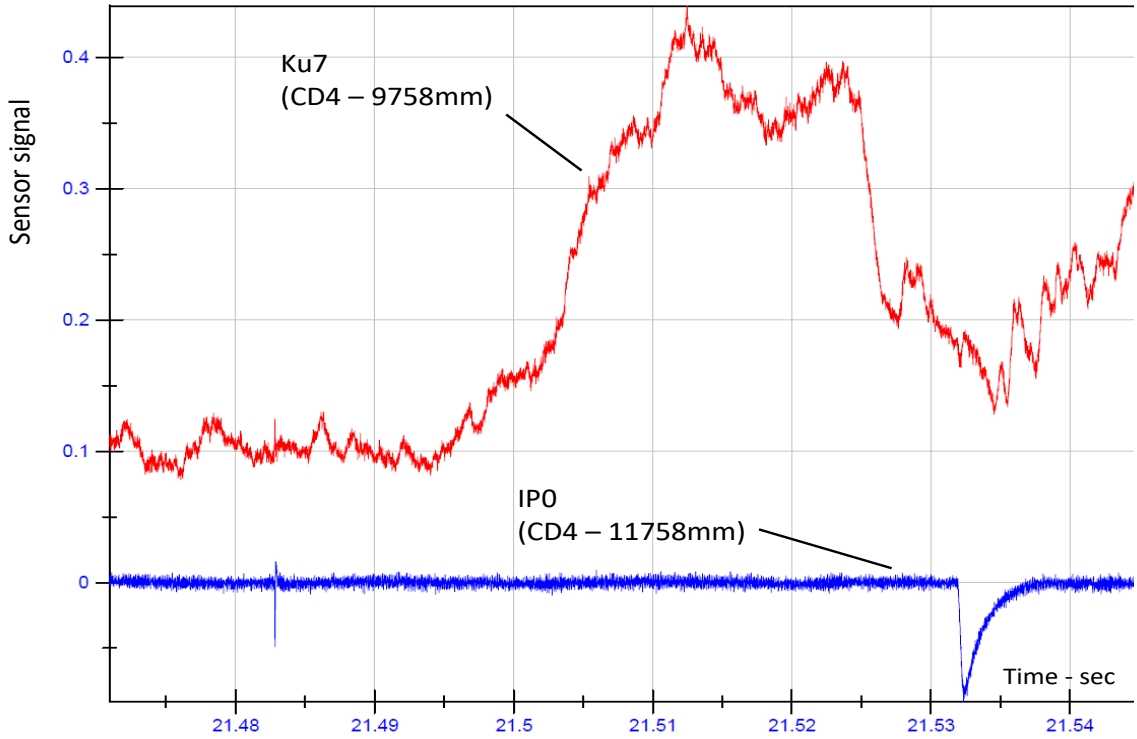

Figure 23: Pressure behaviour at Ku7 near the exit of the circular duct for HRSG Test 7, showing the rise due to volume generation upstream and subsequent fall as cooler exhaust gas is expelled from the system. IP0 shows the exit of flame from the end of the duct.

This figure shows the initial rise on Ku7 for the reasons mentioned, which in this case is around 0.3 barg, and the subsequent fall to a value which is smaller but finite. This rise of 0.3 barg is not the main pressure peak which the end of the circular duct experiences, due to combustion within the HRSG, but it is clear that even this initial pressure may be significant in terms of that which the system can tolerate.

The behaviour described above is found in all of the HRSG tests, with the only exception being Test 12, with 100% H_2, where the duct combustion rate is sufficient to maintain this Ku7 pressure after flame passage.

Referring to the main contribution of the heat exchanger, Figure 24 below emphasises the key part played by the heat exchanger in generating the accelerated combustion associated with the growth of the main pressure wave within the system. This case relates to the open HRSG Test 3 and shows the pressure growth at the centre of the heat exchanger on Ku0 as well as the timings of flame front passage in this region. IP7 is within Section 2, 1.5 m upstream, and it can be seen that pressure does not develop before the arrival of flame at this sensor. IP10 however, is a wall IP on the centre panel of the heat exchanger and its arrival is coincident with the pressure growth, and by assumption the flame acceleration.

This feature has been discussed in earlier sections regarding the transport of this pressure wave through the system and it can be seen again for this case that the width of the pulse is a few msec, which is consistent with the other cases tested, and also with those examined in the circular duct work. This finite pulse width has been interpreted as being due to the finite dimension of the strong turbulence field created by the heat exchanger tubes. This turbulence field is generated both by the steady state exhaust flow, which is around 6 m/s in the full HRSG chamber and around twice this value within the heat exchanger array, plus an additional flow produced by the volume generation of the approaching flame front. It is expected that the combustion intensity will decay as this turbulence field decays downstream of the heat exchanger and this is a useful subject for further numerical study in order to relate the time width of this pressure pulse with the turbulence decay behaviour.

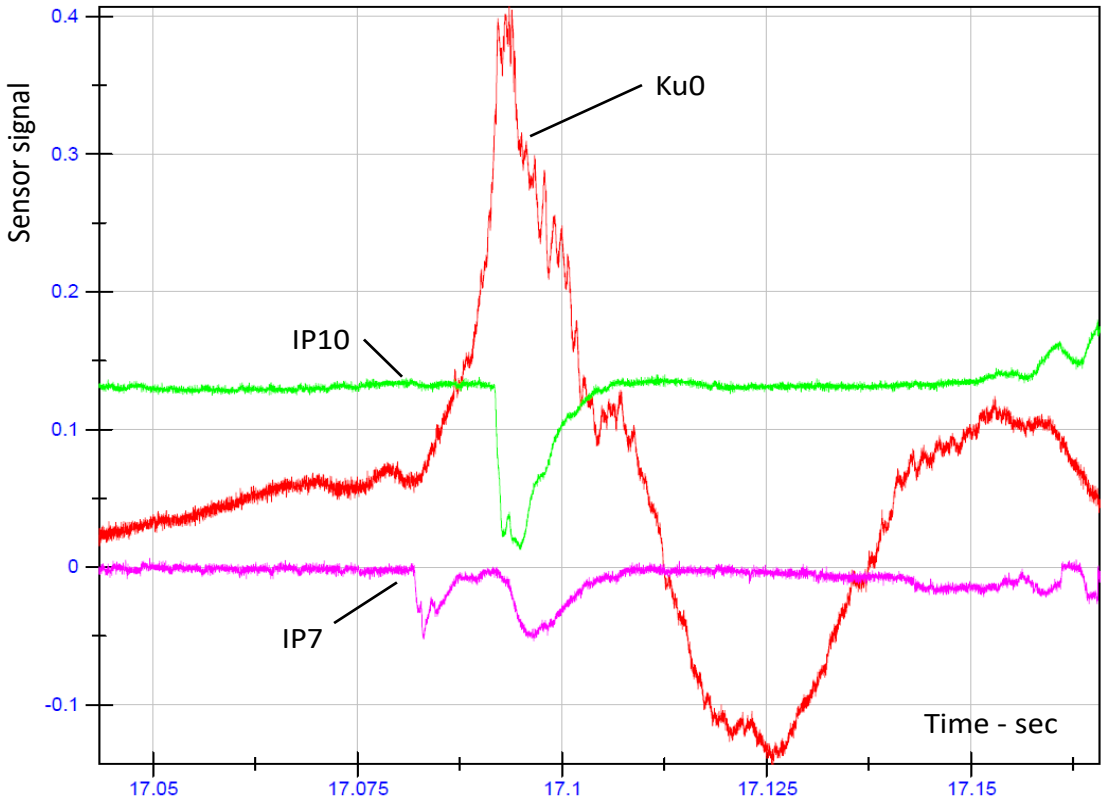

Figure 24: Indication of event timings for HRSG Test 3. Ku0 shows pressure growth in the region of the heat exchanger. IP7 shows flame passage at 1.5m upstream of heat exchanger and IP10 shows flame arrival at the centre of the heat exchanger

It is noted also that the behaviour shown in Figure 24 is manifested in all of the other test cases where useful sensor signals exist.

6.9 COMPARISONS BETWEEN ALL THREE WP 2 DATA SETS.

Section 6.5 discusses the origin of the peak pressure within the HRSG system and the timings of the subsequent wave propagation around the system. In that section it was proposed that the origin of the peak pressure was the accelerated combustion within and

just beyond the heat exchanger. This peak pressure should be independent of any other geometrical features within the HRSG since the pulse width is much narrower than the transit time to the first geometrical boundary, i.e. the end plate. This means that it should be possible to compare this peak pressure for both the open and closed end HRSG as well as the open ended circular duct cases, which is particularly useful when the mixture and EQR values are similar. It has been noted that the pressure pulse widths for the pressure originating around the HRSG are typically 5 msec. Reference can be made to the large number of test cases relating to the circular duct work and it will be seen that pulse widths in the vicinity of the obstacles are also around 5 msec. The interpretation in the latter case is likely to be similar to that previously referred to for the HRSG cases, i.e. that the most intense combustion is in the region at, and downstream of the obstacles, and with flame speeds around 200 - 250 m/s, the 'active' region appears to be around 1 - 1.5 m. Whilst it is less obvious in the HRSG tests, it is also evident that the pulse widths near the exit of the circular duct are narrower than those around the obstacles, which is consistent with expected pressure pulse behaviour.

The peak pressures referred to are compared in Table 13 below for the limited number of HRSG tests undertaken. To aid in the comparison of these cases, the pressures recorded in the immediate vicinity of the heat exchanger (obstacles for the circular duct) have been used. This relates to Ku2 for the HRSG and both Ku5 and Ku6 for the circular duct.

The first six HRSG tests have been paired up for comparison i.e. Tests 3 and 6, Tests 4 and 7 and Tests 5 and 8. The first member of the pair refers to an open ended HRSG (end plate OFF) and the second to the end plate and stack in place (end plate ON). Each of these pairs are otherwise operated under identical conditions of mixture and EQR and it can be seen that the peak pressures in the vicinity of the heat exchanger are very closely similar. This confirms the view that the source pressure wave in this region will be unaffected by upstream or downstream conditions at the time of its generation. The third member of each of these three groups relates to the corresponding case for the circular duct. The mixtures and EQRs are almost identical to those of their corresponding HRSG cases.

Comparing HRSG Tests 3/6 with circular duct Test 30 shows closely similar pulse pressures, although increasing the EQR appears to lead to a separation in behaviour for the next two paired Tests 4/7 with circular duct Test 39, the latter showing less intense combustion and a pulse pressure similar to its lower EQR case. This difference in behaviour is even more apparent for the last CH_4/H_2 case at EQR 0.65 (HRSG Tests 5/8) and circular duct Test 40. These features may be an indication of the relative differences in non-linear behaviour of pressure (i.e. combustion intensity) and EQR for the different geometry setups, where similarity exists at low EQR values but the divergences are more apparent as the non-linear regions are entered.

Two groups of tests are compared using pure hydrogen, i.e. HRSG Test 9 compared with circular duct test 42 and HRSG Tests 10 and 12 compared with circular duct Test 44.

HRSG Test 9 shows a comparable pulse pressure with circular duct test 44 given the slight differences in EQR values. HRSG Test 10 and circular duct Test 44 both show a significant increase in pulse pressure with only a small increase in EQR suggesting the

onset of non-linear behaviour and HRSG Test 12 is included here to show this trend with a doubling of pulse pressure when the EQR is increased by 0.04. Note that there is no corresponding circular duct test of this mixture with the same EQR.

It is noted that there is also an important geometrical difference between the HRSG and circular duct, which is that the flame arrives at the circular duct obstacles ideally as a flat flame perpendicular to the duct axis, whereas in the HRSG the flame arrives at the lower region of the obstacles first due to the orientation of the expansion section. In the HRSG, upward propagation of the flame is impeded due to the fins and horizontal progress meets less resistance. In both cases, the folding of the flow will enhance mixing in the horizontal plane.

Table 13: Comparison of pressure behaviour for similar HRSG and circular duct operating conditions.

Test	Mixture	Eq. Ratio	CH_4 (vol%)	CO (vol%)	H_2 (vol%)	Pressure at obstacles (barg)	End plate
HRSG test 3	CH_4/H_2	0.55	40	0	60	0.35 (Ku2)	OFF
HRSG test 6	CH_4/H_2	0.55	40	0	60	0.39 (Ku2)	ON
Circ duct test 30	CH_4/H_2	0.55	40	0	60	0.25 - 0.28 (Ku5/Ku6)	OPEN
HRSG test 4	CH_4/H_2	0.62	40	0	60	0.63 (Ku2)	OFF
HRSG test 7	CH_4/H_2	0.62	40	0	60	0.59 (Ku2)	ON
Circ duct test 39	CH_4/H_2	0.61	40	0	60	0.25 - 0.39 (Ku5/Ku6)	OPEN
HRSG test 5	CH_4/H_2	0.65	40	0	60	1.41 (Ku2)	OFF
HRSG test 8	CH_4/H_2	0.65	40	0	60	1.30 (Ku2)	ON
Circ duct test 40	CH_4/H_2	0.66	40	0	60	0.40 - 0.53 (Ku5/Ku6)	OPEN
HRSG test 9	H_2	0.47	0	0	100	0.39 (Ku2)	ON
Circ duct test 42	H_2	0.50	0	0	100	0.48 - 0.74 (Ku5/Ku6)	OPEN
HRSG test 10	H_2	0.51	0	0	100	0.92 (Ku2)	ON
Circ duct test 44	H_2	0.51	0	0	100	0.66 - 1.09 (Ku5/Ku6)	OPEN
HRSG test 12	H_2	0.55	0	0	100	1.79 (Ku2)	ON
HRSG test 13	CO/H_2	0.51	0	60	40	0.42	ON
Circ duct test 52	CO/H_2	0.5	0	60	40	0.43 -0.45 (Ku5/Ku6)	OPEN
HRSG test 15	CO/H_2	0.56	0	60	40	0.52	ON
HRSG test 16	CO/H_2	0.59	0	60	40	0.59	ON
HRSG test 17	CO/H_2	0.62	0	60	40	1.21	ON

The last comparison is for HRSG Test 13 and circular duct Test 52 using 40%H_2/60%CO. Note that only a single circular duct test was carried out using this ratio. In this case, where the EQR value is low and the pulse pressure is low, both cases show a similar pulse pressure. It is noted that the circular duct Test 42 for pure H_2 (EQR 0.5) shows a slightly more aggressive combustion than the corresponding Test 52 using H_2/CO mixture (EQR 0.5) and the three remaining H_2/CO HRSG Tests (15, 16 and 17) show less intensity than the corresponding pure H_2 Tests. However, for HRSG Test 17 there can again be seen a doubling of pulse pressure in changing from an EQR of 0.59 to 0.62, which is consistent with the onset of non-linear behaviour shown for pure H_2 (HRSG Test 12).

The results can also be compared with some of those from the extensive range of tests carried out under WP2.1. These tests were mainly carried out with EQR values of 0.8, and pressures for some of the tests were above or below 1 atm. However, the general conclusions were that dilution of hydrogen fuel with methane was significantly different in its reactivity compared with dilution by carbon monoxide. A recommendation of 40% hydrogen in methane was made based on the EQR of 0.8 tested. In the present HRSG work, although 60% hydrogen has been used in methane mixtures, these tests have been confined to the lower EQR values of 0.65. At these levels it has been observed that HRSG pressures (Ku2) have begun to 'take off' and this is consistent with the evidence from the WP2.1 shock tube study. Dilution of pure hydrogen with carbon monoxide was shown to be much more reactive than with methane, and for this reason, a 30% dilution maximum was recommended, again based on an EQR of 0.8. The present work has operated with hydrogen diluted carbon monoxide mixtures at a level of 40% hydrogen (60% carbon monoxide) but has confirmed the findings that such a mixture produces higher peak pressures than the corresponding methane case, being double at comparable EQR values.

Despite the differences in the turbulence generation structure of the HRSG compared to those used in the WP2.1 study, the reactivity differences revealed in the present work are consistent with the earlier results and reveal themselves when the peak pressures are compared from different mixtures at the same EQR due to the fact that the fluid dynamic behaviour experienced by each mixture is the same since, they each pass through the same geometry. An example of this would be the comparison between Tests 6, 12 and 15 at an EQR of 0.55 where peak pressures are 0.39, 1.79 and 0.52 barg for the CH_4/H_2, H_2 and CO/H_2 mixtures respectively.

6.10 EVALUATION OF RESULTS AND THE SAFE OPERATING MODES FOR $H_2/CH_4/CO$ MODEL FUEL MIXTURES

The previous WP 2.2 (Ref. 11) study was concerned with the combustion behaviour using 15 rows of congestion in the circular duct. One of the key outputs from this study was an indication of the limits of EQR for three compositions and based on two peak pressure criteria, i.e. 0.4 bar and 3.0 bar. The graphical output from this study capturing this limit behaviour is repeated in Figure 25 below.

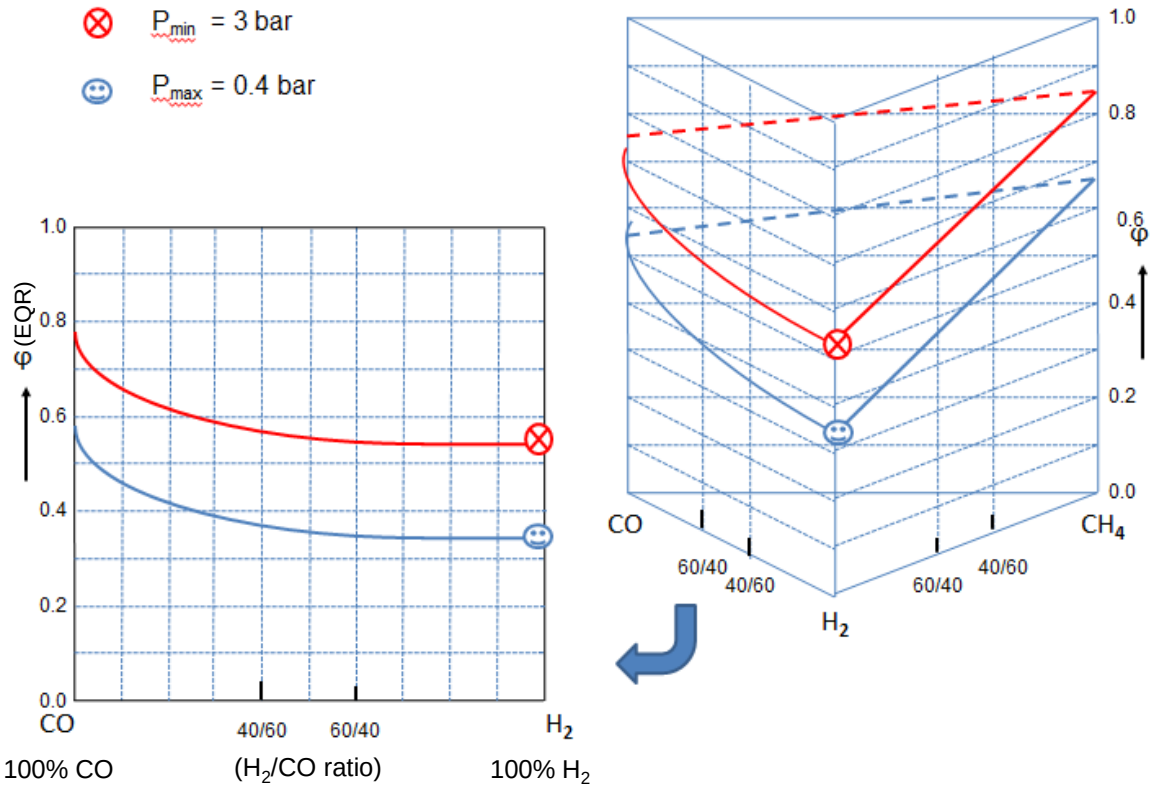

Figure 25: EQR limits based for $CH_4/H_2/CO$ mixtures on two peak pressure thresholds for combustion wave arising within circular duct with 15 rows of obstacles.

The circular duct was designed to withstand much higher pressures than would be observed in practice and it was possible to explore the transition to detonation behaviour as a function of EQR. This indicated that such a transition might occur over a narrow limit of the EQR parameter, e.g. 0.1, and indicated that care needed to be exercised in exploring this parameter in geometries with lower pressure tolerance.

The present phase of work has been concerned with similar limit behaviour arising from combustion wave propagation through the HRSG heat exchanger, and although a lesser number of experiments have been carried out for this system, it is desirable to be able to give an indication of where the safe limits are likely to lie. The circular duct was an open ended system and it has been shown in the discussion above that the end plate within the HRSG, leading to the vertical chimney, gives rise to more complex pressure wave behaviour. It is considered that this pressure transmission behaviour is understood both qualitatively and quantitatively, as the arguments above have shown, although the

interaction of the pressure waves involved with the combustion flame front have only a qualitative interpretation, based largely on the high speed video evidence.

Figure 6 has shown the peak pressure values arising on Ku0 within the heat exchanger for the three mixture combinations as a function of EQR for the limited number of tests carried out. Ku0 was chosen for Figure 6 due to the importance of this region as a source of pressure generation. Table 4 however, indicates that the pressure at Ku0 is not usually the highest within the system due to the various geometrical factors associated with the HRSG, e.g. pressure wave sharpening, wave reflection at the end plate and wave compression through the expansion/reduction section. The highest pressures are usually associated with the transient end plate reflection, where the pressure can double during the period of overlap of the incident and reflected waves at this plate, as has been previously discussed. Referring to Table 4, these pressures at Ku5 have been presented graphically for each of the three mixtures in Figure 26, Figure 27 and Figure 28. Although the number of points in each case is limited, there is some indication of non-linear behaviour, suggesting a 'take-off' point for pressure above a narrow range of EQR.

It is understood that the pressure limits tolerable for industrial size HRSG equipment is likely to be below 1 barg and therefore also incorporated in the figures are approximate EQR limits corresponding to 1 barg and 0.5 barg. It is emphasised that these limits are approximate due to the limited number of data points, and also ignore possible scatter in the data, which is particularly evident in the H_2/CO figure. Reproducibility of test result pressures has not been explored in this series of tests and these are most likely to be at their most sensitive at the lower combustion limits and upper 'take-off' points. A further observation on this point is that combustion limits are almost always quoted for ambient temperature and pressure. Since both parameters have an effect on chemical reaction rates, i.e. temperature via rate constants and pressure via molecular density, then the usual limits are unlikely to apply for the conditions within the HRSG, where exhaust temperature (in K) is around 2.5 times normal room temperature, resulting in a corresponding density reduction at the atmospheric conditions applying.

As a summary of the limits extracted from the graphs, Table 14 provides the numerical values for each mixture.

Table 14: Approximate EQR limit ranges for two peak pressure limits taken from Figure 26 - Figure 28 at each mixture condition

Mixture	EQR Limit (0.5 barg)	EQR Limit (1.0 barg)
60% H_2 / 40% CH_4	0.49	0.62
100% H_2	0.47	0.51
40% H_2 / 60% CO	0.51	0.59

These numerical limits are generally in line with expectations from the previous work on the circular duct, and comparison with Figure 25 reveals a similar relationship between reactivities, i.e. 100%H_2 > 40%H_2/60%CO > 40%H_2/60%CH_4. This is reassuring, although there is an important difference in the origin of the limit pressure for the data of

Figure 25 and Table 14, which is that the latter refers to the 'doubled' reflected wave from the HRSG end plate. The peak pressures used in Figure 26, Figure 27 and Figure 28 could have been taken from other parts of the system which showed similar peak values, in particular the pressure at the end of the circular duct due to the pressure wave at the heat exchanger travelling back upstream and undergoing a compression through the expansion/contraction Section 2. The results however would have been closely similar to Table 14.

Table 14 can be considered as a main correlation emerging from the HRSG test programme and the input and measured parameters associated with Figure 26 - Figure 28, from which it derives, should be weighed in judging the accuracy and limitations of this correlation. The key input parameters are exhaust mass flow rate, exhaust temperature, made up oxygen concentration, mixedness, injected fuel concentration, and target EQR value. The measurement of these has been discussed in the commissioning work and the estimated errors in these, based on the measured run parameters, are given in Table 15.

Table 15: Accuracy associated with input HRSG operating parameters

parameter	target value	unit	estimated accuracy
exhaust mass flow rate	9.3	kg/s	± 1%
exhaust temperature	500	^{o}C	± 1%
oxygen concentration	21	%	± 0.2
mixedness	100	%	± 1%
injected fuel concentration	variable	kg/s	± 1%
EQR	variable	-	± 1%

The main errors in these input parameters arise from knowledge of the exhaust mass flow rate during an actual combustion test which has been observed to have a ± 1% range linked to the exhaust temperature and velocity variation. These have a direct impact on achieved oxygen level and estimated EQR, although the mass flow for the latter is known with higher accuracy.

The observed output parameters, e.g. pressure, are then subject to the natural variability of the combustion process, however their variability has not been explored in the present work. It should also be noted that the results and correlation presented in this section relate to the exhaust temperature indicated in Table 15 and it is known from the small number of tests carried out within WP2.2 that this can be a significant parameter, with reducing temperatures increasing the overpressures for the same mixture conditions. This aspect and the variability between the same data sets are both discussed in the proposal for further work. Similarly there were several mixture combinations investigated as part of the WP 2.2 programme that we were not able to investigate as part of WP 2.3, and which should also be considered for further investigation in order to fill the data base gaps identified in this section.

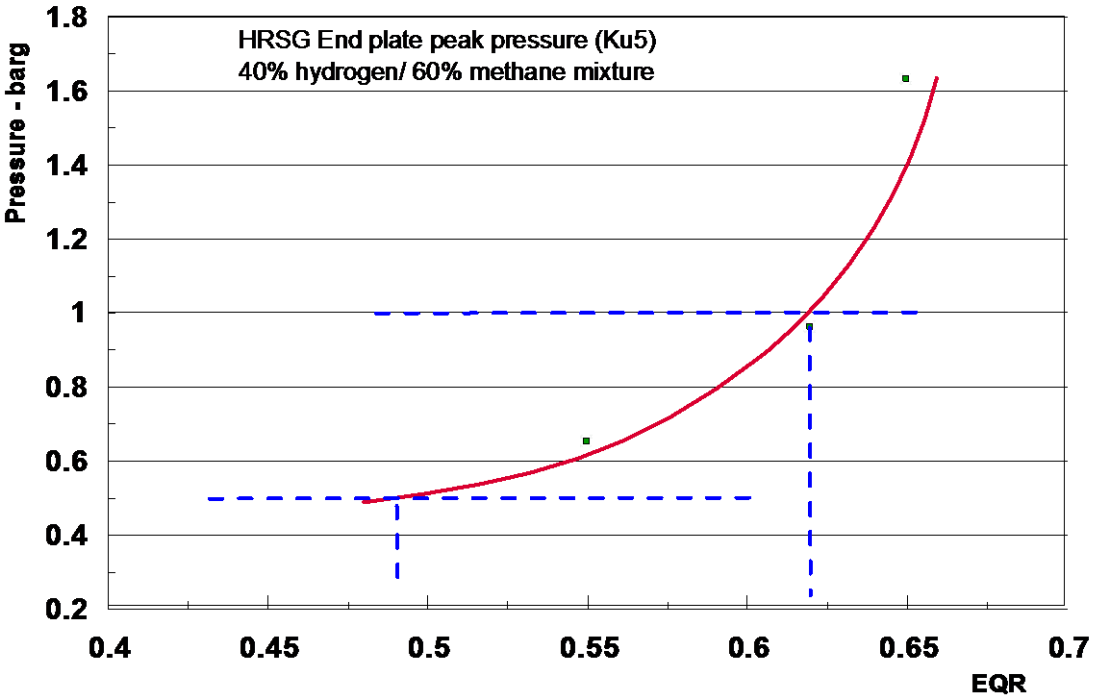

Figure 26: Reflected end plate peak pressures (Ku5) for 40% hydrogen / 60% CO mixture investigated using the HRSG system and at each of the EQR values tested

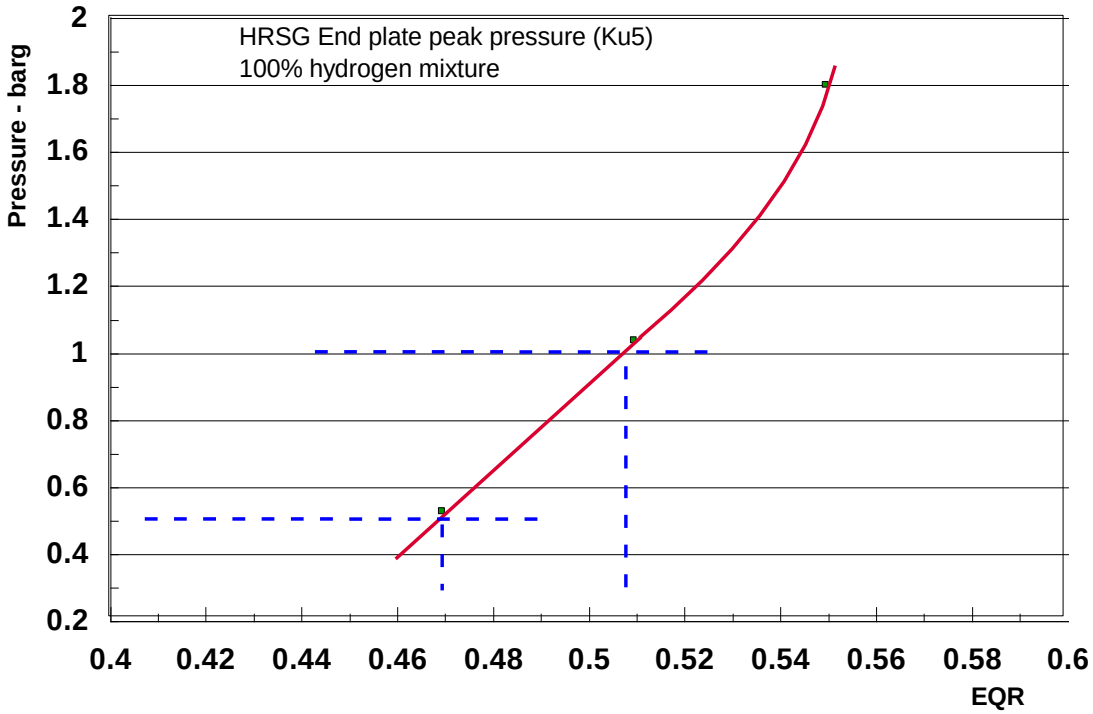

Figure 27: Reflected end plate peak pressures (Ku5) for 100% hydrogen investigated using the HRSG system and at each of the EQR values tested

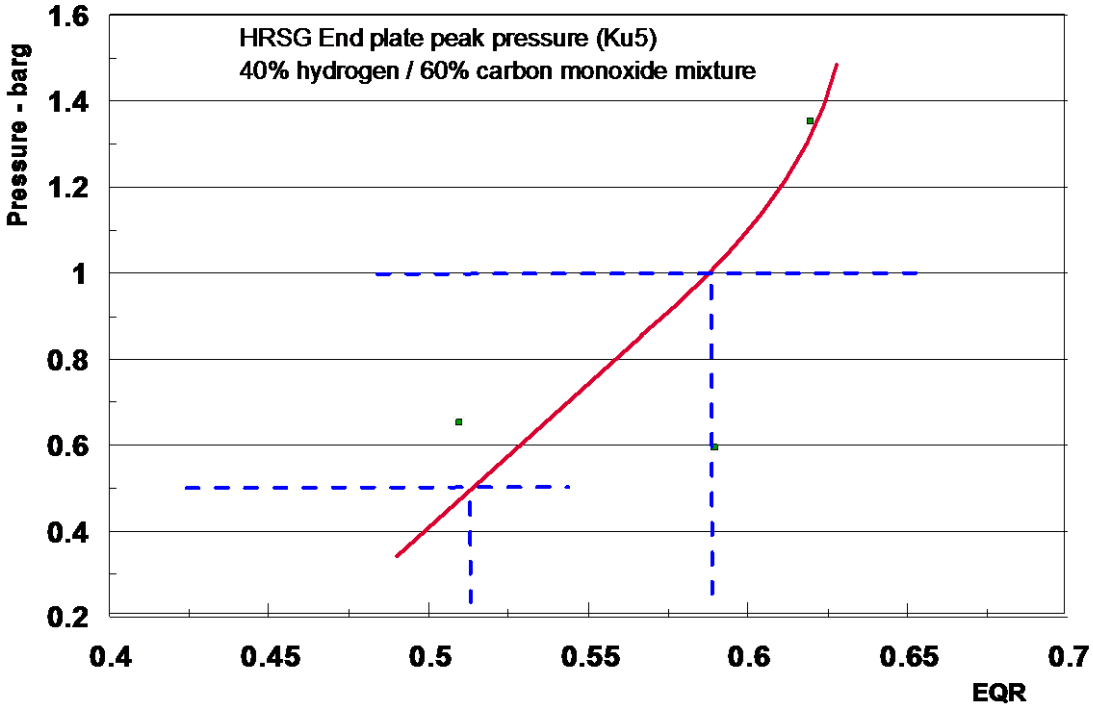

Figure 28: Reflected end plate peak pressures (Ku5) for 40% hydrogen / 60% CO mixture investigated using the HRSG system and at each of the EQR values tested

6.11 SCALING CRITERIA

The scaling criteria requirement as given in the desirable outcomes and also referred to in Appendix 12.2 is to “Outline the applicability of the results by extrapolation to larger duct dimensions and geometries, identifying specific limitations on validity, plus any further work required to increase confidence in the extrapolation process.”

With this in mind the WP 2.3 test system was designed to be geometrically similar to an existing GE 350 MW combined cycle gas turbine (CCGT) design. Thus the test rig is an approximately 1/8th scale model of the existing GE designed CCGT system. The rationale for using this size of rig is based on 1) a compromise between interest in achieving sufficient scale to mimic industrial facilities whilst accommodating (unintended) DDT of highly diluted fuel mixtures, 2) to use as part of the system the WP 2.1 rig with realistic gas velocities across the expanding transition duct, and 3) to limit costs without affecting their relevance.

Furthermore the gas velocities in the model have been kept the same as in the full scale GE unit, as has the finned 38 mm diameter heat exchanger tubing together with the 40% blockage ratio. The scaled distance however, from the beginning of the HE tube bundle to the end of the HRSG was extended beyond the actual scaled distance to allow space for measuring the properties of the flame fronts and pressure waves emerging from the tube bundle (scaled length of 3.95 m extended to 6.35 m). A single tube bank only was used, consisting of fifteen rows of tubes. The temperature and velocity distributions at the entry into the model heat exchanger are the same as those expected within the full scale GE unit and similar units (Maximum HE inlet velocities of around 25-30 m/s and which peak just below the central region of the inlet plane). The measured turbulence levels in the exhaust flows prior to ignition are around 13-15 %, which are also typical of the levels observed on full-scale gas turbine exhaust streams. However the influence of the tube bank in extracting heat from the flow over it was not modelled in the WP 2.3 tests, as it was not practical to utilise a fully representative heat exchanger with water flowing through it. The tubes used did however have a close fitting solid steel rod within them. Reduced flow temperature effects are considered in Section 8 for future work.

Thus in view of the foregoing the observed magnitudes of the pressure waves immediately downstream of the tube bank together with the observed flame speeds are considered to be representative of the values likely to be observed on larger dimensionally similar units. Furthermore the observed flow patterns through the system, following a combustion event are also considered to be representative of what would be observed at full-scale. However as the same flow and combustion velocities are considered to occur irrespective of scale then the time between specific event occurring may be different due to the reduced distances between particular features on the model when compared with full scale. In addition the influence of the reflected pressure wave on the combustion flame front and its subsequent behaviour may differ at full scale because of these inherent time differences, and also because the circular duct was present. However as the influence of the tube bank has been established in respect to the pressure wave increases and the combustion behaviour irrespective of scale, this information can be used in unsteady CFD flow and combustion models to establish the subsequent behaviour/interactions on full scale systems with increased confidence.

Regarding fuel mixtures and EQR values at different scales of investigation, the work of WP2.1, 2.2 and 2.3 have shown consistent relative reactivity behaviour for equivalent hydrogen/carbon monoxide or hydrogen/methane dilution levels and this has been discussed earlier. It is therefore considered that this ranking can be carried forward to the full scale, taking care to note likely differences between different hydrogen dilution levels. Although not strictly a scaling factor, this provides qualitative insight into the effects of these mixtures at the full scale, and is worthy of further exploration as part of a future programme of work.

7 STANDARDS AND REGULATORY ISSUES

7.1 TRANSFERRING HIGH HYDROGEN PROJECT FINDINGS TO INTERNATIONAL STANDARDS

The findings of this project are clearly of considerable value to a range of industrial applications that may give rise to flammable mixtures of hydrogen, including hydrogen with methane and carbon monoxide (syngas, biogas etc.), at elevated temperatures. Two key applications are obviously combined cycle gas turbine and gas engine systems as studied in this project, but the data should be available to as wide an audience as possible. In the first instance, the development of the standard would make available the combustion behaviour data already produced, and then lay the ground for future work on mitigation techniques if appropriate.

In preparation for this, HSL has been raising the awareness of this work to test interest, and specific activities have included presenting the work at a number of events including:

- The International Energy Agency (IEA) Hydrogen Implementing Agreement (HIA) Safety Task (Task 37).
- The International Conference on Hydrogen Safety held in Yokohama, Japan, Autumn 2015.

From these activities incorporation in to standards is clearly the next step. Interest in participation in such an activity has been expressed by a number of countries, positioning the activity at an international level. Recognising this, initial discussions have taken place with the chairman of the International Standards Organisation (ISO) Technical Committee (TC) 197. ISO TC 197 has a scope defined as, “Standardization in the field of systems and devices for the production, storage, transport, measurement and use of hydrogen”. Current sub committees/ working groups with TC197 are listed in Table 16 below.

Table 16: ISO/TC 197 Hydrogen Technologies Subcommittees/Working Groups

Subcommittee/Working Group	Title
ISO/TC 197/TAB 1	Technical Advisory Board
ISO/TC 197/WG 5	Gaseous hydrogen land vehicle refuelling connection devices
ISO/TC 197/WG 15	Gaseous hydrogen - Cylinders and tubes for stationary storage
ISO/TC 197/WG 17	Pressure swing adsorption system for hydrogen separation and purification
ISO/TC 197/WG 18	Gaseous hydrogen land vehicle fuel tanks and TPRDs
ISO/TC 197/WG 19	Gaseous hydrogen fuelling station dispensers
ISO/TC 197/WG 20	Gaseous hydrogen fuelling station valves
ISO/TC 197/WG 21	Gaseous hydrogen fuelling station compressors
ISO/TC 197/WG 22	Gaseous hydrogen fuelling station hoses
ISO/TC 197/WG 23	Gaseous hydrogen fuelling station fittings
ISO/TC 197/WG 24	Gaseous hydrogen fuelling stations ¿ General requirements
ISO/TC 197/WG 25	Hydrogen absorbed in reversible metal hydride
ISO/TC 197/WG 26	Hydrogen generators using water electrolysis
ISO/TC 197/WG 27	Hydrogen fuel quality
ISO/TC 197/WG 28	Hydrogen quality control
Joint working groups under the responsibility of another committee:	
ISO/TC 158/JWG 7	Joint ISO/TC 158 - ISO/TC 197 WG: Hydrogen fuel analytical methods

The business case for ISO TC 197 [6] states that specifically in both the energy and industrial applications, the work of ISO/TC 197 is intended to fulfil the following needs:

- to warrant safety by implementing consensual rules to minimize avoidable risks to persons and goods to an acceptable level; to eliminate barriers to international trade and to simplify the arduous regulatory process by providing hydrogen-specific standards in order to allow the early implementation of the rapidly emerging technologies;
- to control variety by allowing to select the optimum number and types of products, processes and services to meet prevailing needs;
- to harmonise testing methods and quality criteria for the use of hydrogen in all its forms;
- to ensure protection of the environment from unacceptable damage due to the operation and effects of products, processes and services linked to hydrogen.

The Chairman of ISO TC 197 Technical Committee is Dr. Andrei Tchouvelev, and discussion with him confirm that this work would be a good fit for this committee solely, or if required, in conjunction with ISO TC 192 which is concerned with Gas Turbines. He has advised on the next steps to take this forward, which include identify an individual and resources (stressing that to drive acceptance into international standard requires a

strong time commitment over a number of years, generally two to six years, more typically three years) to take forward this activity successfully. The formal process of submitting and developing within ISO includes the stages Proposal (A new work item proposal (NWIP) is submitted to the TC197 Committee) , Preparatory - a working group (WG) is set up by the parent committee to prepare the working draft (WD), Committee, Enquiry and Approval resulting in the publication of the standard.

Dr Tchouvelev stressed the importance of local secretary support from the British Standards Institute, and the likely developments with this work have been discussed in outline with BSI. He also stressed the need for a transfer document to be available to take the activity forward, and initial thoughts are that this could be the final report of the project, or an abridged version.

8 RECOMMENDATIONS FOR FURTHER WORK

8.1 INTRODUCTION

This section contains suggestions for follow-on work based upon observations and analysis of the results from the WP 2.3 test programme together with suggestions contained in the paper by C. Etheridge [7]. The work to date has identified several gaps in the data base that has been put together as a result of the current programme, these include several mixture combinations that were not be fully investigated, repeatability issues, the influence of temperature on combustion behaviour, and means of mitigating the consequences of a flameout. In this section we outline the basis of a follow on test programme based on these aspects, bearing in mind that a separate more detailed proposal [8] is being submitted along with this report to the ETI.

The WP 2.3 work has shown that, following a flameout in the gas turbine of a CCGT system; a flammable gas mixture will enter the exhaust stream as a consequence. If this is subsequently ignited a combustion wave will travel through the system, which is then accelerated as it passes through the tube bank of the HRSG. The test results have shown that the driver of the pressure rise is the acceleration of the flame front velocity through the boiler tubes; the larger the number of tube rows, the higher the resulting pressure rise. This pressure rise may be of sufficient magnitude to destroy the HRSG attached to the turbine, as most HRSG systems are of square or rectangular cross sectional area and will incur significant internal damage if pressure spikes in excess of 0.5 barg occur.

The tests results presented in this report have shown that the peak pressure rises in the HRSG system with an end wall will likely exceed 0.5 barg even at 0.5 equivalence ratios. Internal studies at Solar Turbines [7] have also shown that under certain fuel system failure modes with a flameout, the equivalence ratio could exceed 0.6 and even approach the stoichiometric condition, which in the extreme could drive pressures to well in excess of 10 barg.

Given these possibilities it is important to have a clear understanding of the science driving the combustion behavior in the approach to and through the HRSG, including how the over pressures are influenced by temperature as there are indications that lower temperatures than those used in the WP 2 test programme may occur in practice and will produce higher overpressures as a consequence. It is also important that means of mitigating these consequences are explored with a view to demonstrating their potential and how they may be engineered into CCGT systems in the future.

The following section outlines our suggestions for what should be included in a follow on work programme with a view to filling the identified knowledge gaps as well as examining at least one possible means of mitigation. The proposal for follow on work [8] does provide our views on what the priority areas of further work should be, based on our assessment of the knowledge gaps arising from the current research and our preferred mitigation technique. Several lessons have been learnt in respect of the data collection and processing system, addressing these in the light of the information and knowledge collected are also addressed in [8].

8.2 EXTENSION TO WP 2.3 TEST PROGRAMME

The WP 2.3 test programme was paired down to the bare essentials because of budgetary constraints. As part of a follow on test programme there are several additional tests, including other fuel mixtures that should be included in a follow on programme that would add value to our understanding of the underlining principals as well as extending the range of fuel mixtures considered. In addition we should seek to complete those tests considered necessary for our basic understanding of the behavior of the three fuels/mixtures studied to date, as explained in [8]. A test matrix was originally drawn up as shown in Appendix 12.1; reference to this would form the basis for the selection of future additional tests.

8.3 EFFECT OF MIXTURE TEMPERATURE

The exhaust temperature of an unburned fuel/air mixture is known to influence the extent of the pressure rise as a result of an ignition event. Most of the testing (WP 2.2) in the circular rig was carried out at a temperature of around 550 °C, with a small number of tests being done at the lower temperature of 350 °C. The latter tests did show that for the same test conditions the lower temperature tests produced a significantly higher over pressure than did the higher temperature ones. This agrees with the calculated CJ pressure against equivalence ratio for various pre-ignition mixture temperatures with hydrogen/air mixtures [7]. These plots clearly show that initial mixture temperature has a strong effect on CJ Pressure (designated detonation in the plot).

Evidence from some limited engine testing at Solar Turbines indicates that the initial temperature in a flameout situation could be in the 150 to 200 °C region and this is likely to result in higher pressure rises than those obtained from the current test programme. The information gathered to date clearly shows that more testing to explore temperature effects is needed.

We now consider how in practice the lower temperature can be achieved, either at constant volumetric flow or at constant mass flow conditions. There is a lower intermediate exhaust temperature/mass flow rate combination that can be achieved with the current system, which will be higher than the lowest temperature required. This temperature has been ascertained by removing the existing orifice plate (blockage ratio 0.43), and determining at what temperature the engine will be running at when it is delivering the required volumetric or mass flow rates in the duct. This temperature is in the range of 590 – 610 K, irrespective of whether the volumetric flow or mass flow rates are kept constant, and was measured near the beginning of the third duct section. Under constant mass flow conditions the velocity is reduced to about 60 m/s when the temperature is 600 K. Reducing the temperature further would require operation of the engine combined with the injection into the exhaust of either liquid nitrogen with increased make-up oxygen (provided through the existing system) or alternatively by the injection of liquid air. This will also require the flow to be re-adjusted to give the required mass flow rates of 17.7 kg/s or 9.2 kg/s at 430 K.

An example calculation of the liquid nitrogen/air requirements in order to achieve the 430 K temperature requirement is shown below.

A guide as to the maximum amount of liquefied air required to be injected into the exhaust can be calculated if the maximum operating temperature of 773 K is assumed at the lower engine operating speed. Thus if the exhaust gas is to be cooled from 773 K to 430 K then the rate of heat removal required will be 1.056X9.2X343 = 3.17 MW, where the average C_P is 1.056 kJ/(kg K). If this heat is to be removed by the addition of liquefied air then taking the latent heat of vaporisation for air as 200 kJ/kg, and the BP of air as 80 K the required rate of injection (x) is obtained from 3.17= 1.005X350x + 200x, from which x= 5.74kg/s of liquid air. Thus the total mass flow rate after injection will be 5.74+9.2= 14.94 kg/s, which equates to a duct velocity of 71 m/s.

If the requirement is to maintain a constant volumetric flow then the velocity can be increased to 86 m/s if the ratio of exhaust gas to injected coolant is taken as 1.5, and as a consequence the exhaust mass flow rate increases to 10.88 kg/s from which the corresponding mass flow rate of coolant required becomes 7.13 kg/s. If the requirement is to maintain a constant mass flow rate then the exhaust mass flow rate will need to be reduced to 5.66 kg/s and the injected air to 3.54 kg/s, giving a total flow rate of 9.2 kg/s. These flow rates are within the capability of commercially available high-pressure cryogenic pumps. In respect of storing liquid air two standard cylinders, each of 450 l capacity, would in a worse case provide sufficient volume for a total run time of about 100 seconds, provided that the flow rate was sufficient.

However in view of the likely manufacture and development costs associated with reducing the temperature to 430 K it is not proposed to pursue this approach any further at this stage.

8.4 DUCT BURNER FEASIBILITY STUDY

One way of preventing flame acceleration through the boiler tubes is to ensure that any unburned fuel/air mixture coming out of the GT is combusted immediately before it enters the boiler tubes, and before any flammable gas mixture has had time to fill the overall system. This can possibly be achieved by utilising the already existing technique of using a duct burner to burn off the unburnt fuel as it reaches it. Duct burners in turbine driven systems can typically increase system efficiency by 1-4% by increasing the steam temperature in the HRSG. However they are currently not allowed in systems burning hydrogen based mixtures.

The feasibility of achieving this can be examined by adding a model duct burner to the existing 1/8th scale CCGT test rig. A representative location is near the beginning of the second section of the HRSG expansion section as shown in Figure 4. It is therefore proposed to add a model duct burner to the existing rig, positioned at or near the beginning of the rectangular section of the HRSG expansion section. The duct burner would consist of discrete flames covering the whole or part of the cross-sectional area of the duct, and have sufficient heat output to ensure complete combustion of the injected flammable gas stream. A diffusion propane/air flame is proposed for the burner fuel. The existing engine turbine together with the turbulence generator and the gas injection tubes already replicates the gas turbine exit geometry upstream of the duct burner. These will therefore provide a realistic reflective surface for any pressure waves propagating back upstream during testing. Due to the gas velocity in regions upstream of the duct burner (e.g. 85 m/s) it is not expected that the flame can travel back upstream due to ignition of

unburnt gases arriving at the duct burner and the duct burner will represent the first flame stabilisation structure available to the ignited gas.

The proposed test scenario is that the engine is run up to speed with the exhaust products passing through the rig. The burner is then ignited; a representative range of fuels and oxygen are then injected into the duct using the existing injection system. These will in the main be repeats of tests for which we already have data for but without a duct burner. This mixture will ignite and burn when it reaches the duct burner. The behavior of the resulting flame front will be measured using the existing instrumentation.

The expected outcome is an insignificant pressure rise in any location downstream of the existing turbulence generator. Analysis of the data will be carried out to assess if this approach could be an effective solution.

8.5 WATER DELUGE DETONATION SUPPRESSION SYSTEM

This section outlines the basis of design for a water suppression system, the feasibility of which could be tested on the existing test rig. However detailed proposals including costings are not included, as at this stage of the process it is not the intention to proceed with a practical assessment.

Tests undertaken by Ciccarelli et al [9] at the Brookhaven National Laboratories have shown that the addition of steam to hydrogen/air mixtures reduced flame acceleration and pressure rises for a given equivalence ratio. However this approach is not appropriate for the suppression required in the cases of interest to this project. A water deluge concept is considered more suitable.

The water deluge concept requires flooding the HRSG in the critical area around the boiler tube bundle with water droplets or a fine water mist in order to suppress the flame acceleration. The process envisaged is that a flameout or combustion event is detected by a suitable monitoring system. This is used to trigger the water deluge system which forces water stored under pressure into the HRSG at high velocity through spray nozzles for the period of time that the control system needs to shut off the fuel to the gas turbine. It is envisaged that such a system would be rechargeable and resettable.

HSL has considerable experience in the design and use of water spray systems for explosion and fire suppression as a result of earlier work developing coal dust explosion suppression systems for use in coal mines, as well as developing water mist systems for fire suppression generally. Past work at HSL has also examined the means of detecting the early onset of flame and pressure wave development following an ignition, as well as the optimum location for the water injection process. Both pneumatically and explosively driven water discharge systems have been investigated by HSL in the past. However such systems were designed to operate at the ambient conditions existing in mine roadways, thus air temperatures of around 15-25 ^{O}C and air velocities of around 2 m/s were the norm.

In seeking to adapt mining practices to the CCGT system then the following constraints apply. Firstly the velocities of concern, if a similar location for the water suppression system is to be used to that of the duct burner, then they are going to be in the range of 36 to 16 m/s, depending on whether a constant velocity or a constant mass flow approach

is utilised. Secondly gas temperatures may be in the range 773 to 430 K. Designing on the basis of constant mass flow provides the more realistic operating conditions.

The maximum distance from the ignition point on our test rig to the location of the water barrier is some 12 metres, and given that the measured flame speeds are of the order of 200 m/s, the time from detection of the flame to deployment of the barrier if it is to be established before the arrival of the flame, is 50-60 msec. Typical water spray fluxes quoted in the literature for passive water barriers [10] suggest values in the region of 110-130 l/m^2, whilst comparable values for active water spray barriers are in the region of 10 – 45 l/m^2 [11]. No mention is made in either of these references as to the range of water droplet diameters utilised. However [12], which deals with the use of water sprays generally for explosion suppression, concludes that effective explosion mitigation requires either a significant initial volume fraction of spray at a sub 30 micron droplet diameter, or larger droplets that will readily shatter at low gas accelerations in the flow preceding the flame front. Furthermore the range of larger droplet diameters suggested as the most effective at quenching the flame is in the 1 – 4 mm range. Supportive information is also given in [13].

In practice an active water spray system will be required in view of the limited injection time, which based on current information [11] will require a water injection rate of 0.131 – 0.59 m^3/s. Furthermore the water injection will need to be made at right angles to the flow as the water will need to be stored outside of the HRSG to prevent it boiling. Previous practical designs have consisted of a cylinder containing the required amount of water, which was pressurised with nitrogen gas. A bursting disc or fast acting valve sealed the water into the cylinder, the operation of which released the water through a nozzle. The system was triggered by a signal from a flame sensor placed upstream in an appropriate location. As an example of a practical design if we assume a water capacity of 50 l and a nitrogen capacity of 200 l, then the total capacity of the container will be 250 l with a pressure drop during discharge of around 20%. If the nitrogen is pressurised to 100 bars, and a 75 mm diameter orifice is assumed then the discharge rate will be around 0.6 m^3/s, which is just in excess of the maximum required value. Based on these values a suitable storage vessel of 300 mm diameter would need to be approximately 3.5 metres in length.

Any proposed programme would seek to design and build a suitable delivery system and install it on the existing reduced scale rig. The test programme would quantify its ability to suppress the dynamic pressures resulting from a series of experimental releases in which a wide range of gas mixtures and equivalence ratios are utilised.This would be demonstrated by repeating some of the more energetic tests already completed with the rig.

A successful outcome would be suppressed pressure rise and a system design that allows for a relatively easy reset of the suppression system, as well as optimizing its location.

8.6 BLAST PROTECTION THOUGH THE USE OF LIGHT WEIGHT BLOW OUT PANELS

A further method of suppression is outlined in this section; again it is not proposed to proceed with it at this stage in the programme.

The use of lightweight blow out panels attached immediately upstream, on the side of, or downstream of the tube bundle may also provide a means of mitigating the impact of combustion generated excess pressures in and around the HRSG. In order to achieve sufficient operating time following a combustion event these panels may need to be explosively operated and triggered in advance of the pressure pulse and flame arrival. This may be achieved by sensors upstream of the HRSG, which respond to either the detection of a pressure rise or a flame front once they have formed. The sensor signal then triggering an explosive device, such as a shaped linear charge, which fails the protective panel thus releasing the excess combustion generated pressure pulse.

The technology for such a protective system already exists and it may be the case that what is required is developing a modification of existing systems to the specific needs of HRSG protection, together with a practical demonstration of the system's feasibility.

8.7 END WALL SHOCK ABSORPTION SYSTEM

A further means of mitigating the consequences of combustion overpressures is outlined here, although further work on this proposed method of mitigation will not be pursued as part of this proposal.

It is well known and understood how the peak pressure from a moving combustion wave can be amplified as it is brought to rest by, in this case, the end wall of the HRSG and is then reflected back along its original path. The same is also true for combustion waves hitting a surface obliquely but to a lesser extent. It is also known that there are a number of pressure absorbing materials that could be tested in the reduced scale rig with a modified end wall in place. The idea would be to add a chamber to the end wall of the rig and test candidate materials in it for their pressure absorbing capabilities. This work would involve studying the literature for suitable candidate materials and chamber dimensions then testing them for their effectiveness by repeating some of the tests already carried out as part of the current test programme.

An example of what may be possible is discussed in the article from the Technion Israel Institute of Technology [14] where they discuss the potential pressure absorbing capabilities of using nonlinear acoustic granular meta-materials or "Granular Crystals". An effective demonstration of the potential of materials such as these in the rig could open up the opportunity to protect an HRSG passively under certain applications.

9 CONCLUSIONS FROM THE HSL TEST PROGRAMME

This section provides in summary the conclusions arising from the overall WP 2 test programme. It is split into relevant sections.

9.1 CONCLUSIONS RELATING TO THE PERFORMANCE OF THE WP 2.3 TEST RIG

It was concluded that:

1. The WP 2.3 rig design was successfully implemented as a fully operational test rig.
2. The rig fully met the agreed specification.
3. The rig was commissioned and operated successfully.
4. All the agreed safety standards and operational procedures were met.
5. There were no serious incidents recorded during the operation of the rig.
6. A total of 13 ignition tests were successfully completed for a range of EQRs and gas mixtures.
7. The majority of the tests were undertaken at a maximum temperature of around 500- 550 °C, as measured by the thermocouple probe attached to the pitot-static probe.
8. Valid and consistent data sets were obtained over a wide range of agreed operational parameters. The data however, could be difficult to derive information from due to issues such as noise and sensor drop out making it a time consuming process.
9. Despite the foregoing measurements of flame speed, pressure rise and wave speed were successfully made for all of the tests.
10. High-speed video recordings were made of all of the tests, showing the flame and wave behaviour immediately downstream of the HRSG tube bank.
11. Data from all of the sensors was used collectively to determine as a first priority the critical overpressures and flame speeds generated.

9.2 COMBUSTION BEHAVIOUR CONCLUSIONS

The following observations can be made to summarise the combustion behaviour and resulting measurements that have emerged from the study:

1. The progress of the combustion could be monitored by the measures put in place, including sensors for pressure, flame front detection (both ionisation and optical based) and high speed video.
2. The video record has revealed a degree of complexity in the flame emergence from the heat exchanger finned tube array, such as flame emergence from the bottom of the array initially due to the upstream expansion section orientation

previously discussed, and a weakening of the flame intensity in the downstream half of the HRSG when the end plate and chimney are in place.

3. Mixture reactivities were greatest for pure hydrogen and dilution of hydrogen with methane was more effective at reducing reactivity than dilution with carbon monoxide. For similar mixture dilution levels and EQR values this means that reactivities are in the order of H_2 > H_2/CO > H2/CH_4.
4. The principle pressure generating event was identified with the flame propagation through the heat exchanger and into the turbulent region immediately downstream of this structure, and the pressure wave associated with the rapid combustion in this region could be followed both upstream and downstream with wave speeds consistent with the prevailing gas conditions.
5. The source peak pressures generated around the heat exchanger were of a closely similar magnitude to those generated downstream of the obstacles in the circular duct tests (WP2.2), for a particular mixture and providing the combustion conditions were removed from any strong non-linear behaviour, i.e. in terms of mixture and EQR, which is a useful correspondence for a future combustion modelling effort.
6. The reflection of the pressure wave from the HRSG end plate appeared to interact with the moving flame downstream of the heat exchanger and have an attenuating effect on the progress of this flame. This was evident from the high speed video record and the frequently weaker flame sensor signatures in the downstream half of the HRSG.
7. The highest pressures generated following the flame propagation were usually associated with the period of overlap of the incident and reflected pressure waves at the end plate usually around 5 msec duration, and the upstream pressure associated with the arrival of this reflected wave, following its passage through the duct contraction. This could be twice the pressure generated at the source combustion event around the heat exchanger.
8. Despite the limited number of tests there was evidence of non-linear behaviour in a few of these, suggesting progress toward a more rapid increase of peak pressures with increasing EQR as indicted in Figure 6.

10 OBSERVATIONS FROM THE OVERALL PROGRAMME

10.1 GENERAL OBSERVATIONS

The project has been shown to be able to simulate several of the relevant features of a full scale HRSG system using the current scaled test rig and to demonstrate the development of flame through the system and the generation of pressures, which are believed to be relevant to the understanding of how these will develop at full scale. The commissioning tests carried out have given confidence in the overall operation of the test rig in terms of achieving appropriate gas temperatures, injected fuel mixtures and equivalence ratios; exhaust/injected fuel mixing and HRSG purging times ahead of actual ignition. Detailed flow measurements at selected positions within the system have confirmed the uniformity of the flow in these regions and have provided background turbulence data for future flow and combustion modelling.

The exhaust flow velocity through the HRSG has closely reproduced that in the full scale, i.e. uniformly 6m/s within the main downstream area, and it can be considered that the present heat exchanger/HRSG geometry represents a subset of the full scale in terms of understanding the propagation of flame through and within the downstream region of this structure.

The intensity and duration of the high-speed combustion downstream of the heat exchanger was an unknown at the start of the project and the work has now provided new insights into this aspect of the combustion development. This includes particularly the growth of transient pressure around the heat exchanger, its propagation both downstream and upstream and its interaction with the main flame propagation front. A key output has been the relationship between the peak amplitude of this pressure wave and the mixture conditions giving rise to it, since this is a determining factor in the limiting operating conditions that might be used. Although the number of results is limited, an indication has been given of the likely EQR values which can be used for each of three fuel mixtures in order to limit this peak amplitude within certain limits, as shown in Table 11.

It is important to note that the limited number of tests means that reproducibility of the outputs has not been explored. Whilst the operating conditions have been measured with good precision, the combustion process has an underlying degree of randomness and the body of earlier work (WP2.2) indicates that this can give rise to peak pressure variations, particularly where there is pressure sensitivity to EQR value.

As observed with the circular duct series of tests in WP2.2, the overpressures developed on ignition increased with increasing EQR and the mixtures tested showed relative reactivities, as measured by flame speeds and overpressures, which were consistent with both the WP2.1 and WP2.2 results.

Overall, the data obtained starts to confirm the range of operational conditions, mixtures and EQRs, where overpressures and associated flame speeds are below the indicative agreed limits of 0.5 and 1.0 barg. It is therefore clear that additional data to confirm this behaviour is required and the recommended work of Section 8 seeks to address this aspect.

Several lessons have been learnt in respect of the data collection and processing system, such as dealing with noise issues, sensor dropouts, battery operation and automation of the data analysis. Addressing these in the light of the information and knowledge collected are dealt with in the further work proposal [8].

10.2 OVERVIEW OF PROJECT RESULTS.

This section provides an overview of the results from both the circular duct and HRSG tests when collected together. The circular duct test results have been discussed in the WP2.2 Report and a useful summary of these results is reproduced in Table 17 below.

Table 17 Comparison of peak pressures for the circular duct tests in the immediate region downstream of the obstacles, based on Kulites 5 and 6 for 15-obstacle cases.

Test	Mixture	Eq. Ratio	CH_4 (vol%)	CO (vol%)	H_2 (vol%)	Pressure at obstacles (Ku5/Ku6) (barg)
35	CH_4	0.65	100	0	0	0.22 - 0.27
34	CH_4	0.76	100	0	0	0.37 - 0.49
33	CH_4	0.86	100	0	0	1.52 - 2.50
38	CH_4/H_2	0.60	60	0	40	0.25 - 0.36
36	CH_4/H_2	0.65	60	0	40	0.29 - 0.39
37	CH_4/H_2	0.75	60	0	40	0.90 - 1.03
30	CH_4/H_2	0.55	40	0	60	0.25 - 0.28
39	CH_4/H_2	0.61	40	0	60	0.25 - 0.39
31	CH_4/H_2	0.65	40	0	60	0.84 - 0.93
40	CH_4/H_2	0.66	40	0	60	0.40 - 0.53
41	H_2	0.4	0	0	100	-
28	H_2	0.4	0	0	100	0.26 - 0.32
27	H_2	0.5	0	0	100	0.80 - 1.73
42	H_2	0.50	0	0	100	0.48 - 0.74
44	H_2	0.51	0	0	100	0.55 - 1.09
29	H_2	0.6	0	0	100	3.53 - 7.16
43	H_2	0.60	0	0	100	2.43 - 5.08
46	CO/H_2	0.44	0	100	0	0.099 - 0.114
47	CO/H_2	0.6	0	100	0	0.41 - 0.51

48	CO/H_2	0.77	0	100	0	1.53 - 2.43
50	CO/H_2	0.41	0	60	40	0.23 - 0.23
52	CO/H_2	0.5	0	60	40	0.43 -0.45
49	CO/H_2	0.65	0	60	40	3.30 - 4.66
53	CO/H_2	0.4	0	40	60	0.16 - 0.21
54	CO/H_2	0.5	0	40	60	0.29 - 0.40
56	CO/H_2	0.56	0	40	60	0.35 - 0.42
60	$CH_4/CO/H_2$	0.45	25	35	40	0.12 - 0.21
59	$CH_4/CO/H_2$	0.51	25	35	40	0.31 - 0.40
58	$CH_4/CO/H_2$	0.56	25	35	40	0.75 - 0.85
57	$CH_4/CO/H_2$	0.65	25	35	40	1.22 - 2.19
66 (low T)	CH_4/H_2	0.48	40	0	60	-
65 (low T)	CH_4/H_2	0.5	40	0	60	0.67 - 0.80
64 (low T)	CH_4/H_2	0.58	40	0	60	2.32 - 2.34
63 (low T)	H_2	0.35	0	0	100	0.22 - 0.27
62 (low T)	H_2	0.45	0	0	100	0.44 - 0.63
61 (low T)	H_2	0.5	0	0	100	1.23 - 1.35
67 (low T)	CO/H_2	0.51	0	60	40	0.85 - 0.94

These results relate specifically to the 15 row obstacle tests, which produced the greatest of the pressures in all of the three geometry scenarios investigated and, as discussed in the WP2.2 report, the pressure sensors chosen to represent these tests are Kulite 5 and 6 in the immediate downstream region of the obstacle pipe array. These are comparable with the corresponding pressure sensor (Kulite 2) used to represent the pressure generation region of the HRSG in the present report and shown previously in Table 13.

To enable a more visual comparison of these two test campaigns,

Figure 29, Figure 30 and Figure 31 present the entire key results graphically. For the circular duct cases, the pressure plotted is the average of the Ku5 and Ku6 sensors. The figures group the tests roughly according to mixture.

Figure 29 plots methane and methane/hydrogen mixture. The behaviour of the curves confirms the previous discussion and shows a clear progression in combustion intensity in moving from 100% CH_4 to 60%H_2/40%CH_4. There is also a clear distinction between 60%H_2/40%CH_4 and 40%H_2/60%CH_4, again reflecting the increased activity for the circular duct tests as would be expected. However, interestingly there is also a definite increase in combustion intensity associated with the HRSG compared with the circular duct for the 60%H_2/40%CH_4 mixtures; although for the duct tests the data is more variable. Particularly noticeable is the effect of temperature reduction on the

60%H_2/40%CH_4 mixture with the circular duct (operating at 350°C). Only two data points are available for this case and the effect cannot be exactly quantified with certainty but at least a doubling of generated pressure would appear to be justifiable from this limited data, which clearly indicates a need for further study.

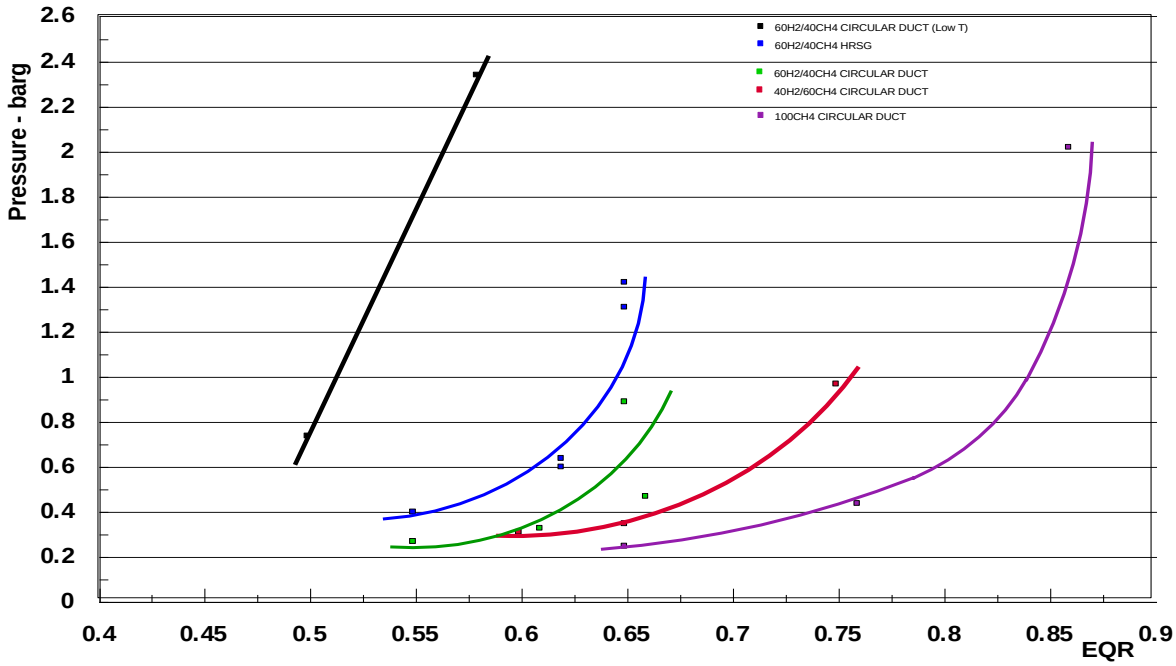

Figure 29: Methane and Methane/Hydrogen Mixtures.

The 100% H_2 cases are compared in Figure 30 and although the data points are limited, the HRSG and circular duct curves occupy similar regions, with the HRSG showing a slightly steeper pressure/EQR gradient tendency. It is noted that the upper points for the circular duct case relate to detonation behaviour. Three points are provided at lower temperature in the circular duct tests for pure hydrogen and again these show a higher resultant pressure, being approximately double those of the higher temperature cases.

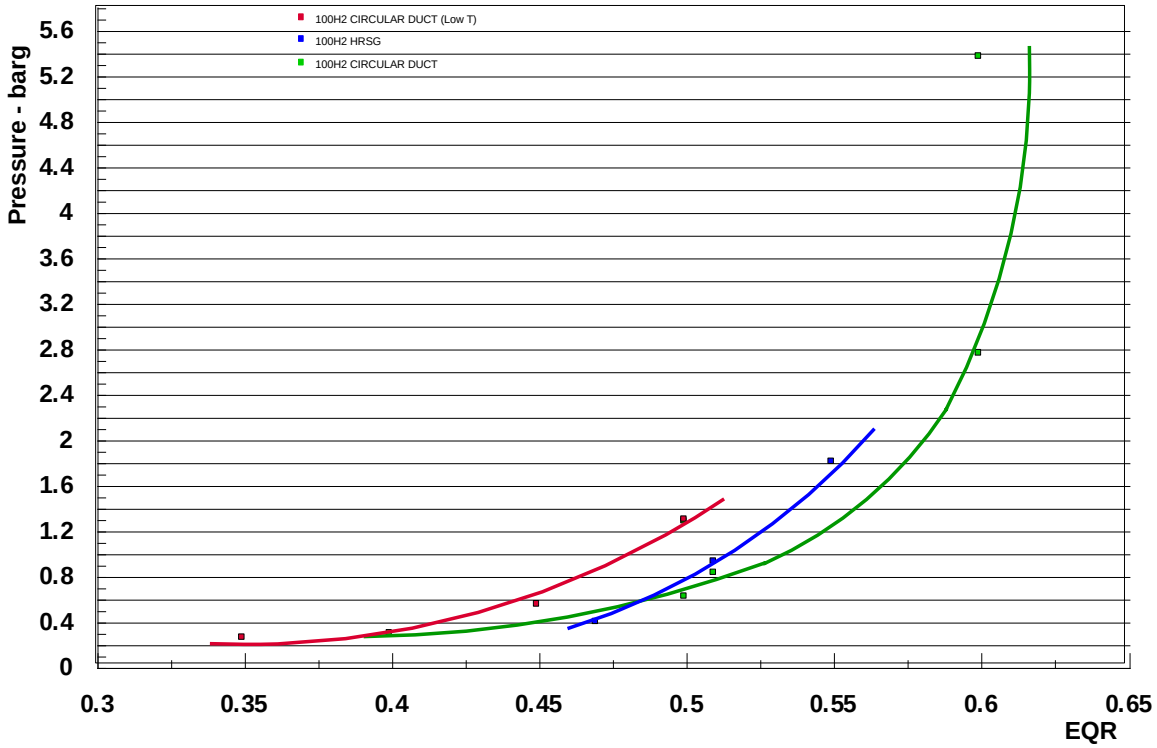

Figure 30: 100% Hydrogen.

Figure 31 presents six sets of data involving mixtures of carbon monoxide, including 100% CO. Regarding the 40%H_2/60%CO for the circular duct and HRSG, the pressures for the duct appear to be slightly higher, which is different to that observed for the H_2 and H_2/CH_4 mixtures already discussed, although the data is limited and slightly variable for certainty on this point. Also the 60%H_2/40%CO case for the circular duct appears to occupy the same pressure region as the weaker H_2/CO mixture which would not be expected. This clearly is an area worthy of further investigation in order to understand this apparent anomaly. The 40%H_2/35%CO/25%CH_4 pressure curve for the circular duct follows three points on a good curve, lies above but generally close to the other curves at low EQR, and does not follow the detonation behaviour of the 40%H_2/60%CO duct case at an EQR of 0.65 due to the mitigating effect of the methane. The weakest of the group is that of 100% CO in the circular duct, which appears slightly more reactive than the 60%H_2/40%CH_4 example. Only a single lower temperature points exists for the 40%H_2/60%CO mixture in the circular duct and this is consistent with an approximate doubling of peak pressure in reducing to 350 °C.

Comparisons between the HRSG and circular duct tests should also note that the entrance velocities into the obstacle arrays are different for the two systems, being 21 m/s for the circular duct and around 5- 40 m/s for the HRSG, noting that in the latter the expansion section generates a recirculation zone and hence a velocity profile. The free stream turbulence intensity upstream in the circular duct was around 5% whereas with the higher upstream velocities used for the HRSG (85 m/s) this was around 15%. As has been discussed, it is expected that the flow folding within the obstacle arrays and the turbulence generated downstream of these will likely dominate burning velocity behaviour.

Qualitative comparisons of mixture reactivities observed in the HSL duct and HRSG work with the experimental studies WP2.1 have already been made in this and the WP2.2 report, and this was to confirm that the general ranking of mixtures in the two areas of study was the same. The data sets in both bodies of work do not completely overlap and the main points of comparison are likely to be the shock tube studies carried out in WP2.1. These however, concentrate mainly on an EQR value of 0.8 and the tests were also carried out at ambient temperature, which is likely to generate significant differences as discussed above. Where comparisons can be made, e.g. with 40% and 60% hydrogen mixtures, it was generally found that the pressure ratios between these were less in the shock tube tests than in the circular duct tests, demonstrating the importance of scale for the full development of the overpressure with these generally lean (stoichiometry below unity) mixtures. It has already been pointed out that one of the three elements in generating combustion intensity is the obstacle geometry, and the shock tube test geometry is very different from that of the duct or HRSG, making anything but qualitative comparisons more difficult.

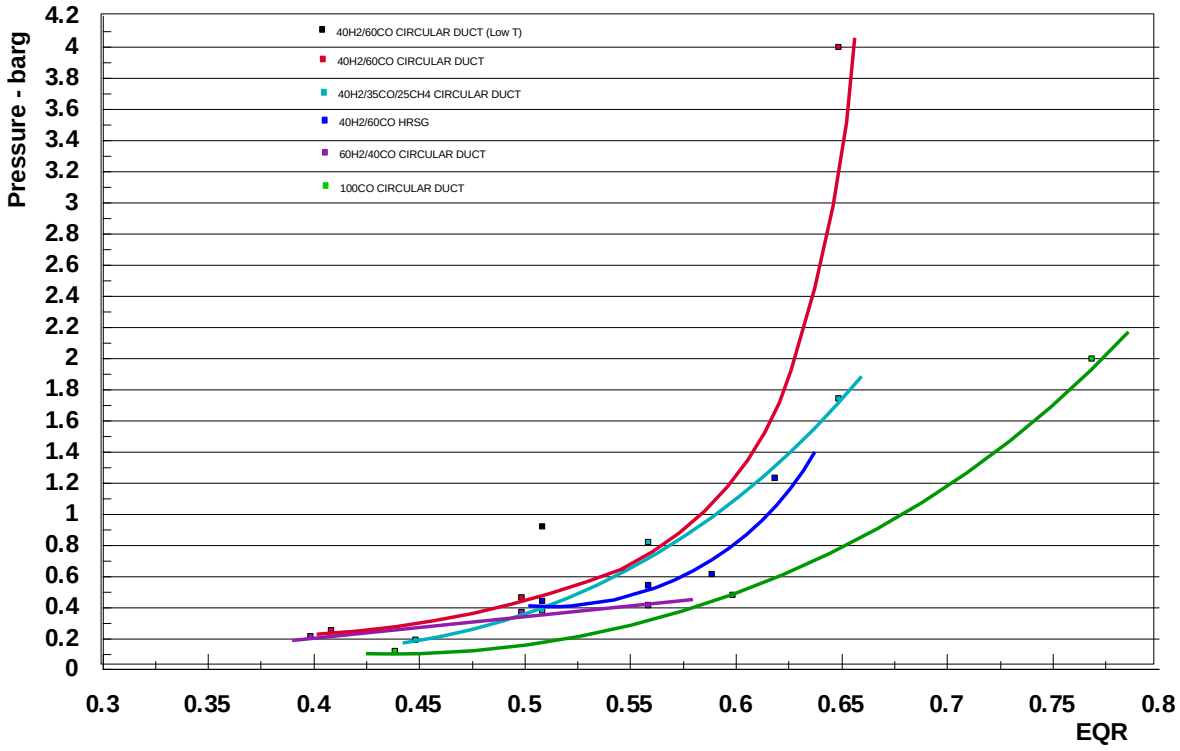

Figure 31: Carbon Monoxide and Hydrogen/Carbon Monoxide Mixtures.

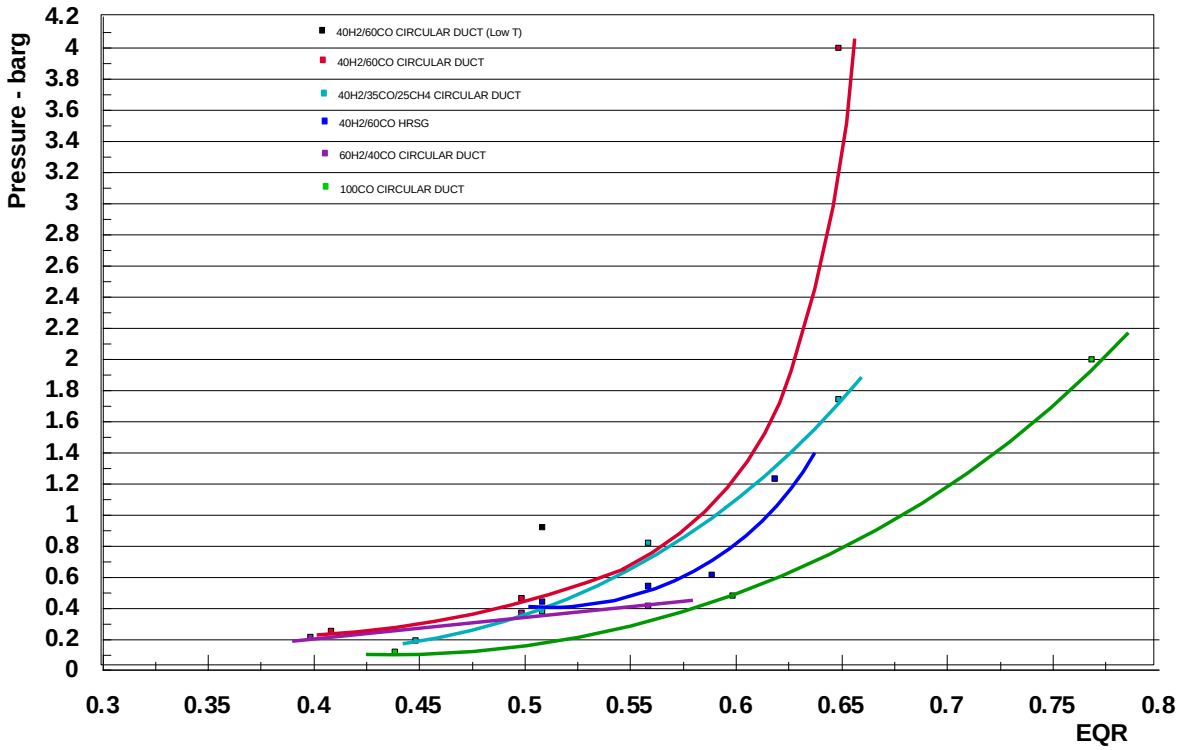

Figure 31 carry a limited number of data points per curve, but they do demonstrate important trends in behaviour with modest variability within each data set. The curves clearly have a predictive capability which should enable interpolation between points with some confidence. This is valuable in designing additional experiments in order to test the security of the pressure curves, as the graphs of

Figure 29, Figure 30 and Figure 31 are able to guide recommendations for further work to fill certain perceived gaps in the knowledge base, which industry operators are likely to need. Regarding the H_2/CH_4 mixtures,

Figure 29 indicates that more data is required at both lower and slightly higher EQR values for the 60%H_2/40%CH_4 mixture, in order to confirm the pressure behaviour below EQR 0.55 and also the steepness of the rise above EQR 0.65, where the test rig still has some margin of safe operation. Also missing from this data set is the pressure behaviour for the 40%H_2/60%CH_4 mixture, which was studied in the circular duct. It would be useful to confirm the margin of difference with the 60%H_2/40%CH_4 mixture as was observed in the circular duct tests.

Figure 30 for 100%H_2 suggests that the data points are well behaved, although the EQR values occupy a narrow range. It is therefore important to extend this range at both the lower and upper ends, although some care is required above EQR 0.55 since the safety margin available here is only modest. The effect of temperature seems less pronounced, as this is an important aspect needing further investigation.

Concerning mixtures containing CO, only one of these was tested in the HRSG work, i.e. 40%H_2/60%CO. In order to fill the mixture matrix more completely, it is suggested that the richer mixture of 60%H_2/40%CO be tested as well as two ternary mixtures involving

H_2/CO/CH_4, which are more representative of those fuel mixtures likely to be used in the future by industry. This would allow data interpolation between mixtures to be carried out with more confidence. It would also confirm or otherwise the apparent lack of sensitivity when changing the H_2 fraction between 60% and 40% as was observed in the circular duct.

The graphs of

Figure 29, Figure 30 and Figure 31 reveal the likely importance of reduced temperature in influencing the peak pressures obtained, where in each case that was tested at a modest temperature reduction, higher pressures were observed. Future work should therefore benefit from a more thorough investigation of the temperature parameter, with tests at as low a temperature as can be achieved being carried out. Ideally, this should be performed with a range of mixtures in a similar way to that suggested previously. This is considered an important aspect for further investigation, as it has been shown in studies by Solar (Private communication) that during an actual flame out the exhaust temperatures are lower than those tested in this study.

Referring back to the earlier figures in this report, e.g. Figure 10, Figure 11, Figure 12, Figure 13 and Figure 23, reference was made to the initial pressure rise at the upstream position associated with the flame development and the generation of gas volume within the circular duct. As was indicated, this arises from the pressure required to drive the generated volume through the downstream blockage of the heat exchanger and in the tests this was typically 0.2 - 0.4 barg at its peak. It has also been discussed in several places of the report that the main region for pressure generation has been the heat exchanger and the region immediately downstream of it. This indicates that the prevention of flame propagation into the heat exchanger region should result in the avoidance of this pressure rise. It is therefore particularly relevant to consider flame mitigation/extinction measures upstream of the heat exchanger as a means of reducing the pressure to the lowest values achievable. This is likely to be the initial pressure rise which Figures 10 etc. referred to above, have indicated is 0.2 - 0.4 barg. It is expected that this pressure range is within that tolerable by full scale equipment.

The results presented in this report are based upon our analysis of the data currently available, and depending on future results and further analysis at a later stage, some of the findings and opinions expressed may or will be reviewed.

11 REFERENCES

1. Moodie, K., *Basis of Design Document for HSL WP2 Task 2 test rig for ETI*. 2014, Health and Safety Laboratory.

2. Moodie, K., *Basis of Design Document for HSL WP2 Task 3 HRSG test rig for ETI*. 2015.

3. Moodie, K. and B. Ewan, *Commissioning Report HSL WP2 Task 2 Test Rig*. 2014, Health and Safety Laboratory.

4. Moodie, K., et al., *HSL Commissioning Report for WP2 Task 3 Test Rig*. 2016, Health and Safety Laboratory.

5. Michels, H., *Results from IC WP2.1 Report*. Imperial College London.

Q. F M Global, publications, http://www.fmglobal.com/

6. ISO. *ISO/TC 197 Business Plan*. 2005 [cited 2016; Available from: http://isotc.iso.org/livelink/livelink/fetch/2000/2122/687806/ISO_TC_197__Hydrogen_technologies_.pdf?nodeid=852624&vernum=-2.

7. Etheridge, C., *Hydrogen Exhaust Test Request for 2016 Activity*. 2016, Solar Turbines.

8. Moodie, K. and B. Ewan, *Proposal for Follow-on Work*. 2016, Health and Safety Laboratory.

9. Ciccarelli, G., et al., *The effect of initial temperature on flame acceleration and deflagration-to-detonation transition phenomenon*. 1998, Brookhaven National Lab., Upton, NY (United States); Nuclear Regulatory Commission, Div. of Systems Technology, Washington, DC (United States); Nuclear Power Engineering Corp., Tokyo (Japan).

10. Medic Pejic, L., et al., *Full scale test for explosion water barriers in small cross-section galleries.* 2011.

11. Zou, D. and S. Panawalage, *Passive and triggered explosion barriers in underground coal mines-A literature review of recent research.* CANMET Natural Resources Canada, 2001.

12. Thomas, G. and J. Brenton, *An investigation of factors of relevance during explosion suppression by water sprays*. 1996: Great Britain, Health and Safety Executive.

13. Ewan, B. and M. Moatamedi, *The study of induced water flow devices in the suppression of gas explosions.* Process Safety and Environmental Protection, 2002. **80**(3): p. 126-134.

14. *Granular Shock Absorbers*. 2016, Israeli Institute of Technology.

15. *ETI WP2 Task 2 Interim Project Report*. 2016, Health and Safety Laboratory.

16. Clay, M., *General Area and Visitor Risk Asessment*. 2014, Health and Safety Laboratory.

17. Clay, M., *Hydrogen Test Rig, Mixed Gas System Risk Assessment*. 2014, Health and Safety Laboratory.

18. Clay, M., *Modification of Rig. Operational Risk Assessment.* 2014, Health and Safety Laboratory.

19. Clay, M., *Oxygen System Risk Assessment*. 2014, Health and Safety Laboratory.

20. Clay, M., *Hydrogen Project. Toxic (CO) Risk Assessment*. 2014, Health and Safety Laboratory.

12 APPENDICES

12.1 PROGRAMME TEST MATRIX FOR WP 2.3 TESTS

The fuel compositions and concentrations proposed for these tests are designed to build on the key tests from the WP2.2 circular duct programme and aim to determine the lowest hazardous (P_{max} ≈ 3.0 bar) and highest safe fuel concentrations (P_{max} = 0.4 bar) for operation in the WP2.3 model HRSG facility. As previously, the programme is designed to achieve the objectives in a safe and progressive manner, building on previous experience, and additional knowledge that will be gained about the operational characteristics of the new facility. Also, as in WP2.2, the boundaries will be determined from an approach employing a minimum of three, ideally four experiments for each base mixture (H_2, H_2/CH_4 and H_2/CO) at constant fuel mixture composition but varying equivalence ratio in air.

These compositions are optimum based on the findings from the circular duct. The boundaries are in the first instance expected to be approximately 0.2 EQR apart. As inlet temperatures in the HRSG facility will be below those of the circular duct experiments, the first test will be at or just above (+ 0.05 EQR) the safe boundary value of the latter. EQRs of the second and third, and ideally the fourth test will then be chosen in the light of evidence from the first test. In addition, the program includes a tertiary mixture, for which a minimum of three equivalence ratios are also required to be tested.

The programme of tests described below was agreed at HSL on 3 February 2016. Present were Prof Hans Michels, Keith Moodie, Paul Winstanley, Bruce Ewan, John Gummer, John Allen and Stuart Hawksworth.

12.1.1 Programme priorities

In an ideal world, all 32 tests shown in Table 18 would be performed, but clearly resources are limited and so a process of prioritisation has been carried out which is indicated by the following colour coding:

- [ ] – These tests are essential and need to be completed in the following order to ensure the safe operation of the facility

    i. Three EQR ratios for H_2/CH_4 60:40 with no end wall, that is to say an open HRSG. These tests will build the link between the open circular duct and the open HRSG; and are the initial link to determining performance with the end wall in place for all mixtures. One of these tests has already been completed as part of the commissioning, a second (provisionally at an EQR of 0.6) will also be completed as part of the commissioning programme, and the third will be performed as test 1 of the full programme.

    ii. Repeat the three EQR ratios (following review of the results from i. by the team) for H_2/CH_4 60:40 with the closed end wall. These tests will provide the next link, open HRSG to closed HRSG, and will overall relate the behaviour in the open circular duct to the performance in the closed HRSG. These tests will be number 2, 3 and 4 of the main programme.

iii. Three EQR ratios with 100% H_2 fuel with the HRSG closed end wall. These will be chosen based on the performance from the circular duct of 100 H_2, cross referenced with the results from i. and ii. above. These tests will number 5, 6 and 7 of the main programme. These will provide comparative H_2 to H_2/CH_4 behaviour in the same closed HRSG configuration.

iv. Following review of all of the results above, the provisional plan is to then test three H_2/CO 40:60 mixtures. The aim of the review is to ensure that following i to iii above that these are still the priority tests. These tests will number 8, 9 & 10 of the main programme.

- ▭ - These are second priority tests, and ideally all 9 should be carried, but as a minimum one composition set (one row of three tests) should be completed at a later stage to provide data on the tertiary mixtures and on the open end wall configuration.
- ▭ – In an ideal world these tests should also be completed, to provide greater confidence in the data trends. However they are of lower priority than the above tests.
- ▭ – Lowest priority tests.

Note that effects of temperature etc. are not included in this matrix, but are instead included in future work (see earlier).

Table 18: Proposed test matrix (EQR values in brackets indicate actual values finally used)

Test Mixture	Composition	EQR 1		EQR 2		EQR 3		EQR 4	
		open	Closed	open	closed	open	closed	open	closed
1	100% H_2	0.45	0.45 (0.47)	t.b.d.	t.b.d. (0.51)	t.b.d.	t.b.d. (0.55)	t.b.d.	t.b.d.
2	40/60 CH_4/H_2	0.53 (0.55)	0.53 (0.55)	t.b.d. (0.62)	t.b.d. (0.62)	t.b.d. (0.65)	t.b.d. (0.65)	t.b.d.	t.b.d.
3	60/40 CO/H_2	0.58	0.58 (0.51)	t.b.d.	t.b.d. (0.56)	t.b.d.	t.b.d. (0.59)	t.b.d.	t.b.d.
4	25/35/40 $CH_4/CO/H_2$	0.45	0.45	t.b.d	t.b.d	t.b.d.	t.b.d	t.b.d.	t.b.d

12.2 DELIVERABLES AND ACCEPTANCE CRITERIA

The following are the relevant project deliverables as listed in the contract:

The following are the relevant project deliverables as listed in the contract and the sections of the report where the deliverables are presented:

1. A description of the WP2.2 and WP2.3 test facilities, their commissioning, and their means of operation (Sections 12.3. - Section 12.5).
2. The results obtained during the WP2.2 and WP2.3 test programme (Ref. [15], Section 5 and Section 6).
3. A comparison of the results for the flammability, any hot surface/induced/auto ignition and DDT potential for the selected fuel mixtures for WP2.2 and WP2.3 with the data collected during the smaller-scale studies at Imperial college (WP2.1).
4. A full description of the set of engineering scaling methods which correlate results at all three scales tested. (Section 6.11)
5. A description of the extent to which the above correlations for the model fuel mixtures tested in this work programme can be used, given their limitations/ accuracy, by system designers and operators towards identification of safe operating limits in the downstream ducts of industrially-relevant scales and configurations of CCGT and CCGE systems (Ref [16], Section 6.10).
6. A detailed discussion of the limitations and accuracy of the engineering correlations developed and identification of how these might be improved through further test work on the WP2.2 or 2.3 or other larger-scale test rigs (Section 6.10).
7. Report and guidance on future engagement with standards and regulatory bodies in this area, to work with them to understand and develop robust guidelines for such applications, including identification of further work, where necessary, to achieve these objectives. (Section 7).
8. Conclusions and recommendations based clearly on the evidence provided in the report (Section 6.10, Section 8).
9. An Executive Summary capturing all the key findings within the report (Page 8).
10. A comprehensive photographic record of the WP 2.3 test rig and an HS video record of the tests completed (provided separately).
11. Raw and analysed data from all of the tests completed for WP 2.3 in a suitable digital format (provided separately).

The following are the relevant acceptance criteria:

1. The report will comprehensively cover all items set out in the deliverable description.
2. The report will be written in a clear and concise style to aid informed decision making at the end of the project, and in a form that can be used by industrial users to inform design and operational decisions for CCGT and CCGE systems operating on high hydrogen fuels.

3. The report will be provided as an MS Word compatible document and in PDF format.
4. A catalogue of high quality photographs suitable for publicity purposes will be generated.
5. Quality-checked data files for each test run performed will be produced; the data will be issued electronically with a folder for each test run. Each folder will contain:
    i. Rig mass flow calculations
    ii. Pitot test
    iii. Pro forma Excel work book
    iv. GDS test pro forma mixed fuel filling operation / details / calculations
    v. TDMS file
    vi. CCTV footage of test from all three cameras
    vii. Photographic and HS video records of the tests
6. The root folder of the issued data will contain:
    i. The test matrix
    ii. A table describing each test; giving each test a unique number
    iii. The test folder's name, starting with this number. Where a test has been aborted after starting, an explanation of the issue with the test should be given. The folder will then not contain the data file but should contain all the other information for tasks undertaken before the failure
    iv. Each file type in the folder will also start with the test number
7. A brief report outlining the early engagement with standards and regulatory bodies in this area, and a costed road map for working with them, in order to understand and develop robust guidance for these applications. The lessons learnt from the bodies will help to shape the report structure and the details of this format are to be explained.

12.3 FINAL DESIGN SPECIFICATION

1. The main component of the rig is a scale model of an HRSG that includes an expansion section, a tube bank and an exhaust stack. It is connected to the end of the 12 m long by 600 mm diameter stainless steel duct that forms the WP 2.2 rig. The maximum operating pressure for the HRSG is 5 barg, and the maximum wall design temperature is 400 °C.
2. A Rolls-Royce Viper, type 301, gas turbine, running on butane, and supplying a vitiated exhaust stream to the duct.
3. A maximum mass flow rate of 9.2 kg/s was used during the WP 2.3 test programme. The accuracy to which this was measured is defined by the resolution of the pressure transducer(s) used to measure the dynamic pressure across the duct. This is within ± 1% full scale deflection (FSO) for the

transducer used, which corresponds to an error of ± 0.2 kg/s for the maximum mass flow rate.

4. The mass flow rate is controlled by an orifice plate in combination with an exhaust diverter that allows some of the flow to be exhausted to atmosphere before entry into the duct. Control of the mass flow through the diverter section gives velocities along the test duct of between 60 and 90 m/s. The measured values are within ± 2% FSO of the transducer used.

5. Test gas mixtures and make-up oxygen are injected into duct in the transition section just before the entrance to the duct. Three spray bars, equi-angled across the section are used for injecting the test mixture and a further three for injecting make-up oxygen. The injection pressure is of the order of 20 barg, through 52 holes, 1.7 mm diameter, in each spray bar.

6. Test gases and oxygen are prepared and stored in four 220-litre pressure vessels (two connected in parallel for each gas). Their flow rates are measured and controlled via Coriolis flow meters linked to flow controllers operating at a pressure of no more than 45 barg.

7. Turbulence is generated in the duct by a 50 mm square grid located at the beginning of the duct.

8. A heat exchanger tube bank comprising fifteen rows of 38 mm diameter pipes running vertically is located at the start of the HRSG. The blockage ratio is 40% for the tubes alone, but increases to 48% when the tube fin area is taken into account. There are a total of 218 tubes.

9. Instrument ports are located diametrically opposed along both sides of the duct at a distance of 500 mm apart. In addition, there are quartz viewing ports 500 mm from the start of each duct section together with a further instrument port on the top of each section at a distance of 250 mm from the section start as shown below.

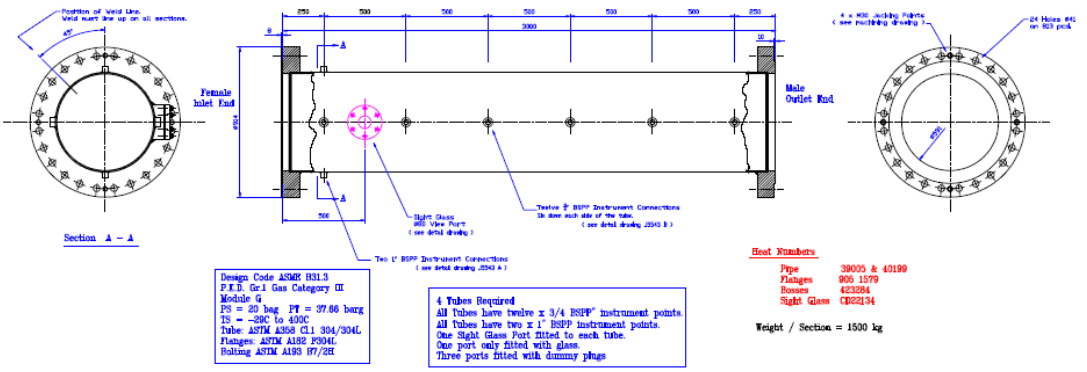

Figure 32: Circular duct section showing instrument port positions.

1. Instrumentation consists of fast response pressure transducers, ionisation probes, optical probes and thermocouples. A pitot-static probe is also used to obtain the velocity profile across the duct at the start or end of each test run or series of runs. It is located 500 mm from the beginning of the fourth duct

section. A gas analyser, located in the fourth section of the duct, is also used to measure the oxygen concentration in the exhaust stream.

2. The HRSG contains over seventy instrument ports and six optical windows as shown in Figure 2.
3. Operating temperatures in the duct (after addition of fuel and oxygen) are within the range 350 to 600 °C. Measurements are within ± 1% of the required values. Temperatures are measured using type 'K' thermocouples and are to the manufacturer's specified accuracy of ± 2 °C at 600 °C.
4. Provision is made for injecting sufficient oxygen to restore levels to 21% in the exhaust stream when operating at 15 kg/s. This is equivalent to a maximum oxygen mass flow rate of 1.12 kg/s. Measurements are within ± 2% of the required FSO range of the device. The Emerson Coriolis flow meters used are types F050S and F100S, accurate to better than ± 0.2% FSO, which in this case is ± 0.003 kg/s.
5. Provision is made for injecting fuel mixtures up to 15% by volume of the total flow at the highest operational mass flow rate used. Measurements are within ± 2% of the FSO values for the respective gases. Mass flow rates are measured using Emerson Coriolis flow meters, types F050S and F100S, accurate to better than ± 0.2% FSO.
6. The fuels are mixtures of hydrogen, methane and carbon monoxide, or each gas individually up to maximum mass flow rates of 0.2 kg/s, 1.0 kg/s and 2.0 kg/s respectively. The revised values are those required to give at least 15% of the total flow when operating at the maximum flow rate of about 9.2 kg/s: higher percentages are possible for lower flow rate conditions.
7. Oxygen concentrations during the test programme are measured using a Servomex gas analyser, accurate to ± 1% of FSO.
8. .A calibrated pitot-static probe with a thermocouple attached, and which could be traversed across the duct, is used to obtain both temperature and velocity profiles. These are measured to accuracies within the stated tolerances for the pressure sensors and thermocouples used, namely ± 1% of FSO
9. The velocity profiles and turbulence levels (x and y directions only) across the entry plane to the HRSG are measured with the HSL-owned TSI-manufactured LDA system. The measurements obtained are within the tolerances specified for the instrument used. The system uses X-optics operated in back-scatter mode and a Dantec BSA-F80 processor to convert the optical signals to flow velocities in the axial and vertical directions.
10. Measurements are made of both the temperatures and dynamic pressures along the duct and throughout the HRSG during testing. These are measured to within the levels of accuracy specified by the manufacturers for the instruments used, namely Kulite and PCB pressure sensors and type 'K' thermocouples, all within ± 1% of FSO. The type 'K' thermocouples are to the same accuracy as specified previously. However, there is a noticeable lag in the thermocouple measurements due to their thermal mass. The pressure sensors are within the specified accuracy, being in both cases 0.1% of FSO.

11. Ionisation probes and optical (photoconductive) sensors are used to measure flame front velocities. These are on/off devices, designed and manufactured by Chementech. These units are tested prior to installation by subjecting them to a flame front and observing the response. Since the ionisation sensors are purely conductive devices their response times are short, e.g. less than 1 μsec, whilst the quoted time response of the Hamamatsu photoconductive sensors is 2 μsec.
12. An ignition system comprising an 8-10 Joule spark is positioned on the centreline of the rig. It sparks repeatedly at a rate of once every 1.5-2 seconds. It is situated for test purposes on the rig centreline, 250 mm downstream from the beginning of the second section of duct.
13. The data logging and processing system has a resolution to 16 bit or better, with a maximum sampling rate of 1MHz, but typically 100 kHz. Data from the foregoing sensors, except the thermocouples, are sampled at a rate of 100 kHz per channel using a National Instruments logger and processor. It was acknowledged during design discussions that the above sampling rates are acceptable for non-detonation events, which form the main focus of the work. However the occurrence of detonating events is still identifiable. National Instruments Diadem software is used for data analysis. The data logger used is a National Instruments PXI system with data acquisition cards to provide the required channel count. This system is PC based using the Windows 7 operating system. The data collection system and associated software is written in LabVIEW. During testing this system is operated remotely from the control room.
14. The engine control and gas delivery systems are operated by their own PLC systems, which are NI-cRIO for the engine control and a PXI real-time system for the gas delivery. Both of these systems record data at a rate of 10 Hz and transmit it over the network to the high speed data acquisition PXI system, which incorporates these data along with the data collected at high speed. This alleviates the need to synchronise all three systems. The thermocouples attached to the high speed data acquisition system are recorded at a rate of 5 kHz but are then averaged to an effective data rate of 10 Hz and included in the TDMS file. On the high speed data acquisition system the individual DAQ card sample clocks are synchronised with each other from the PXI chassis so that there is no significant uncertainty regarding timing of samples from across channels.

12.4 DESCRIPTION OF THE WP 2.3 TEST SETUP (ADDITIONAL INFORMATION)

12.4.1 Gas turbine

The Rolls-Royce Viper gas turbine was converted to run on liquid butane, in order to minimise the possibility of soot particles and other additives affecting the deflagration to detonation transition (DDT) behaviour of the gases being tested. Consequently, the engine was controlled by an external variable speed positive displacement pump that metered the fuel flow into the engine. The engine exhaust gas temperatures immediately

after the turbine varied up to a maximum of 650^{0}C depending on the operating conditions being used. Increasing the fuel flow increased the engine speed, which increased the mass flow through the engine and the exhaust temperature as a consequence. The engine output was variable from idle conditions, when the mass flow rate was approximately 5 kg/s, up to the maximum power used for these tests which corresponded to a mass flow rate of around 9.2 kg/s.

12.4.2 Diverter and transition sections

There was both a diverter section and a transition section incorporated between the engine's turbine and the start of the 600 mm diameter duct. The first of these provided a pathway from the engine turbine into the duct. It also provided a means of controlling the amount of exhaust flow that entered the test duct by enabling some of the exhaust flow to be diverted sideways to atmosphere. The flow rate into the duct was controlled by an orifice plate in combination with the diverter. The orifice plate used for these tests is shown in Figure 33. Depending on engine speed, this allowed velocities along the duct of between 60-90 m/s to be achieved, these being typical of those occurring in actual CCGT's

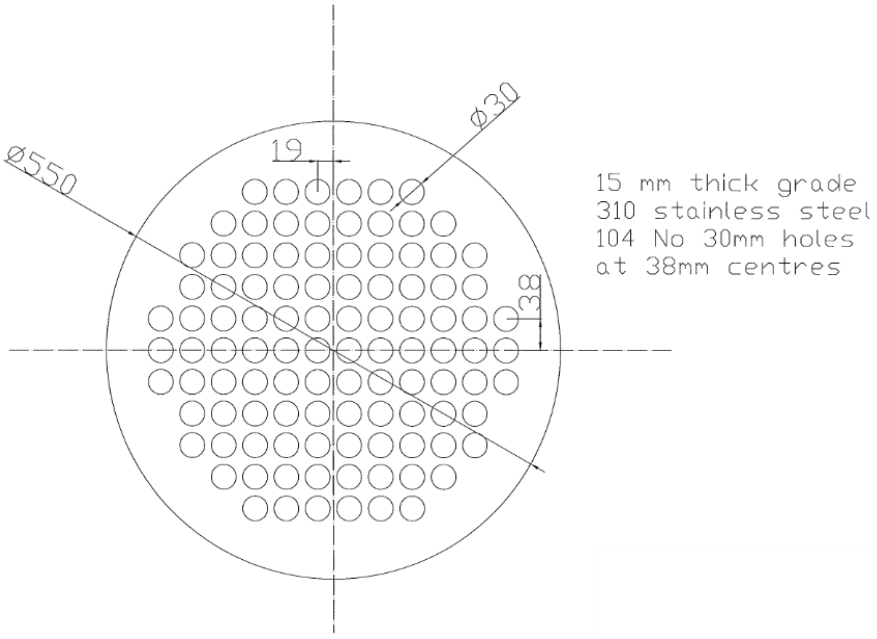

Figure 33: Orifice plate used for the WP 2.3 rig.

The transition section expanded the flow from the engine turbine into the duct. Six spray bars each containing 52 holes were incorporated into this section to provide the means of injecting and mixing the test gas mixtures circumferentially into the main hot gas exhaust flow from the engine. The holes were spaced to ensure a uniform mass flow rate across the section. The gases were injected at about ambient temperature, thus minimising the risk of ignition at this point. The first three spray bars were used to inject oxygen such that the oxygen concentration was restored to 21%. The second group of three were used to inject the test gases to give mixtures of differing EQRs.

12.4.3 Injection and mixture systems

The means of injecting the oxygen and gas mixtures was a flow-through system, injecting directly into the exhaust stream and relying on the injection process to ensure that the gases were fully mixed with the exhaust stream. This avoided waste and reduced the risk of a flashback. The mass flow rates of the injected gases were measured using individual Coriolis mass flow meters and controlled using mass flow controllers. The supply line pressures were regulated using pressure regulators (55 bar maximum, but typically 40 bar). This method of flow control and monitoring provided precise control over the mixture concentrations injected, over a wide range of mass flow rates and EQRs.

The gas mixture and oxygen supply systems were positioned to the side of the main building housing the duct and engine. The system of gas mixture and oxygen supply individually consisted of two steel pressure vessels with a maximum capacity of 450 litres and a maximum working pressure (MWP) of 200 barg. One pair of vessels contained oxygen, the other the fuel mixture. The latter comprised mixtures of hydrogen/methane/carbon monoxide and nitrogen as required. Specific gas mixtures were prepared from individual gas cylinder packs using a Haskel booster pump. Mixtures were quantified using partial pressures. Mixtures and individual gases up to 100% concentration were prepared in this way.

12.4.4 Turbulence generator and igniter

There was a turbulence generator at the entrance to the first section of the duct; this consisted of a 50 mm by 50 mm square grid fitted with small deflector plates. It was sandwiched between the end of the transition section and the beginning of the duct. There was a spark igniter located 250 mm downstream from the beginning of the second duct section; it was attached through the top instrument port. The spark igniter itself was positioned on the centreline of the duct. This position was chosen to give the maximum run-up distance for the developing flame front. This was also consistent with CFD simulations, which had showed that the injected fuel and oxygen would be fully mixed into the engine exhaust stream before this point.

12.4.5 Velocity profile measurements

A pitot-static probe that traversed right across the duct was located through the optical viewing port on the fourth section of duct. This was used to obtain the pressure profiles across the duct, from which the mass flow rates along the duct were calculated for the test flow conditions. It was driven across the duct by a traverse operated by a stepper motor and its position recorded using a rotary encoder. The pressure profiles were recorded for each test or occasionally after a run of two/three tests if these had been completed in quick succession. These served as both a check on the consistency of the measurements and also as a basis for calculating the required oxygen and test fuel injection rates.

12.4.6 Building housing the rig

The complete test facility comprising the jet engine and the duct, with its associated components, was housed in an approximately 15 metre long by 3 metre wide by 3.5 metre high cross-section ventilated agricultural style building. The test duct was attached

directly to a substantial concrete pad, which could withstand the resulting dynamic reaction loads should a detonation occur within it. The duct was fixed at one point only, through an anchor plate attached at the entrance area of the duct. The rest of the duct was simply supported on bogies in order to allow for thermal expansion. The Rolls-Royce viper engine was mounted independently with a variable length connection between the exit from the turbine and the beginning of the diverter section. The HRSG part of the rig was housed in a 5 metre high by 6 metre wide extension to the original building.

The engine itself was housed in a semi open rectangular building isolated from the test section by a steel blast wall designed to prevent any fragments from a failed engine reaching the test area. The building walls were made from concrete blocks with a steel roof, and it was open at one end, being designed to contain any fragments resulting from the accidental release and ignition of flammable butane escaping from the engine fuel system. The building was also designed to contain any fragments that may result from a failed engine.

12.4.7 Engine control system

The engine control system makes use of a National Instruments cRIO system, which is effectively a PLC device that records engine parameters, and also has the ability to operate valves and switch pumps on/off using relays and pneumatic valves. This system records the following parameters: engine rpm, bearing oil pressure, fuel supply pressures in the butane fuel system (3 in total), exhaust temperatures, vibration, intake pressure, intake temperature, atmospheric pressure, fuel flow rate, and the status of all valves and oil level switches in the butane supply valves. Some of these parameters are used to calculate the engine intake mass flow rate. A variable speed positive displacement pump driven by a 3-phase inverter controls the speed of the engine. The cRIO communicates with the inverter drive to vary the speed of the pump, which in turn regulates the amount of fuel delivered to the engine. The engine operator from the control room alters the fuel demand to the engine.

This system communicates all its parameters via an ethernet link to a computer in the control room hosting software written in LabVIEW, which allows the user to operate the engine. The transmitted data is recorded locally on the engine control PC and is also received and recorded by the high speed data acquisition system. This means that it is not necessary to synchronise the two systems as the high speed DAQ system receives the data at the same time as the engine control PC does, at a rate of 10 Hz. The engine control system has remained the same basic system as used for WP 2.2. All recorded engine parameters are displayed on the computer in numerical and graphical form. The control system software for the engine was an adaptation of the established control system developed and used by SCITEK when running the Viper engine in its normal mode on kerosene.

This dedicated PLC system was programmed to control and ensure the prescribed safe operation of the engine, rig and facility. The engine is started using an electrical motor that spins it between 700-900 rpm; fuel is then injected using the pilot fuel injectors and ignited. When the engine speed goes above 2000 rpm the PLC switches the fuel to pass through the main fuel injectors, which are then used to bring the engine up to idle speed at around 5000 rpm. The engine control PLC is separate from the gas delivery PLC system.

Hardwired manual ESTOPs are provided on the engine frame and in the control room that can be used to shut down the engine in the case of an emergency. The PLC also monitors all measured parameters and initiates a software ESTOP condition if any parameter exceeds defined limits. The PLC prevents the engine from being restarted until all hardwired and software ESTOPs have been reset/cleared.

The PLC was located in a building close to the engine whilst the PC responsible for displaying and storing the engine parameters is located in the control room. For safety reasons this was situated approximately 90 metres from the engine and test area. Engine start, speed settings and shutdowns were always carried out from the control room.

12.4.8 Gas delivery control system

The engine operation and the fuel/oxygen injection systems were both controlled from the control room situated approximately 90 metres from the test rig, but in line-of-site.

A National Instruments PXI-SCXI system running a real-time operating system was used to facilitate operation of the gas delivery system. This system was essentially a PLC device with interfaces to record pressures at various points in the mixed gas and oxygen pipe work as well as mass flow rates. It also had the ability to activate valves and pressure regulators. Another important function that it carried out was PID control of the valves that regulated the flow rate for both the oxygen and mixed gas lines. As different mixtures of gasses were used with varying density it offered the ability to vary the PID parameters from the control room to suit each test condition. The GDS PLC also allowed the operator to activate the spark igniter inside the rig to initiate ignition of the injected gas mixture. It also had the ability to initiate data acquisition on the high speed data acquisition system.

As with the engine control PLC, all gas delivery system parameters were logged and transmitted over the ethernet network to a PC in the control room that featured a user interface that allowed the system to be operated remotely. The data transmission rate was 10 Hz. This system also recorded the engine speed (rpm) signal (the same signal that the engine control PLC was recording) for reference purposes. In order to avoid the need for synchronising each system, the same data transmitted to the GDS was also received by the high speed data acquisition system and was recorded with the high speed data in the same TDMS file. The user interface software for the GDS also recorded the data locally so that a separate file was generated for reference purposes and as a backup.

12.4.9 High speed data acquisition system

SCITEK designed and installed the data acquisition system on the rig, using hardware from National Instrument. This took the form of a PXI system with a number of fast data acquisition card, providing 64 channels of data that were sampled at a sampling rate of 100 kHz. The PXI system was also connected to an SCXI system which provided signal conditioning for thermocouples and other analogue input signals that did not require fast sampling. Thirty-two channels were available for thermocouples and eight channels were used to record the oxygen level, pitot traverse position, the pitot-static pressure across the duct, and engine rpm; the remainder being left as spare channels. On the SCXI all channels were sampled at 5 kHz but averaged down to a rate of 10 Hz. For these channels the response rate of the sensors was slow so a high recording rate was not

considered to be of any benefit, especially as averaging improved the accuracy of the measurements. In order to alleviate the need to synchronise all three data recording systems, the high speed data acquisition system was able to receive the data streams transmitted by the engine control and GDS PLCs over the network and record them, along with the high speed data, so that all data was time synchronised by default.

The PXI system used for the fast data logging was PC based running Windows 7. The data acquisition sampling rates were chosen to suit the response characteristics of each group of sensors. The gas delivery system and engine control parameters were streamed via the network at a rate of 10 Hz, and were recorded synchronously with the fast data streams. For the main ignition event, sensors for pressure, flame ionisation and optical flame sensing were sampled at 100 kHz. As stated above, a single TDMS file was generated by this system that included all 64 high speed channels, the 32 thermocouple channels, the 8 slow analogue input channels, and also the engine control and GDS parameters. The data acquisition software was written by SCITEK using LabVIEW. Data processing and analysis was facilitated using a commercially available software package called DIAdem, which is marketed by National Instruments and was ideal for analysing the large volumes of data generated. The size of each TDMS file generated by an ignition test varied from 0.3 to 2 GB so it was not possible to analyse such a volume of data using tools such as Microsoft Excel. It was also the case that the original hard drive in the PXI system was not always able to cope with the throughput of data streamed to it and was therefore upgraded to a fast solid state drive to alleviate the potential loss of data during recording.

12.5 INSTRUMENTATION

12.5.1 Sensor types and locations

The permanent instrumentation attached to the rig comprised type ‘K’ thermocouples, pressure transducers and optical sensors; both flame ionisation (IP) probes and optical flame (OP) probes. There were up to twenty-four flame ionisation probes positioned along the rig, together with twelve optical probes. There were also four rakes placed across the HRSG section of the rig, each containing three IP probes, giving an additional twelve ionisation probes. There were up to ten piezo-resistive pressure transducers, manufactured by Kulite, situated in strategic locations throughout the rig, together with an additional fast-response piezo-electric pressure transducer manufactured by PCB Piezotronics. This was only used to measure the incident pressure on the end wall of the HRSG when it was fitted.

There were also several type ‘K’ thermocouples attached to the duct for measuring both the gas and wall temperatures. The thermocouples measuring the gas temperature were inserted through the duct wall using the fixed transducer locations and protruded at least 50 mm into the flow in order to be clear of the thermal boundary layer. Those thermocouples measuring the wall temperatures were bonded to the external wall surface under the layer of insulation. There was a sampling probe near the end of the duct section of the rig that was used for gas sampling; but during testing it was connected to a Servomex oxygen gas analyser and measured the oxygen concentration in the flow.

Over seventy sensor ports were built into the HRSG extension to the rig in order to provide sufficient sensor location options to cover all of the perceived requirements. The

sensor port locations are shown in Figure 2. The actual sensor locations were decided upon initially following the commissioning trials, but were changed as the trials progressed to meet particular requirements. The intention had been that these remained the same throughout the test programme, however changes had to be made when, for instance, a sensor proved to be faulty or when additional information was needed, as was the case when the end wall was in place. Upon completion of a test a data template was prepared and issued to the ETI, showing amongst other things the precise locations of all of the sensors for that particular test. A typical example of the data template format used to indicate the types and locations of the sensors is shown in Appendix 12.7. Tests were only started when all the sensors fitted to the rig for that test were indicating that they were responding as expected prior to commencing a test. Occasionally, and upon completion of a test, an IP, rake or OP sensor did appear to have responded incorrectly or not responded at all. However, it was not always the case that a signal was to be expected, as no data from these types of sensors could be as important as the presence of data, as it could be the case that no flame was present at that particular location.

12.5.2 Flame ionisation (IP) Sensors

The flame ionisation sensors were manufactured in-house. Each of the 24 sensors used to detect flame arrival within the duct and HRSG was based on the principle that currents generated from the flame front arose from the raised but small conductivity change associated with the flame and were in the 5 µA range. This gave rise to voltages in the 0.2 - 1 V range when a load resistor of 100 kΩ was used. The devices were bench tested using a hand held propane flame, which was considered adequate for this purpose as the device is not sensitive to which particular flame ions are responsible for conduction. The hand-held propane torch flame was passed quickly through the sensor tips in the case of the IPs and passed across the front of the aperture for the OPs.

Since the circuit was purely resistive, response times were fast (e.g. < 0.1 µsec) and much less than the sampling intervals used within the data collection system, which were 10 µsec for flame detection. Due to the small signal currents, the sensor body needed to be kept dry as dampness in the external environment could give rise to a leakage current and a resulting DC offset voltage, which could be several volts. They were kept dry by heating each of the sensor tips at the start of each day's testing.

It was noted that, since the IPs were point measurement sensors, they only provided a signal if a high temperature flame front passed their location. Depending on the complexity of the flame development, this criterion was not always met at all locations. This was particularly true for weak combustion mixtures, such as those with relatively low EQR values.

12.5.3 Optical flame (OP) sensors

The twelve optical sensors were also made in-house and were located along the length of the duct and HRSG. These used a PbSe photoconductive element for sensing radiation in the visible and near IR range. The sensing cell used a Hamamatsu P9696 device, which is 3 x 3 mm in size with a reported response time (t_{90}) of 2 - 3 µsec. The sensor had wavelength sensitivity in the visible region and out to 4.5 µm wavelength, which made it suitable for the detection of water vapour and carbon dioxide emissions from vibrational stretching modes at around 3 µm. Note that this differs from UV detection

from OH radicals, which would not be suitable for the present application. Water vapour is of course also present in the engine exhaust during normal running, but this only becomes visible to the detector when the flame front is present due to the temperature difference between the exhaust gas and the combustion flame front. As with the IP devices, the OPs were tested using a hand-held propane flame, which again was appropriate due to the wide detection bandwidth of the detector.

The detection circuit was set up in order to block the large DC offset arising from the 28V power supply, so the output was the first derivative of the input signal due to the rate of flame radiation arriving at the sensor. The input side of the photocell was sitting at around -15V and, as the resistance dropped with flame radiation arriving, this voltage went more +ve. The first change seen on the output was therefore a signal rise and for a radiation pulse input, the output was a sharp +ve pulse followed by a sharp -ve pulse. The cross-over point at zero volts corresponds to the maximum of the flame radiation (i.e. where the derivative is zero).

In general, for a flame front arriving, which is followed by high temperature combustion gases (i.e. a step change in temperature), the signal took the form of a positive pulse, where the maximum corresponded to the maximum rate of change of radiation emission within the flame front or brush.

The receiving aperture at the open end of the device body set the viewing angle subtended from the sensor. For these tests a sapphire receiving lens of 50 mm focal length was used, with the objective of creating a collimated collection path of around 15 mm diameter. In principle, since the OPs were collecting radiation from across the duct diameter, they provided a different flame detection opportunity from the IPs and would generate a signal when some individual IPs would not.

It was also noted that the IPs and OPs were considered 'on' or 'off' devices with the sole purpose of detecting when a flame front arrived. There was no intent with these to extract any particular flame properties and therefore no calibration procedures for these were undertaken prior to use. Each of the devices was bench-tested to confirm flame detection prior to use and this process was repeated regularly to confirm correct operation. During this procedure, the data collection system was used to sample the signal in the normal way to confirm correct operation.

12.5.4 Pressure sensors

The primary types of pressure sensors (ten in total) used during the test programme were those based on piezo-resistivity, manufactured and supplied by Kulite in the UK. The particular series used was Kulite XTEH-10L-180 (M). Several different sensors from this series were used depending on availability, thus sensors with different pressure ranges and threads were used. Additional protection was provided for the sensors by mounting them in water-cooled jackets. These types of sensor are able to withstand operating temperatures of up to 540 °C, thus making them more suitable for the operational environment of the experiments being conducted.

These sensors were also chosen because they offered a higher operating temperature range than piezo-electric alternatives, although their frequency responses were less (being typically 50-100 kHz). A protective diaphragm placed across the sensing element limited their response. This was not considered to be an issue as the sampling rate of

the data logger was set at 100 kHz. This limiting value was chosen on the assumption that the tests would produce mild to fast deflagrations with flame speeds well below the sound speed of the exhaust gas mixture and with the pressure waves travelling sonically.

A single PCB Piezotronics-supplied 0-70 bar pressure sensor, Type 113B24, was used in some of the tests to measure the pressure reflected off the end wall of the HRSG. This sensor was also fitted into a water-cooled jacket as supplied by the manufacturer.

Further information regarding the pressure sensors is given in the Basis of Design and Commissioning reports for the task 2 and task 3 test rigs [1-4].

12.5.5 Velocity measurements

The velocity profiles across the duct were determined using a pitot-static probe to measure the dynamic pressure of the flow. The probe was manufactured and calibrated by Kimo UK. This probe also had a thermocouple attached near the tip and this was used to obtain temperature profiles across the duct at the same time as the pressure profiles. An RS supplied GEMS differential diaphragm pressure transducer, type 5266250LBHT1C-RS, 0 – 250 Pa, was used for the pressure measurements,. These measurements were made at the start of or immediately after each test during the test programme. In this way velocity profiles across the whole of the duct were obtained, from which duct mass flow rates were obtained by integration of the velocity and density profiles.

12.5.6 Temperature measurements

Temperature measurements were made using between twenty one and twenty four type ‘K’ thermocouples for all of the wall and gas temperature measurements made on the rig. They were supplied calibrated to be within ± 2 ^{0}C at 600 ^{0}C. They were sampled at a rate of 10 Hz and logged on the engine and control system loggers. Their outputs were time-synchronised with the rig’s high speed logging system and their locations were as shown on the data templates used to summarise the test results, a typical example of which is shown in Appendix 12.7.

The sampling rate of 10 Hz was considered appropriate for the thermocouples given that their dynamic response times in the gas phase were several seconds, depending on the turbulence levels and the resulting heat transfer coefficient. Typically, flame temperatures were established in less than a second after an ignition, but the thermocouple response grew over the following few seconds, which was a measure of their normal time response under the test conditions. Consequently, the thermocouples were unable to record the peak gas temperatures but did provide an indication that an ignition had occurred and to some extent its severity.

Accurate measurements were made of the gas and wall temperatures prior to any ignition as there was ample time allowed for these temperatures to stabilise.

12.5.7 Ignition system

The ignition system used to provide a spark ignition source was an 8-10 Joule spark unit supplied by Rolls-Royce. Once triggered by the gas injection system it sparked repeatedly at a rate of once every 1.5-2 seconds. The spark plug was a standard gas turbine igniter as supplied by Vibrometer. It was located on the axis of the duct through

a rigid plug extension, which maintained it normal to the flow along the centreline. It was located through the top of the second duct section, 250 mm from the beginning of it. Other locations were available but were not used in these tests. It was noted that the discharge of the igniter capacitor produced an electrical pulse on a number of signal channels. This is not unusual on signal acquisition systems where large EM fields are present. It did not interfere with the measurements on the signal channels. Due to the narrowness of this pulse (~5 µsec) it could also be used when necessary as an indicator of the time of an ignition. The occurrence of this pulse on the signal channels after the start of data acquisition was variable due to the time it took for the discharge capacitor to reach its discharge voltage.

12.5.8 LDA Velocity and turbulence measurements

The velocity profiles and turbulence levels (x and y directions only) across the entry plane to the HRSG tube bank were measured with the HSL-owned TSI-manufactured LDA system. The measurements were made at five different vertical locations as shown in Figure 2, using the same 2 metre long traversing mechanism that was used for traversing the pitot-static probe across the 600 mm duct section of the rig. The optics were arranged so that the laser beams entered through the 150 mm diameter quartz glass optical viewing windows situated as shown, starting at the lowest and working upwards. The end plate was attached to the rig thus ensuring that the set-up was representative of a typical industrial HRSG with the flow exiting through a vertical stack.

The system utilised fibre optics to transmit four beams, two blue and two green, from a 4W Lexel 95 argon ion laser source. The system used a probe volume size of around 1 mm in length and 0.1 mm in width. An advantage of this system was that the probe was factory set and the beams always crossed so it greatly reduced the risk to the experiment as well as providing good quality data. This system was operated in back scatter mode which again had the advantage that the scattered light came down an optical fibre that was factory set with no adjustment being necessary. The working distance of this system was close to 1 metre as a longer through-lens could not be borrowed or hired from anywhere, because it was not something that was widely used. Although this path length did not cover the full width of the HRSG it was considered the best option in order to obtain good quality measurements across the majority of the width of the HRSG. A Dantec BSA-F80 two component signal processor was used to convert optical signals to flow velocity in the axial and vertical directions.

The Dantec transmission optics were considered unsuitable as they had steerable beams and also steerable receiving optics which, although good for a laboratory environment, were known to be affected by temperature changes. They were therefore considered vulnerable to the open air environment of the HRSG rig and the hot exhaust temperatures within it. It was therefore decided that using these optics would have significantly reduced the chances of obtaining good quality data.

- The high temperature of the flow stream necessitated the use of solid particle seeding using the SCITEK LS-10 seeder. The seeding material used was titanium oxide powder with a grain size of one micron. An extensive literature database supports the use of this seeding material and this size range for gas flow measurements. Provided that aggregation is avoided by keeping the material dry, then this particle size and material is known to be able to follow the

flow and turbulence fluctuations up to several kHz. The seeding was injected across the flow using a rake located just downstream of the gas injection pipes though one of the ports along the centreline of the rig. It proved necessary to dry and then heat the air going to the seeder to ensure that the powder was dry enough to be dispersed effectively into and across the rig.

- The rake was downstream of the turbulence generator screen. The LDA and seeding systems were operated remotely from the control room. Some time and effort was spent getting the seeding system to work satisfactorily and providing sufficient particles to give statistically meaningful results.

All of the LDA measurements were made with the engine running at 11,800 rpm, which corresponded to an average velocity in the duct section of the rig of 85 m/s at a temperature of 550 °C. The results obtained were the mean velocity, which was usually averaged from up to several thousand particles passing through the LDA probe volume, and the turbulence intensity, comprising the distribution of velocity about the mean velocity. Both measurements were calculated by the system and presented as the results. Each traverse took approximately one hour due to the time required by the LDA system to acquire the data.

12.6 RIG OPERATING PROCEDURES

12.6.1 Safety procedures

Several HAZOP studies and risk assessments were undertaken to explore and control the hazards associated with the operation of the rig and the subsequent trials. The initial HAZOP studies were split into three areas; the butane isolation, its separation, and the gas feed system. Further HAZOP studies were made of the fire and explosion hazards associated with the test rig and the engine. A basis of safety was established from these HAZOP studies that applied to the design and construction of the rig itself and subsequently to its routine operation. The latter included the handling of the flammable and toxic gases used for the test programme. Outcomes from the HAZOP studies were incorporated into the rig operational risk assessments Refs [16-20].

Consequently, during the trials the main basis of safety was the exclusion of personnel from the experimental test rig and the 200 metre exclusion zone which surrounded it. This exclusion zone was calculated to ensure that personnel were protected from blast, ejected parts, thermal radiation, noise and toxic hazards. The exclusion zone was enforced by HSL staff (sentries), which is standard practice for many other experiments undertaken at the HSL site. In the unlikely event that there was an incursion into the exclusion zone, the sentries could immediately advise the trials officer in the experimental control room. Consequently the experiment would be abandoned and the rig placed into isolation mode. This was achieved immediately, remotely and securely by key switch operation.

After a trial was completed the basis of safety shifted to the isolation of both the butane and gas feed systems. Due to the use of asphyxiating, oxidising and flammable gases, isolation was paramount.

12.6.2 Hazards associated with the trials

The potential hazards of the trials were:

- Fire

  There was a potential for fire as flammable fuels were used on site including butane, methane, hydrogen and carbon monoxide. The designs of the gas storage compounds and the gas injection systems ensured that there were separated isolated states for these systems when not in use.

- Explosion

  A study was undertaken by HSL's Explosives Team using the US NRC (US Nuclear Regulatory Commission) model. This study modelled the blast overpressure of a detonation of either methane or hydrogen in the most undesirable (i.e. a stoichiometric) mixture in the duct. The pressure resulting on the area around the rig was then determined. This modelling provided:

  - Assurance that the walls erected around the rig would remain intact and therefore provide on-going protection to adjacent plant (e.g. bulk gas storage) resulting from direct blast and/or ejected parts.
  - A separation distance between the rig and people that would protect them against effects of blast.

- *Toxic Exposure*

  A study was undertaken by HSL's Consequence Modelling and Risk Assessment Team using the PHAST (Process Hazard Analysis Software Tool) system. This modelled a rapid release of carbon monoxide whilst the engine was running. This was based upon a release of some 4 kg of carbon monoxide, a volume of approximately 4,000 litres at NTP. A HAZOP study was then undertaken to identify and implement control measures to ensure the safe handling of potential asphyxiates.

- Noise

  The hazard that determines the largest exclusion zone was exposure to noise. Here a minimum exclusion zone of 230 metres from the rig was indicated. The noise associated with the running of the Viper engine cannot be reduced therefore control measures such as personnel exclusion and the use of ear protection were introduced.

12.6.3 Calibration procedures

Of the four sensor types installed in the test rig (pressure transducers, thermocouples, optical probes and ionisation probes) only the pressure transducers and thermocouples were subject to a formal calibration procedure. The optical probes and ionisation probes did not require calibration as their mode of operation effectively makes them indicators only.

Calibration of the pressure transducer and thermocouple channels was carried out using a Druck DPI620 calibrator (see Table 19), which was supplied and maintained by SCITEK and calibrated annually by the Drück Standards Laboratory. The Drück unit is

calibrated in accordance with the requirements of UKAS and international standards ISO/IEC 17025.

Table 19: Details of Drück calibrator used for calibration of pressure and temperature measurement channels

	Manufacturer	Druck
	Model	DPI620
	Serial Number	02918726
	Calibration certificate number	0058874

12.6.4 Pressure Transducers

The pressure transducers were supplied complete with certificates of calibration but were re-calibrated 'in situ' as a complete unit comprising sensor, amplifier (where fitted) and data acquisition card. This calibration was carried out prior to first use and then periodically during the test programme.

The gain and offset for each of the pressure sensor channels was set to 1 and 0 respectively. The sensors were each then systematically subjected to known pressures using the Drück calibrator at a minimum of 5 points and across the full sensor range. The data obtained was plotted and a linear regression applied to produce scaling (gain) and offset factors which were applied to the appropriate channel output. All the sensors calibrated showed excellent linearity with correlation coefficients (R^2 value) of 1.

The periodic checks on the calibrated sensors were carried out, usually following a period of inactivity or significant change in configuration i.e. sensor relocation. These were done using the Drück calibrator, with a known pressure being applied to the sensor and compared with the displayed value (in barg). Any significant variations in these results would require the sensor unit to be recalibrated. However, all of the calibration checks have proven to be consistently accurate and recalibration has not been necessary.

The calibration of the PCB pressure transducer was carried out in a similar way but due to drift it was essential that the application of pressure was achieved rapidly. A methodology was developed whereby a known pressure was applied to a small pressure vessel to which the sensor was attached. The output from the sensor was zeroed before rapidly discharging the stored pressure to 0 barg, which generated a negative signal whose amplitude was proportional to the gauge pressure to which the vessel had been charged. This occurred within 10 seconds of the zeroing procedure, during which time no drift was observed. This procedure was carried out at a number of pressures across the range 0 to 10 bar. The obtained data was plotted and a linear regression applied to produce scaling and offset factors that were applied to the appropriate channel output in the data acquisition software. During normal testing, any drift on the PCB was used as the baseline from which combustion generated pressures were measured.

12.6.5 Thermocouples

All the type 'K' thermocouples conformed to British Standard BS EN 60584-1:2013. The temperature measurement channels were calibrated using the Drück DPI620 calibrator,

which supplied voltage values in accordance with standard IEC 584. The range of temperatures and measurement uncertainties are shown in Table 20.

Table 20: Temperature calibration ranges of Drück DPI620 calibrator and measurement uncertainty values

Type	Standard	Temperature Range				Total uncertainty	
		°C		°F		°C	°F
		From	To	From	To		
K	IEC584	-270.00	-220.00	-454.00	-364.00	4.00	7.20
		-220.00	-160.00	-364.00	-256.00	1.00	1.80
		-160.00	-60.00	-256.00	-76.00	0.50	0.90
		-60.00	800.00	-76.00	1472.00	0.30	0.54
		800.00	1370.00	1472.00	2498.00	0.50	0.90

Each of the temperature channels were calibrated at several temperatures and the applied value compared to the temperature reading value. The results of the calibration were recorded and in all cases showed the output value to be within ±1 °C of the applied temperature.

12.6.6 Ionisation Probes

The ionisation probes were not calibrated as they are effectively indicators, sensing the arrival of the flame along the tube wall. However, functionality of the sensors was periodically checked by taking them out of the rig and applying a flame from a butane torch across each of the sensor tips.

Further details of the operation of the ionisation probes can be found in Section 12.5.2.

12.6.7 Optical Probes

The optical probes were *not* calibrated as they are effectively indicators, sensing the arrival of the flame front across the diameter of the horizontal centreline in the tube.

Further details of the operation of the optical probes can be found in Section 12.5.3 and a discussion of the performance of both the optical and ionisation probes can be found in Section 6.4.

12.6.8 Operating procedures

Operating procedures were developed during commissioning as the process developed and staff became familiar with the system's idiosyncrasies and safety requirements. After several iterations two written operational procedures were developed, one covered operation with flammable gases only, the second with toxic gases added. These were used to draw up check lists that the system operators were required to follow during the experimental test programme.

The essence of these procedures was as follows:

- On the designated test day, checks were made for, and to ensure, correct functioning of all the required instrumentation by following the prescribed procedures.
- The test gas mixture required was then made up by filling the gas reservoir with the lightest gas first then adding the next heavier component(s). The correct gas mixture ratio was obtained using partial pressures. When a toxic gas was being used any person approaching and opening the toxic gas bottle filling valve was required to wear BA.
- The gases were thoroughly mixed by recirculating through the Haskel gas pump for a minimum of one hour.
- The liquid butane, which would fuel the Viper gas turbine, was also recirculated through the butane supply system at approximately the same time.
- The engine control software and the data logging system were readied for operation.
- The appointed Trials Officer then placed lookouts at chosen points on the exclusion zone boundary. They were in radio contact.
- Given the all clear, the gas turbine was started and run up to the operating speed of 11,800 rpm.
- After some five to ten minutes of running to allow the gas temperature to stabilise, a pitot-static probe traverse was made across the duct. The results were used to obtain the mass flow rate from which the required fuel mixture and oxygen injection rates were calculated to meet the EQR requirements of the particular test conditions being investigated. The results were logged and filed.
- After a series of safety checks, the siren was sounded and then the actual test proceeded with the injection first of all of sufficient oxygen to restore the level in the exhaust stream to a maximum of 21%. This was followed by injection of the required fuel to give the required EQR. These were injected into the exhaust downstream of the engine turbine. This procedure reduced the exhaust stream temperature by approximately 50 °C.
- The flammable gas/oxygen mixture injection process lasted for no more than 10 seconds, during which time ignition of the mixture was undertaken using the electrical spark situated axially downstream of the fuel injection point. This also started the data recording process. Immediately after ignition the fuel and oxygen supplies were automatically stopped by the controlling software.
- If an ignition occurred the engine was slowed down and a check made of the data, which was subsequently filed and backed up.

In order to stabilise the gas temperature along the duct, the operating procedure required the engine to run for up to ten minutes prior to injecting fuel and oxygen. A typical operating gas temperature, after injecting the test gas and oxygen, was expected to be about 500-550 °C. During this process the duct walls were heating up but at no point in the test did they reach thermal equilibrium. However, the heat losses to the duct walls

were minimal but in any case the wall temperatures were recorded throughout the test period.

During each test the dynamic pressure and static temperature were measured across the diameter of the duct using the pitot-static probe and thermocouple with the engine running at 11,800 rpm. This information was used to calculate the exhaust mass flow rate, from which the required injected mass flow rates of oxygen and fuel mixture were calculated based on the required EQR for that particular test. It was observed that the exhaust mass flow rate was very reproducible during all of the tests at a value of 9.24 kg/s. The exhaust oxygen was monitored using a Servomex analyser and this provided a repeatable value of 17.2% at the agreed running condition. This resulted in an oxygen make-up injection rate of 0.501 kg/s. Note that a deviation from this injection rate of ± 0.02 kg/s results in a deviation in the exhaust oxygen level from 20.85 to 21.15%. It was in fact observed that the controller operation resulted in a usual range for the oxygen injection level of 0.48 - 0.52 kg/s. For each test a target EQR was set and the fuel mass flow rate calculated and entered into the control system parameters. Following a test, the actual fuel mass flow rate was extracted from the data and the actual EQR re-calculated. This was the value quoted for each test.

The composition of the engine exhaust gas has been reported in the earlier Commissioning Report [4] and these values have been used to calculate the molecular weight of exhaust gas, both for fuel injection calculations and sound speed estimations when required. The molar % values used for the engine exhaust were as follows: N_2 76.46, O_2 16.50, H_2O 3.72, CO_2 2.47, and Ar 0.88. The input values to this calculation were based on the user's choice for the particular test being run. For example, the fuel mixture composition was input as the mole fractions of each gas in the mixture already prepared and the oxygen mole fraction in the exhaust was measured separately with the engine running at the normal operating condition. The exhaust mass flow rate was calculated separately as previously discussed.

The recording system was triggered to start recording by the ignition spark and it was terminated by the closing of the mixture supply valve. During the WP 2.2 set of tests using carbon monoxide it was observed that auto-ignition had occurred shortly after commencing the fuel mixture injection process and before the ignition system had been triggered. As a consequence the data recording system had not recorded the event. A modification was therefore made to the software controlling the data recording system which allowed the recording system to be started manually. This was used for the carbon monoxide based tests reported herein. It resulted initially in larger data files but these were clipped to contain only the relevant data prior to being issued.

12.6.9 Safety record during testing

During the course of the test programme there were no significant safety related incidents that brought into question the originally established basis of safety as identified through the HAZOP and risk assessment studies undertaken originally.

During commissioning of the rig for the WP 2.2 test programme there were some modifications made to the system that could be considered safety related. These were detailed in the WP 2.2 test report [15] and remained in place for this the WP 2.3 test programme.

After completion of the tests with the end of the HRSG being left open, a vent stack was designed and fitted to the top of the HRSG exit slot in order to vent the combustion products upwards and out of the building enclosing it, once the end wall was attached to the HRSG. The original stack design proved to be inadequate as it was damaged in the course of testing by the negative pressure wave resulting from the expulsion of combustion products through the vent. Modifications were made in the form of strengthening ribs welded around the original stack together with the welding of a mounting bracket around the perimeter of the exit slot. The latter provided a more substantial base for attaching the stack to the HRSG. These modifications proved satisfactory as the modified stack served its purpose for the remainder of the test programme.

The final design of the exit stack is shown in Figure 34.

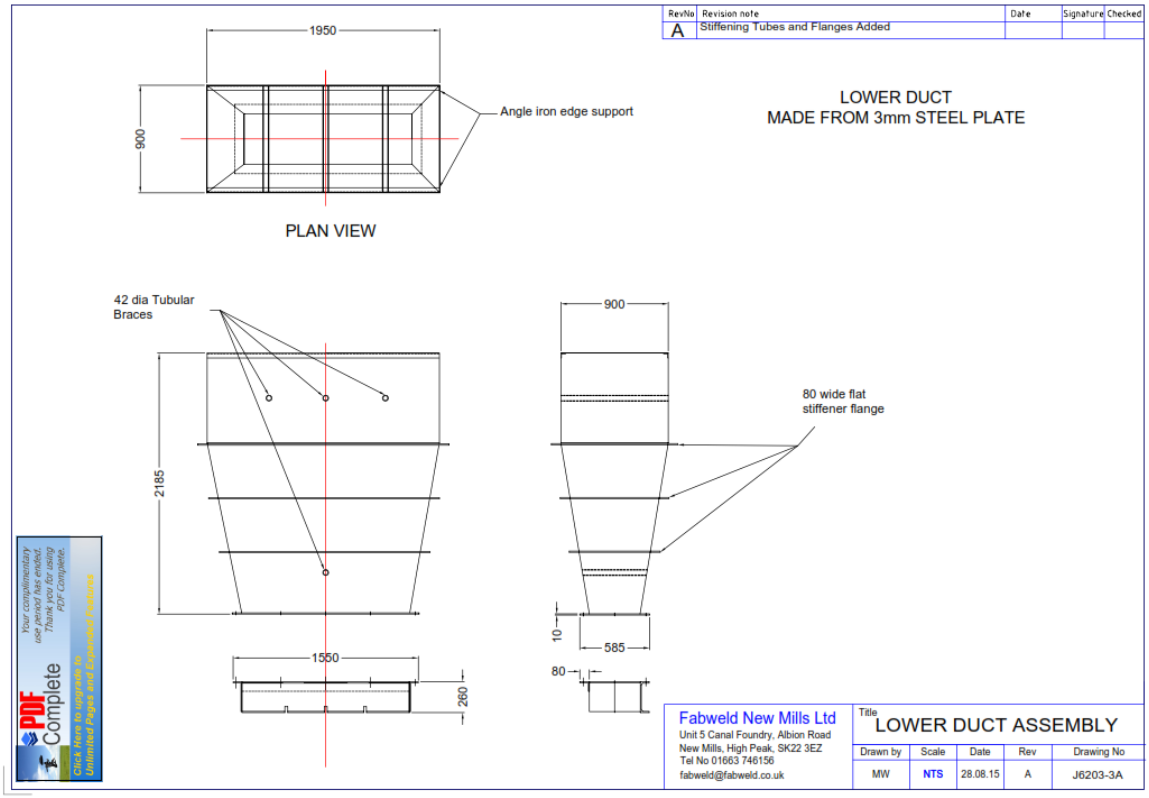

Figure 34: Design of vent stack.

12.7 TEST DATA OUTPUT TEMPLATE (DOT) SCREENSHOTS

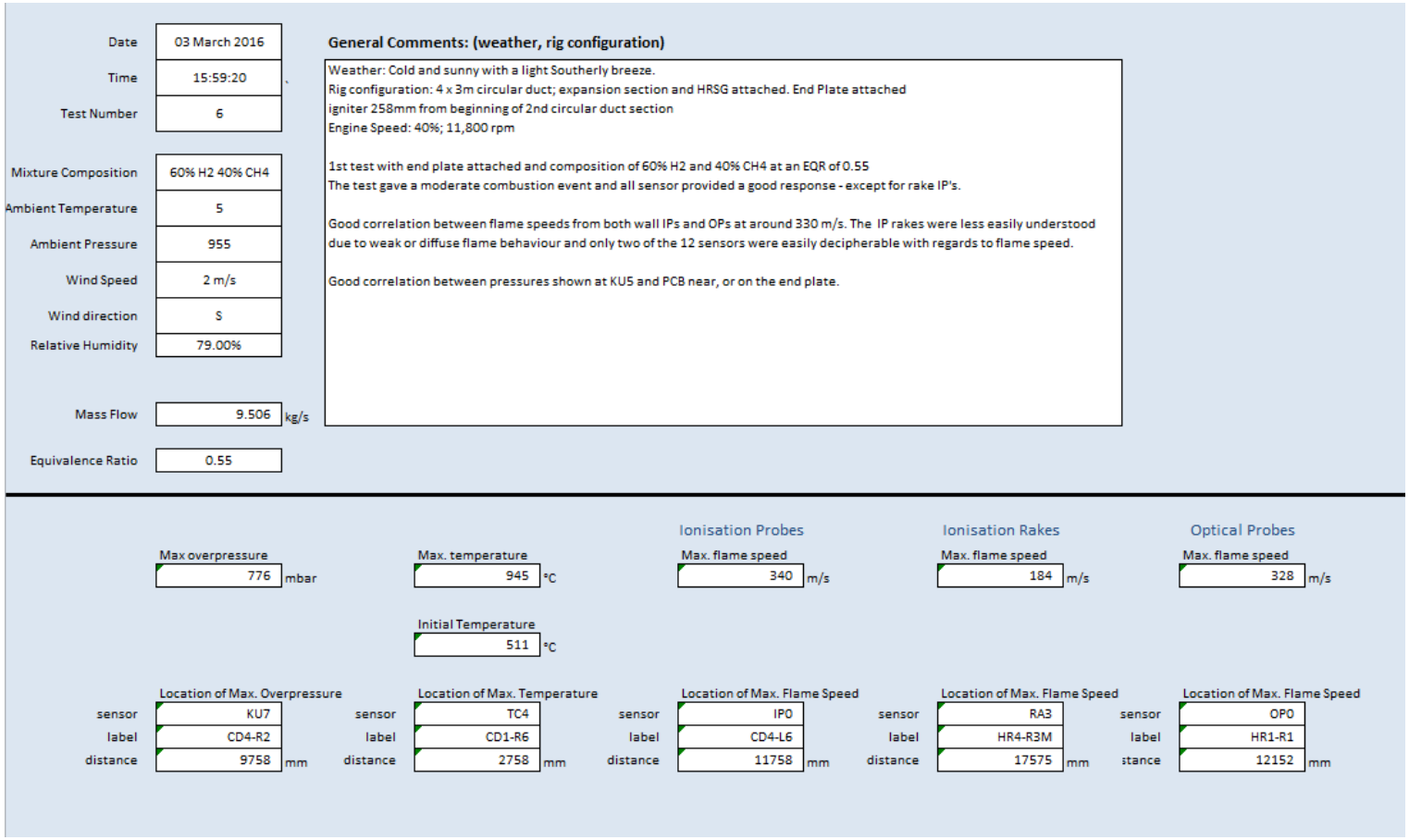

Date	03 March 2016
Time	15:59:20
Test Number	6
Mixture Composition	60% H2 40% CH4
Ambient Temperature	5
Ambient Pressure	955
Wind Speed	2 m/s
Wind direction	S
Relative Humidity	79.00%
Mass Flow	9.506 kg/s
Equivalence Ratio	0.55

General Comments: (weather, rig configuration)

Weather: Cold and sunny with a light Southerly breeze.
Rig configuration: 4 x 3m circular duct; expansion section and HRSG attached. End Plate attached
igniter 258mm from beginning of 2nd circular duct section
Engine Speed: 40%; 11,800 rpm

1st test with end plate attached and composition of 60% H2 and 40% CH4 at an EQR of 0.55
The test gave a moderate combustion event and all sensor provided a good response - except for rake IP's.

Good correlation between flame speeds from both wall IPs and OPs at around 330 m/s. The IP rakes were less easily understood due to weak or diffuse flame behaviour and only two of the 12 sensors were easily decipherable with regards to flame speed.

Good correlation between pressures shown at KU5 and PCB near, or on the end plate.

		Ionisation Probes	Ionisation Rakes	Optical Probes
Max overpressure	Max. temperature	Max. flame speed	Max. flame speed	Max. flame speed
776 mbar	945 °C	340 m/s	184 m/s	328 m/s
	Initial Temperature			
	511 °C			

Location of Max. Overpressure		Location of Max. Temperature		Location of Max. Flame Speed		Location of Max. Flame Speed		Location of Max. Flame Speed	
sensor	KU7	sensor	TC4	sensor	IP0	sensor	RA3	sensor	OP0
label	CD4-R2	label	CD1-R6	label	CD4-L6	label	HR4-R3M	label	HR1-R1
distance	9758 mm	distance	2758 mm	distance	11758 mm	distance	17575 mm	stance	12152 mm

Figure 35 DOT - test summary sheet

Location of igniter 3258 mm Time of ignition 19.06463 seconds

IP Number	Location label	Data Name	Position in tube (mm)	Flame arrival time (s)	Avg Flame speed from last sensor (m/s)
IP4	CD4-L1	Flameion_4	9258	19.1064	144
IP5	CD4-R1	Flameion_5	9258	19.1056	146
IP2	CD4-L5	Flameion_2	11258	19.1139	268
IP3	CD4-R5	Flameion_3	11258	19.1128	281
IP0	CD4-L6	Flameion_0	11758	19.1153	340
IP1	CD4-R6	Flameion_1	11758	19.1144	303
IP6	HR1-R2	Flameion_6	13160		
IP7	HR2-R3M	Flameion_7	14140	ND	
IP8	HR2-R5M	Flameion_8	14745	ND	
IP10	HE2-R1M	Flameion_10	16090	19.1034	-394
IP12	HR4-R1M	Flameion_12	16985	19.1139	85
IP13	HR4-L1L	Flameion_13	16985	19.1139	
IP14	HR4-R5M	Flameion_14	18165	19.1140	196
IP15	HR5-R2M	Flameion_15	18775	19.1141	
IP16	HR5-L2L	Flameion_16	18775	19.1296	114
IP17	HR6-R1M	Flameion_17	19985	19.1446	40
IP19	HR6-L3L	Flameion_19	20575	ND	
IP18	HR6-R5M	Flameion_18	21165	19.1427	182
IP20	HR6-L5L	Flameion_20	21165	19.1453	152
IP9	#N/A	Flameion_9	#N/A		
IP11	#N/A	Flameion_11	#N/A		
IP21	#N/A	Flameion_21	#N/A		
IP22	#N/A	Flameion_22	#N/A		
IP23	#N/A	Flameion_23	#N/A		

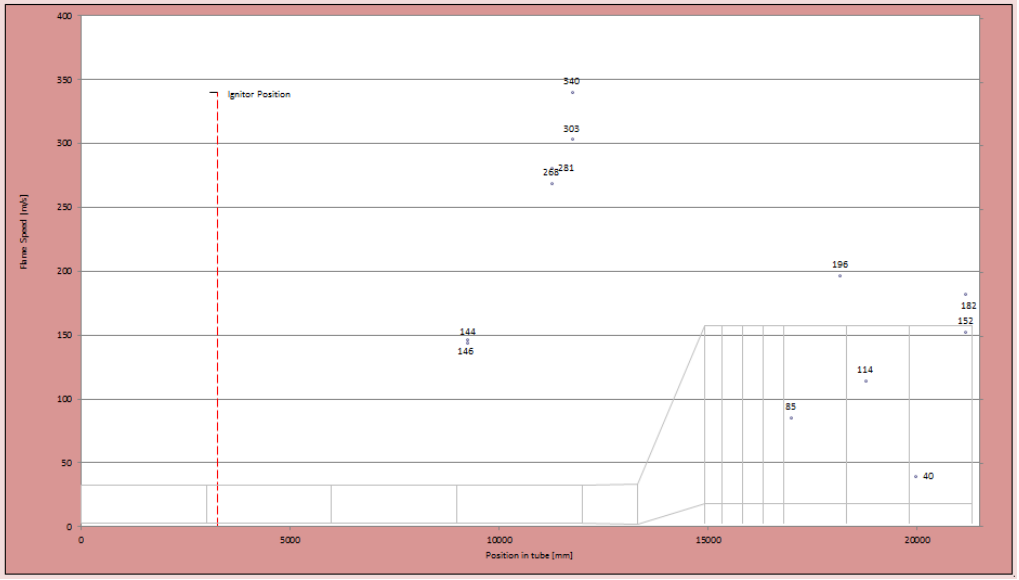

Figure 36 DOT - wall ionisation probe data summary

Location of igniter 3258 mm Time of ignition 19.06463 seconds

Rake Number	IP Number	Location label	Data Name	Position in tube (mm)	Flame arrival time (s)	Avg Flame speed from last sensor (m/s)
RA1	IP24	HR2-R2M	IP24	13785	ND	
RA1	IP25	HR2-R2M	IP25	13785	ND	
RA1	IP26	HR2-R2M	IP26	13785	ND	
RA2	IP27	HR2-R4M	IP27	14475	ND	
RA2	IP28	HR2-R4M	IP28	14475	ND	
RA2	IP29	HR2-R4M	IP29	14475	ND	
RA3	IP30	HR4-R3M	IP30	17575		
RA3	IP31	HR4-R3M	IP31	17575	19.1472	173
RA3	IP32	HR4-R3M	IP32	17575	19.1425	184
RA4	IP33	HR5-R4M	IP33	19375	ND	
RA4	IP34	HR5-R4M	IP34	19375	ND	
RA4	IP35	HR5-R4M	IP35	19375	ND	

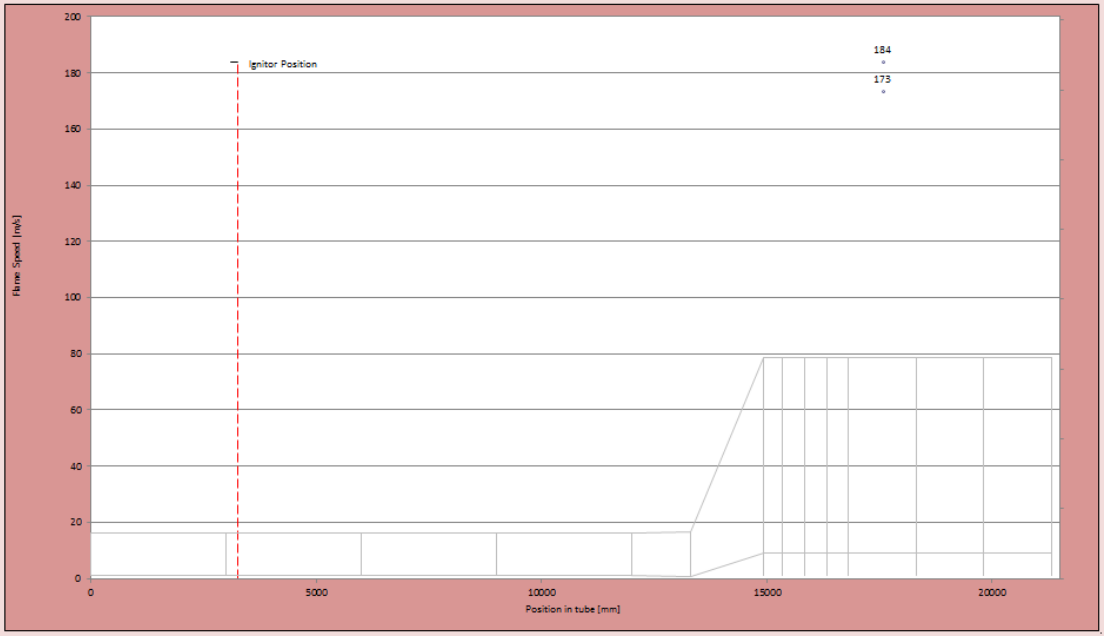

Figure 37 DOT - rake ionisation probe data summary

Location of igniter 3258 mm

Transducer number	Location	Position in tube [mm]	ΔPmax [mbar]	TimeΔPmax [mbar]
KU6	CD3-R5	8258	757	19.1648
KU7	CD4-R2	9758	776	19.1650
KU8	HR2-T5	14745	455	19.1579
KU9	HR3-L1L	15140	400	19.1588
KU0	HE1-R1U	15600	467	19.1373
KU1	HE3-R1L	16580	361	19.1538
KU2	HR4-R1U	16985	390	19.1426
KU3	HR5-R2L	18775	500	19.1507
KU4	HR5-L2M	18775	454	19.1506
KU5	HR6-L5M	21165	648	19.1463
PCB	EP-1M	21330	741	19.1463
KU10	#N/A	#N/A		
KU11	#N/A	#N/A		

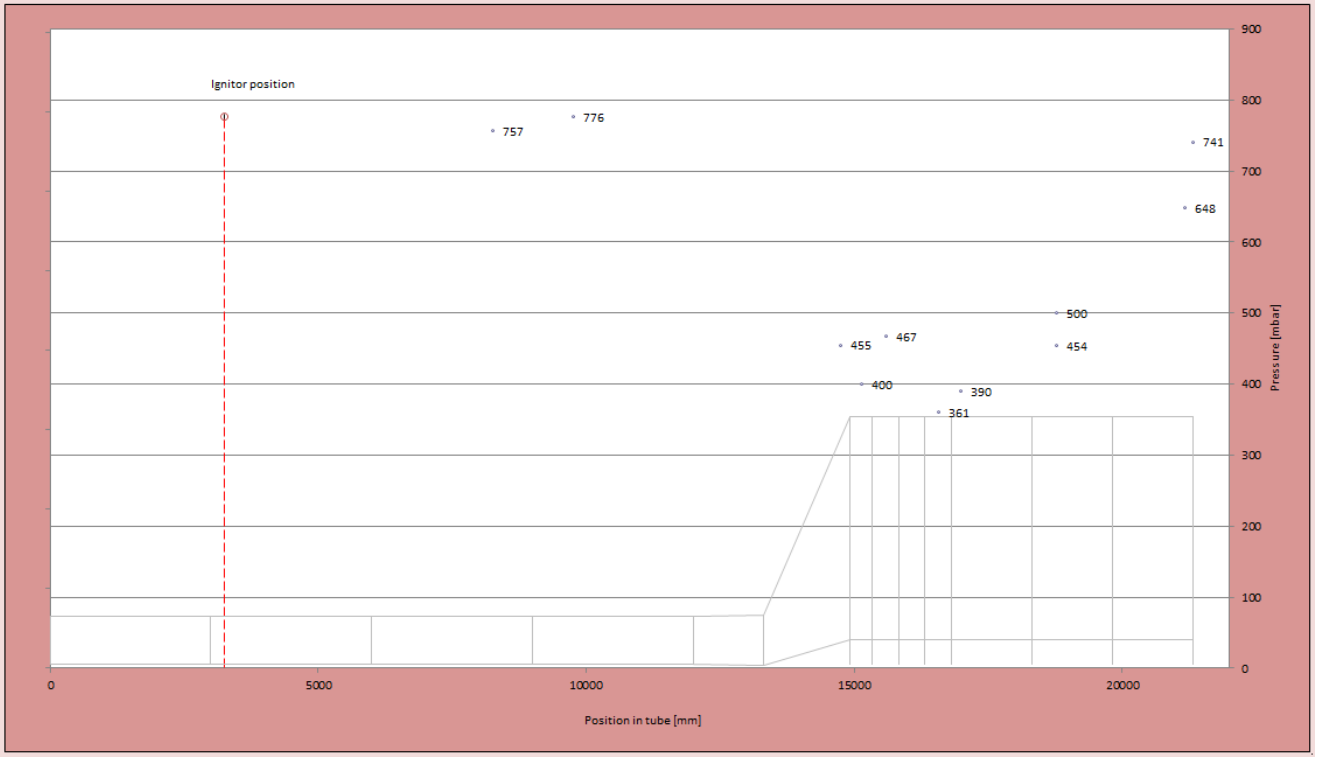

Figure 38 DOT - pressure transducer data summary

Location of igniter 3258 mm Time of ignitio 19.06463 seconds

OP Number	Location label	Position in tube (mm)	Flame arrival time (s)	Average flame speed (m/s)
OP11	CD4-L3	10258	19.1119	
OP10	CD4-R4	10758	19.1136	306.7
OP0	HR1-R1	12152	19.1178	328.0
OP1	HR2-T3	14215	19.1342	125.9
OP2	HR2-L5M	14745	19.1354	190.9
OP3	HE1-T1	15600	19.1364	185.1
OP4	HE3-T1	16580	19.1502	
OP5	HR4-R1L	16985	19.1412	291.6
OP6	HR4-T1	16985	19.1417	263.8
OP7	HR5-T2	18775	19.1509	193.5
OP8	HR6-T3	20575	ND	
OP9	HR6-R5U	21165	ND	
OP12	#N/A	#N/A		
OP13	#N/A	#N/A		
OP14	#N/A	#N/A		
OP15	#N/A	#N/A		

Flame detected on OP4 happens later than would be expected compared to other probes and so reliable flame speed calculation not possible.
The flame arrival at OP7 is not at its maximum intensity.

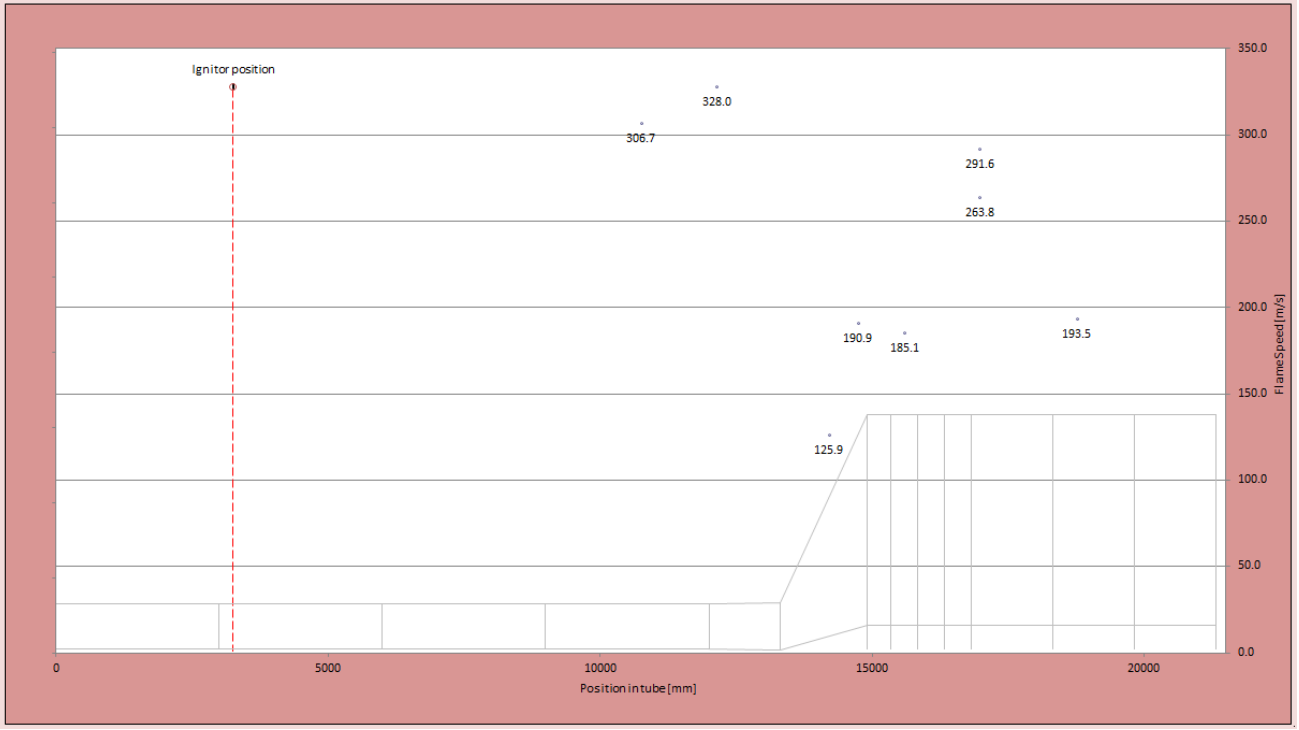

Figure 39 DOT - optical probe data summary

Location of igniter 3258 mm

Thermocouple number	Location	Position in tube (mm)	T_{max} (deg C)	T_i (deg C)
TC0	CD1-R3	1258	469	467
TC2	CD1-R4	1758	499	496
TC3	CD1-R5	2258	574	487
TC4	CD1-R6	2758	945	511
TC5	CD2-R2	3758	186	170
TC7	CD3-R2	6758	928	446
TC9	CD3-R6	8758	841	426
TC11	#N/A	#N/A		
TC12	#N/A	#N/A		
TC13	#N/A	#N/A		
TC14	#N/A	#N/A		
TC15	#N/A	#N/A		
TC16	HR2-R5L	14745	675	396
TC17	HE2-R1U	16090	267	256
TC18	HR6-R3L	20575	218	153
TC19	#N/A	#N/A		
TC20	HE2-R1L	16090	412	375
TC22	#N/A	#N/A		
TC23	HR6-R5L	21165	277	239
TC24	HR2-L3M	14140	573	359
TC25	HR2-L5L	14745	634	367
TC26	HR3-L1M	15140	676	388
TC27	HR3-L1U	15140	584	392
TC28	HR4-L1M	16985	250	224
TC29	HR5-L2U	18775	262	219
TC30	HR6-L3U	20575	275	214
TC31	HR6-L5U	21165	337	291

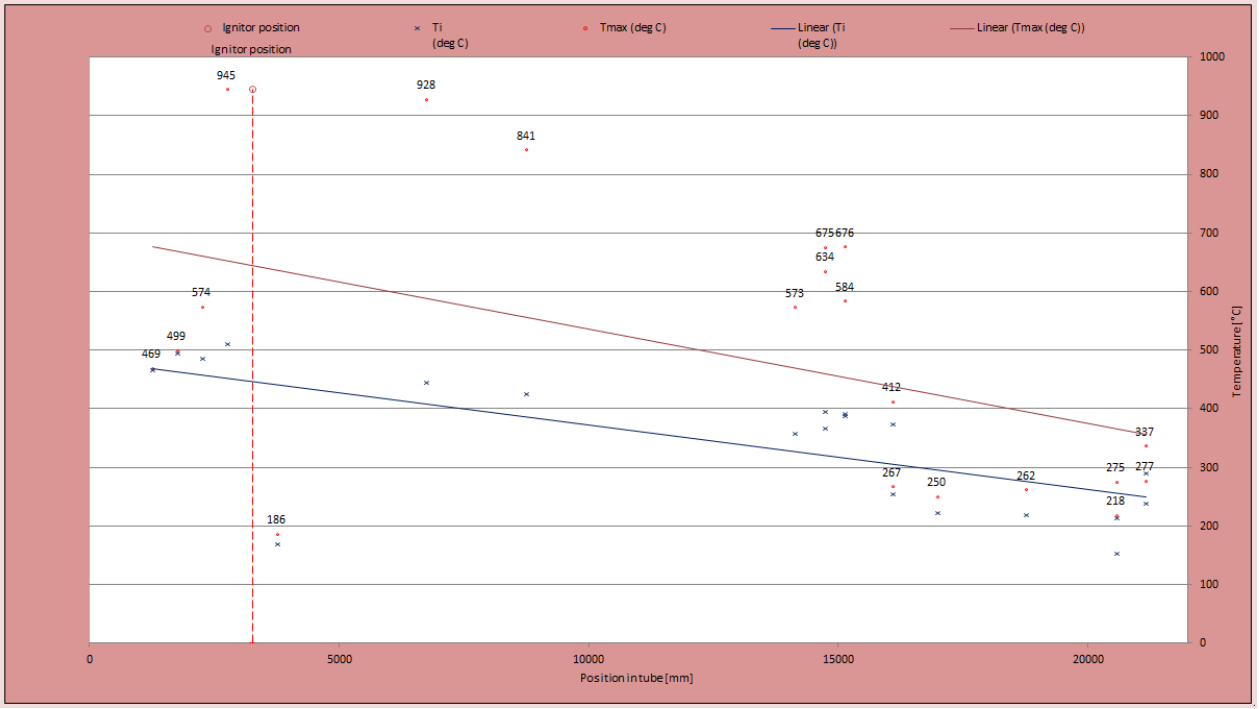

Figure 40 DOT - thermocouple data summary

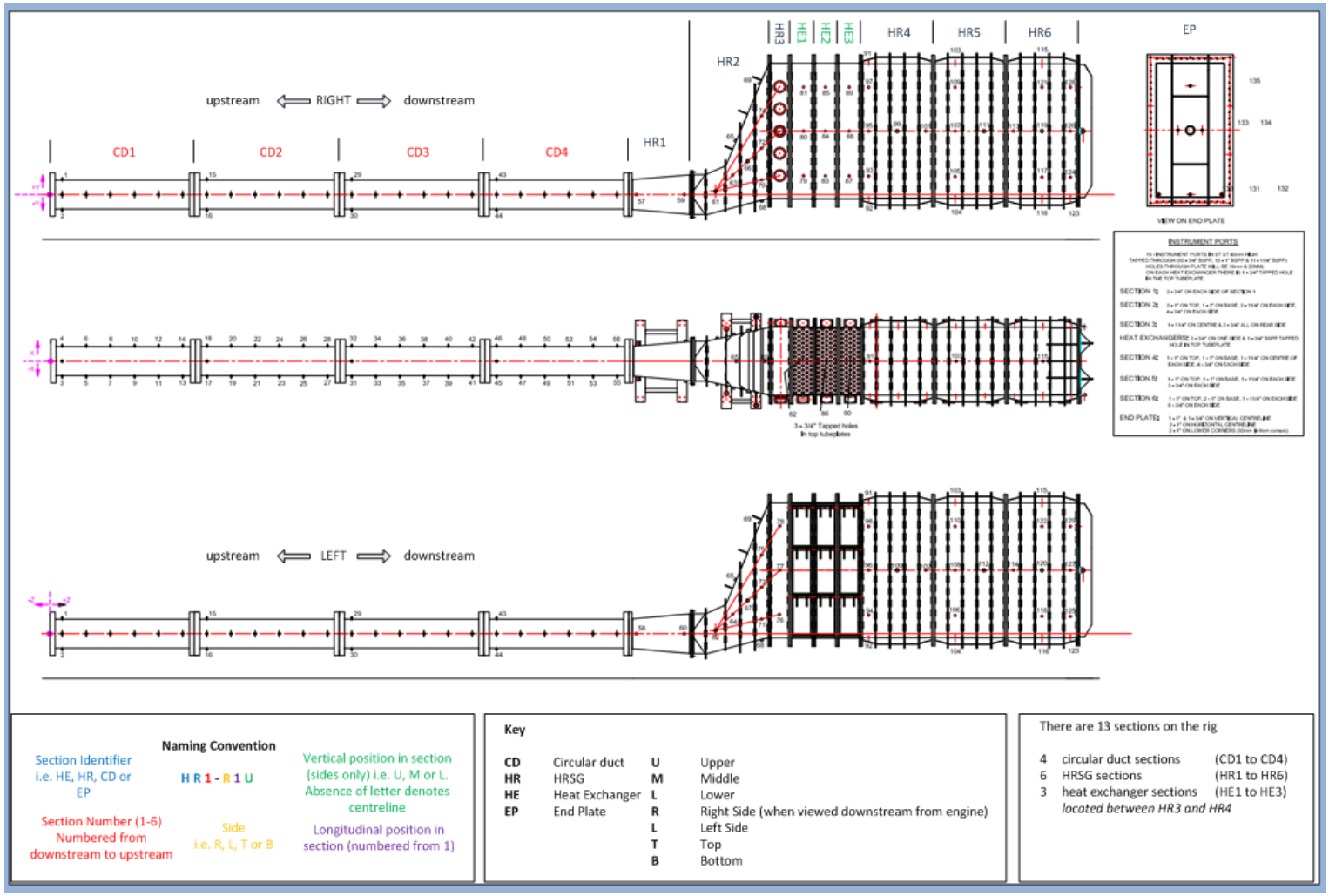

Figure 41 DOT - rig drawing and key

Figure 42 DOT - port and sensor position table

Sensor	OLD DESIGNATION	NEW DESIGNATION	Section	Section Number	Side	Horizontal Location	Vertical Location	PORT REF	SIZE	"X"	"Y"	"Z"
-		CD1-T1	CD	1	T	1		1	1" BSPP	0	298	258
TC1	TS1-1	CD1-T2	CD	1	T	2		NA	SURFACE	0	298	1508
-		CD1-B1	CD	1	B	1		2	1" BSPP	0	-298	258
-	NS1-1	CD1-R1	CD	1	R	1		3	3/4" BSPP	298	0	258
-	FS1-1	CD1-L1	CD	1	L	1		4	3/4" BSPP	-298	0	258
-	NS1-2	CD1-R2	CD	1	R	2		5	3/4" BSPP	298	0	758
-	FS1-2	CD1-L2	CD	1	L	2		6	3/4" BSPP	-298	0	758
TC0	NS1-3	CD1-R3	CD	1	R	3		7	3/4" BSPP	298	0	1258
-	FS1-3	CD1-L3	CD	1	L	3		8	3/4" BSPP	-298	0	1258
TC2	NS1-4	CD1-R4	CD	1	R	4		9	3/4" BSPP	298	0	1758
-	FS1-4	CD1-L4	CD	1	L	4		10	3/4" BSPP	-298	0	1758
TC3	NS1-5	CD1-R5	CD	1	R	5		11	3/4" BSPP	298	0	2258
-	FS1-5	CD1-L5	CD	1	L	5		12	3/4" BSPP	-298	0	2258
TC4	NS1-6	CD1-R6	CD	1	R	6		13	3/4" BSPP	298	0	2758
-	FS1-6	CD1-L6	CD	1	L	6		14	3/4" BSPP	-298	0	2758
IGN		CD2-T1	CD	2	T	1		15	1" BSPP	0	298	3258
TC6	TS2-1	CD2-T2	CD	2	T	2		NA	SURFACE	0	298	4508
-		CD2-B1	CD	2	B	1		16	1" BSPP	0	-298	2358
-	NS2-1	CD2-R1	CD	2	R	1		17	3/4" BSPP	298	0	3258
-	FS2-1	CD2-L1	CD	2	L	1		18	3/4" BSPP	-298	0	3258
TC5	NS2-2	CD2-R2	CD	2	R	2		19	3/4" BSPP	298	0	3758
-	FS2-2	CD2-L2	CD	2	L	2		20	3/4" BSPP	-298	0	3758
-	NS2-3	CD2-R3	CD	2	R	3		21	3/4" BSPP	298	0	4258
-	FS2-3	CD2-L3	CD	2	L	3		22	3/4" BSPP	-298	0	4258
-	NS2-4	CD2-R4	CD	2	R	4		23	3/4" BSPP	298	0	4758
-	FS2-4	CD2-L4	CD	2	L	4		24	3/4" BSPP	-298	0	4758
-	NS2-5	CD2-R5	CD	2	R	5		25	3/4" BSPP	298	0	5258
-	FS2-5	CD2-L5	CD	2	L	5		26	3/4" BSPP	-298	0	5258
-	NS2-6	CD2-R6	CD	2	R	6		27	3/4" BSPP	298	0	5758
-	FS2-6	CD2-L6	CD	3	L	6		28	3/4" BSPP	-298	0	5758

Sensor	OLD DESIGNATION	NEW DESIGNATION	Section	Section Number	Side	Horizontal Location	Vertical Location	PORT REF	SIZE	"X"	"Y"	"Z"
-		CD3-T1	CD	3	T	1		29	1" BSPP	0	298	6258
TC8	TS1-1	CD3-T2	CD	3	T	2		NA	SURFACE	0	298	7508
-		CD3-B1	CD	3	B	1		30	1" BSPP	0	-298	6258
-	NS3-1	CD3-R1	CD	3	R	1		31	3/4" BSPP	298	0	6258
-	FS3-1	CD3-L1	CD	3	L	1		32	3/4" BSPP	-298	0	6258
TC7	NS3-2	CD3-R2	CD	3	R	2		33	3/4" BSPP	298	0	6758
-	FS3-2	CD3-L2	CD	3	L	2		34	3/4" BSPP	-298	0	6758
-	NS3-3	CD3-R3	CD	3	R	3		35	3/4" BSPP	298	0	7258
-	FS3-3	CD3-L3	CD	3	L	3		36	3/4" BSPP	-298	0	7258
-	NS3-4	CD3-R4	CD	3	R	4		37	3/4" BSPP	298	0	7758
-	FS3-4	CD3-L4	CD	3	L	4		38	3/4" BSPP	-298	0	7758
KU6	NS3-5	CD3-R5	CD	3	R	5		39	3/4" BSPP	298	0	8258
-	FS3-5	CD3-L5	CD	3	L	5		40	3/4" BSPP	-298	0	8258
TC9	NS3-6	CD3-R6	CD	3	R	6		41	3/4" BSPP	298	0	8758
-	FS3-6	CD3-L6	CD	3	L	6		42	3/4" BSPP	-298	0	8758
-		CD4-T1	CD	4	T	1		43	1" BSPP	0	298	9258
TC10	TS1-1	CD4-T2	CD	4	T	2		NA	SURFACE	0	298	10508
-		CD4-B1	CD	4	B	1		44	1" BSPP	0	-298	9258
IP5	NS4-1	CD4-R1	CD	4	R	1		45	3/4" BSPP	298	0	9258
IP4	FS4-1	CD4-L1	CD	4	L	1		46	3/4" BSPP	-298	0	9258
KU7	NS4-2	CD4-R2	CD	4	R	2		47	3/4" BSPP	298	0	9758
-	FS4-2	CD4-L2	CD	4	L	2		48	3/4" BSPP	-298	0	9758
-	NS4-3	CD4-R3	CD	4	R	3		49	3/4" BSPP	298	0	10258
OP11	FS4-3	CD4-L3	CD	4	L	3		50	3/4" BSPP	-298	0	10258
OP10	NS4-4	CD4-R4	CD	4	R	4		51	3/4" BSPP	298	0	10758
-	FS4-4	CD4-L4	CD	4	L	4		52	3/4" BSPP	-298	0	10758
IP3	NS4-5	CD4-R5	CD	4	R	5		53	3/4" BSPP	298	0	11258
IP2	FS4-5	CD4-L5	CD	4	L	5		54	3/4" BSPP	-298	0	11258
IP1	NS4-6	CD4-R6	CD	4	R	6		55	3/4" BSPP	298	0	11758
IP0	FS4-6	CD4-L6	CD	4	L	6		56	3/4" BSPP	-298	0	11758
OP0		HR1-R1	HR	1	R	1		57	3/4" BSPP	308	0	12152
-		HR1-L1	HR	1	L	1		58	3/4" BSPP	-308	0	12152

Sensor	OLD DESIGNATION	NEW DESIGNATION	Section	Section Number	Side	Horizontal Location	Vertical Location	PORT REF	SIZE	"X"	"Y"	"Z"
IP6		HR1-R2	HR	1	R	2		59	3/4" BSPP	393	0	13160
-		HR1-L2	HR	1	L	2		60	3/4" BSPP	-393	0	13160
RA1		HR2-R2M	HR	2	R	2	M	61	11/4" BSPP	448	70	13785
RA1		HR2-L2M	HR	2	L	2	M	62	11/4" BSPP	-448	70	13785
IP7		HR2-R3M	HR	2	R	3	M	63	3/4" BSPP	528	410	14140
TC24		HR2-L3M	HR	2	L	3	M	64	3/4" BSPP	-528	410	14140
OP1		HR2-T3	HR	2	T	3		65	1" BSPP	0	1122	14215
RA2		HR2-R4M	HR	2	R	4	M	66	11/4" BSPP	598	700	14475
RA2		HR2-L4M	HR	2	L	4	M	67	11/4" BSPP	-598	700	14475
-		HR2-B5	HR	2	B	5		68	1" BSPP	0	-100	14745
KU8		HR2-T5	HR	2	T	5		69	1" BSPP	0	2315	14745
TC16		HR2-R5L	HR	2	R	5	L	70	3/4" BSPP	662	310	14745
TC25		HR2-L5L	HR	2	L	5	L	71	3/4" BSPP	-662	310	14745
IP8		HR2-R5M	HR	2	R	5	M	72	3/4" BSPP	662	975	14745
OP2		HR2-L5M	HR	2	L	5	M	73	3/4" BSPP	-662	975	14745
-		HR2-R5U	HR	2	R	5	U	74	3/4" BSPP	662	1660	14745
-		HR2-L5U	HR	2	L	5	U	75	3/4" BSPP	-662	1660	14745
KU9		HR3-L1L	HR	3	L	1	L	76	3/4" BSPP	-700	400	15140
TC26		HR3-L1M	HR	3	L	1	M	77	11/4" BSPP	-700	1335	15140
TC27		HR3-L1U	HR	3	L	1	U	78	3/4" BSPP	-700	2270	15140
-		HE1-R1L	HE	1	R	1	L	79	3/4" BSPP	700	400	15600
-		HE1-R1M	HE	1	R	1	M	80	3/4" BSPP	700	1335	15600
KU0		HE1-R1U	HE	1	R	1	U	81	3/4" BSPP	700	2270	15600
TC20		HE2-R1L	HE	2	R	1	L	83	3/4" BSPP	700	400	16090
IP10		HE2-R1M	HE	2	R	1	M	84	3/4" BSPP	700	1335	16090
TC17		HE2-R1U	HE	2	R	1	U	85	3/4" BSPP	700	2270	16090
KU1		HE3-R1L	HE	3	R	1	L	87	3/4" BSPP	700	400	16580
-		HE3-R1M	HE	3	R	1	M	88	3/4" BSPP	700	1335	16580
-		HE3-R1U	HE	3	R	1	U	89	3/4" BSPP	700	2270	16580
OP3		HE1-T1	HE	1	T	1		82	3/4" BSPP HOLE	-47	2735	15600
-		HE2-T1	HE	2	T	1		86	3/4" BSPP HOLE	0	2735	16090
OP4		HE3-T1	HE	3	T	1		90	3/4" BSPP HOLE	-47	2735	16580

Sensor	OLD DESIGNATION	NEW DESIGNATION	Section	Section Number	Side	Horizontal Location	Vertical Location	PORT REF	SIZE	"X"	"Y"	"Z"
OP6		HR4-T1	HR	4	T	1		91	1" BSPP	0	2735	16985
-		HR4-B1	HR	4	B	1		92	1" BSPP	0	-65	16985
OP5		HR4-R1L	HR	4	R	1	L	93	3/4" BSPP	700	400	16985
IP13		HR4-L1L	HR	4	L	1	L	94	3/4" BSPP	-700	400	16985
IP12		HR4-R1M	HR	4	R	1	M	95	3/4" BSPP	700	1335	16985
TC28		HR4-L1M	HR	4	L	1	M	96	3/4" BSPP	-700	1335	16985
KU2		HR4-R1U	HR	4	R	1	U	97	3/4" BSPP	700	2270	16985
-		HR4-L1U	HR	4	L	1	U	98	3/4" BSPP	-700	2270	16985
RA3		HR4-R3M	HR	4	R	3	M	99	11/4" BSPP	700	1335	17575
RA3		HR4-L3M	HR	4	L	3	M	100	11/4" BSPP	-700	1335	17575
IP14		HR4-R5M	HR	4	R	5	M	101	3/4" BSPP	700	1335	18165
-		HR4-L5M	HR	4	L	5	M	102	3/4" BSPP	-700	1335	18165
TC21		HR5-R1M	HR	5	R	1	M	NA	SURFACE	700	1200	18455
OP7		HR5-T2	HR	5	T	2		103	1" BSPP	0	2735	18775
-		HR5-B2	HR	5	B	2		104	1" BSPP	0	-65	18775
KU3		HR5-R2L	HR	5	R	2	L	105	3/4" BSPP	700	400	18775
IP16		HR5-L2L	HR	5	L	2	L	106	3/4" BSPP	-700	400	18775
IP15		HR5-R2M	HR	5	R	2	M	107	3/4" BSPP	700	1335	18775
KU4		HR5-L2M	HR	5	L	2	M	108	3/4" BSPP	-700	1335	18775
-		HR5-R2U	HR	5	R	2	U	109	3/4" BSPP	700	2270	18775
TC29		HR5-L2U	HR	5	L	2	U	110	3/4" BSPP	-700	2270	18775
RA4		HR5-R4M	HR	5	R	4	M	111	11/4" BSPP	700	1335	19375
RA4		HR5-L4M	HR	5	L	4	M	112	11/4" BSPP	-700	1335	19375
IP17		HR6-R1M	HR	6	R	1	M	113	3/4" BSPP	700	1335	19985
-		HR6-L1M	HR	6	L	1	M	114	3/4" BSPP	-700	1335	19985
OP8		HR6-T3	HR	6	T	3		115	1" BSPP	0	2735	20575
-		HR6-B3	HR	6	B	3		116	3/4" BSPP	0	-65	20575
TC18		HR6-R3L	HR	6	R	3	L	117	3/4" BSPP	700	400	20575
IP19		HR6-L3L	HR	6	L	3	L	118	3/4" BSPP	-700	400	20575
-		HR6-R3M	HR	6	R	3	M	119	11/4" BSPP	700	1335	20575
-		HR6-L3M	HR	6	L	3	M	120	11/4" BSPP	-700	1335	20575
-		HR6-R3U	HR	6	R	3	U	121	3/4" BSPP	700	2270	20575

Sensor	OLD DESIGNATION	NEW DESIGNATION	Section	Section Number	Side	Horizontal Location	Vertical Location	PORT REF	SIZE	"X"	"Y"	"Z"
TC30		HR6-L3U	HR	6	L	3	U	122	3/4" BSPP	-700	2270	20575
-		HR6-B5	HR	6	B	5		123	1" BSPP	0	-65	21165
TC23		HR6-R5L	HR	6	R	5	L	124	3/4" BSPP	700	400	21165
IP20		HR6-L5L	HR	6	L	5	L	125	3/4" BSPP	-700	400	21165
IP18		HR6-R5M	HR	6	R	5	M	126	3/4" BSPP	700	1335	21165
KU5		HR6-L5M	HR	6	L	5	M	127	3/4" BSPP	-700	1335	21165
OP9		HR6-R5U	HR	6	R	5	U	128	3/4" BSPP	700	2270	21165
TC31		HR6-L5U	HR	6	L	5	U	129	3/4" BSPP	-700	2270	21165
-		EP-1L	EP			1	L	130	1" BSPP	650	-15	21330
-		EP-2L	EP			2	L	131	1" BSPP	0	-15	21330
-		EP-3L	EP			3	L	132	1" BSPP	-650	-15	21330
PCB		EP-1M	EP			1	M	133	1" BSPP	250	1335	21330
-		EP-2M	EP			2	M	134	1" BSPP	-250	1335	21330
-		EP-1U	EP			1	U	135	3/4" BSPP	0	2270	21330

12.8 LDA TEST RESULTS.

The data acquired from the LDA measurements carried out at each of the 5 windows in section 3 of the HRSG are summarised in Table 21, Table 22, Table 23, Table 24 and Table 25 on the following pages.

12.8.1 Bottom window

Table 21: LDA measurements from bottom window

Row	X (mm)	Offset from Window (mm)	Count (1)	Count (2)	Data rate (1) (#/s)	Data rate (2) (#/s)	Validation (1) (%)	Validation (2) (%)	Horizontal Velocity	Vertical Velocity	LDA1 RMS (m/s)	LDA4 (2) RMS (m/s)	Turb. Int. Horizontal (%)	Turb. Int. Vertical (%)	Velocity Vector	Vector Angle
1	0	15	2000	2000	315.66	25.29	99.1	99.8	4.4	6.19	29.76	31.34	676.3636	506.3005	7.5944783	54.5938751
2	50	65	2000	485	41.36	4.2	92.88	98.17	-5.37	17.71	14.89	11.48	-277.281	64.82213	18.506242	-73.131725
3	100	115	2000	520	61.39	4.38	98.6	97.07	6.58	21.58	12.6	10.97	191.4894	50.83411	22.560869	73.0429095
4	150	165	2000	760	42.85	6.76	98	97.45	14.54	21.84	9.69	9.7	66.64374	44.41392	26.237325	56.3462723
5	200	215	2000	495	43.3	4.17	98.63	98.55	17.29	20.22	9.45	7.35	54.65587	36.35015	26.60437	49.4664474
6	250	265	2000	2000	204.19	114.61	97.61	98.86	19.54	16.69	8.91	7.44	45.59877	44.57759	25.697621	40.502142
7	300	315	2000	1641	56.36	13.91	99.23	98.9	25.08	14.62	11.75	6.96	46.85008	47.60602	29.030171	30.2393891
8	350	365	2000	735	106.54	6.2	99.17	97.75	33.06	14.75	11.56	7.42	34.96673	50.30508	36.201189	24.0444456
9	400	415	2000	966	42.85	10.92	98.47	99.18	36.29	14.82	11.38	7.01	31.3585	47.30094	39.199445	22.2139732
10	450	465	2000	758	29.06	8.43	98.71	99.26	38.17	15.22	10.94	7.25	28.66125	47.63469	41.092546	21.7392694
11	500	515	2000	598	28.54	6.77	98.67	99.28	40.53	14.31	10.01	7.32	24.69775	51.15304	42.982054	19.4466896
12	546	561	1093	398	12.21	4.46	94.62	99.55	38.1	14.7	10.74	6.5	28.18898	44.21769	40.837483	21.0979496
13	600	615	2000	2000	266.94	265.34	99.59	95.23	37.43	12.78	11.62	8.92	31.04462	69.79656	39.551654	18.8518213
14	650	665	2000	505	101.5	5.83	99.62	96.87	35.1	15.01	11.09	7.81	31.59544	52.03198	38.174731	23.1532631
15	700	715	2000	210	26.45	2.5	99.59	99.21	32.04	13.55	11.52	7.57	35.95506	55.86716	34.787413	22.9239327
16	750	765	1782	192	20.08	2.29	99.79	100	29.81	13.26	11.26	7.95	37.77256	59.95475	32.62612	23.9803198
17	800	815	2000	158	27.32	1.9	97.5	95.67	25.69	12.09	11.63	8.15	45.27053	67.41108	28.392679	25.2021977
18	850	865	2000	177	130.6	2.14	98.35	97.78	22.63	11	11.18	7.5	49.40345	68.18182	25.161814	25.9234793
19	900	915	949	64	10.82	0.78	99.19	95.97	19.12	10.64	10.32	7.88	53.9749	74.06015	21.881133	29.0952971
20	950	965	332	19	4.05	0.3	97.62	100	17.21	14.04	12.2	7.56	70.88902	53.84615	22.210486	39.2077295
21	990	1005	79	12	0.93	0.14	100	100	14.94	13.39	11.02	5.73	73.76171	42.79313	20.062295	41.8683374

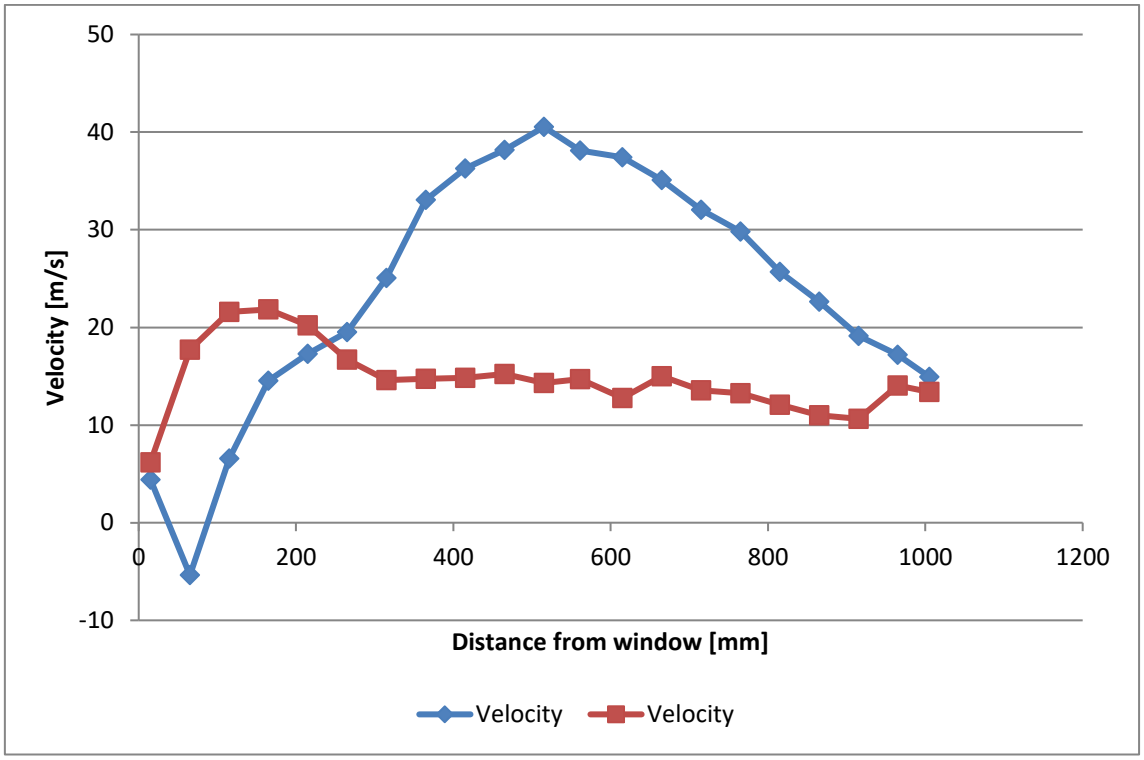

Figure 43 Gas Velocities across width of HRSG (bottom window)

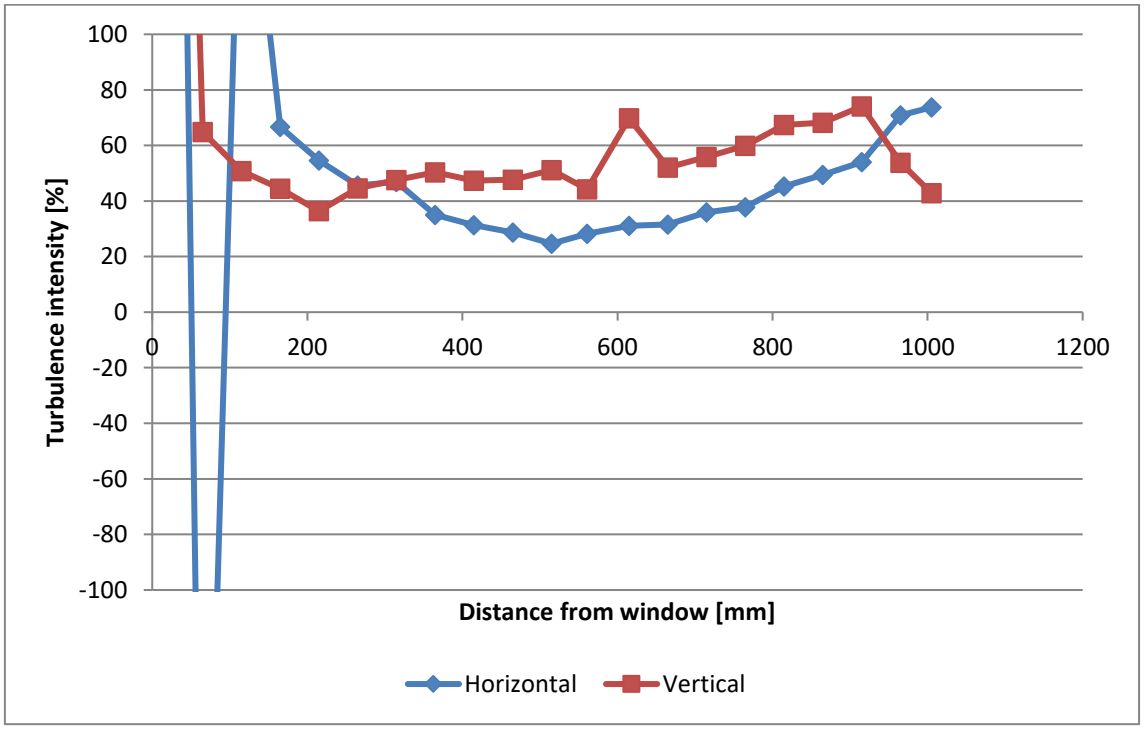

Figure 44 Turbulence intensity across width of HRSG (bottom window)

12.8.2 2nd window from bottom

Table 22: LDA measurements from 2nd window

Row	X (mm)	Offset from Window (mm)	Count (1)	Count (2)	Data rate (1) (#/s)	Data rate (2) (#/s)	Validation (1) (%)	Validation (2) (%)	Horizontal Velocity	Vertical Velocity	LDA1 RMS (m/s)	LDA4 (2) RMS (m/s)	Turb. Int. Horizontal (%)	Turb. Int. Vertical (%)	Velocity Vector	Vector Angle
1	0	15	2000	2000	163.77	88.64	5.72	2.43	3.21	-6.28	30.49	43.19	949.8442	-687.739	7.052836	-62.9263
2	50	65	2000	1178	136.37	13.22	95.87	88.93	-8.19	25.14	9.64	8.46	-117.705	33.65155	26.44042	-71.9557
3	100	115	2000	1014	68.25	11.54	96.74	91.4	-1.93	25.4	10.02	8.28	-519.171	32.59843	25.47322	-85.6548
4	150	165	1424	376	15.85	4.22	98.03	92.49	5.15	22.67	8.45	8.66	164.0777	38.20026	23.24761	77.2012
5	200	215	652	163	7.29	1.87	97.46	87.99	8.21	22.03	7.19	7.53	87.57613	34.18066	23.5101	69.5609
6	250	265	494	117	5.56	1.33	95.48	91.38	8.86	18.11	6.85	8.32	77.31377	45.94147	20.16114	63.93062
7	300	315	356	77	3.97	0.96	97.72	82.44	8.03	13.77	6.44	6.91	80.19925	50.18155	15.94032	59.75132
8	350	365	1320	286	14.74	3.21	96.78	81.35	5.63	10.32	6.1	6.34	108.3481	61.43411	11.75582	61.38565
9	400	415	487	197	5.49	2.24	96.69	85.79	5.21	7.55	5.47	5.62	104.9904	74.43709	9.173146	55.39175
10	450	465	244	119	2.79	1.45	92.12	86.05	4.96	5.74	5.39	5.87	108.6694	102.2648	7.586119	49.16933
11	500	515	919	251	10.26	2.87	96.65	80.55	3.48	4.32	4.66	4.87	133.908	112.7315	5.547324	51.14663
12	550	565	1598	754	17.88	8.41	69.33	30.41	3.35	1.51	7.12	21.7	212.5373	1437.086	3.674588	24.26329
13	600	615	2000	2000	370.72	287.19	96.55	84.1	2.7	3.25	4.98	5.57	184.4444	171.3846	4.225222	50.28124
14	650	665	1330	500	15.41	6.19	98.39	88.55	2.4	3.59	4.44	5.68	185	158.2173	4.318345	56.23633
15	700	715	539	498	6.11	5.79	95.75	91.39	2.2	4.26	4.46	4.42	202.7273	103.7559	4.794539	62.68673
16	750	765	162	140	1.81	1.79	97.69	76.13	1.93	4.34	4.55	4.98	235.7513	114.7465	4.749789	66.02526
17	800	815	616	457	7.39	5.2	97.51	83.58	2.16	5.46	4.14	4.83	191.6667	88.46154	5.871729	68.41603
18	850	865	210	220	2.48	2.54	99.64	96.16	2.14	3.42	3.36	5.07	157.0093	148.2456	4.034352	57.96451
19	900	915	78	157	0.89	1.8	97.66	91.67	0.13	6.92	4.92	6.06	3784.615	87.57225	6.921221	88.92376
20	950	965	18	28	0.23	0.38	100	91	0.49	6.41	6.47	6.25	1320.408	97.5039	6.428701	85.62864
21	990	1005	10	82	0.14	0.98	100	96.3	3.27	1.83	0.53	4.32	16.20795	236.0656	3.747239	29.23282

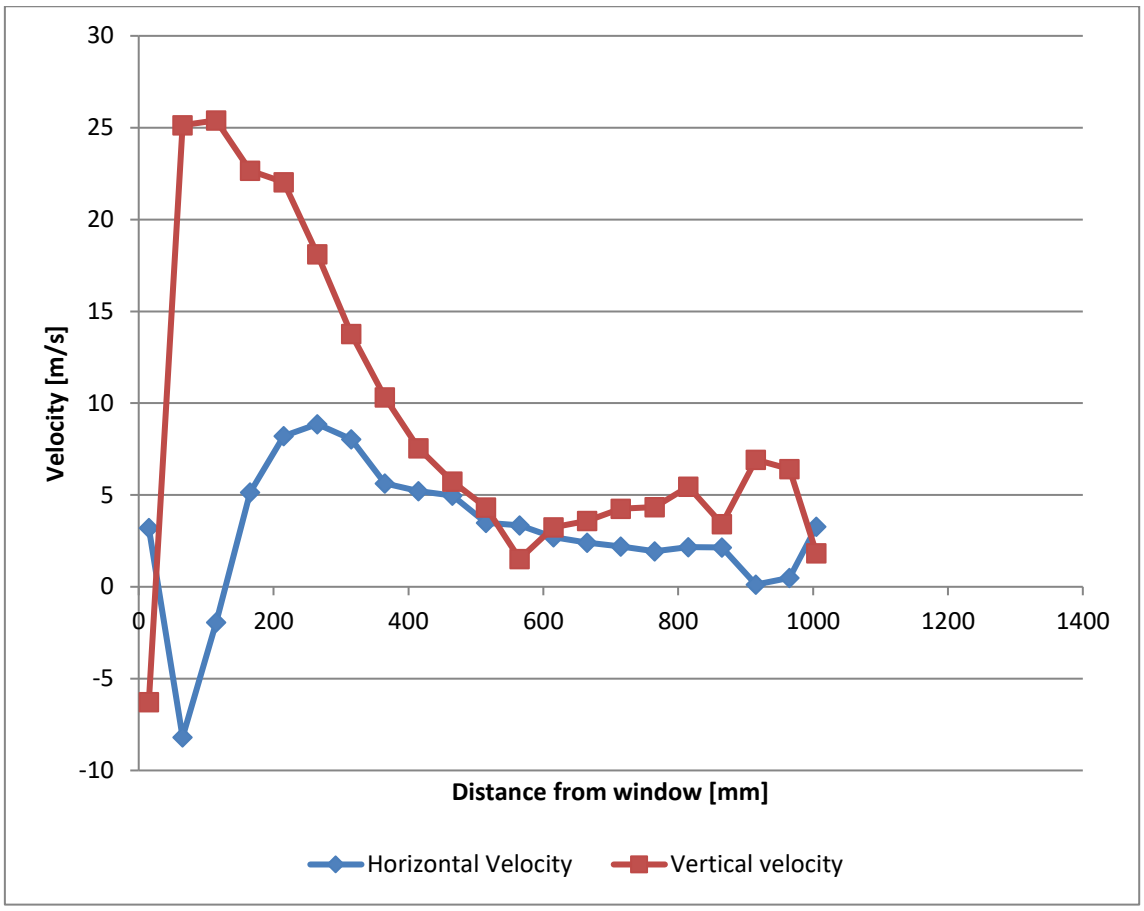

Figure 45 Gas velocities across width of HRSG (2nd window from bottom)

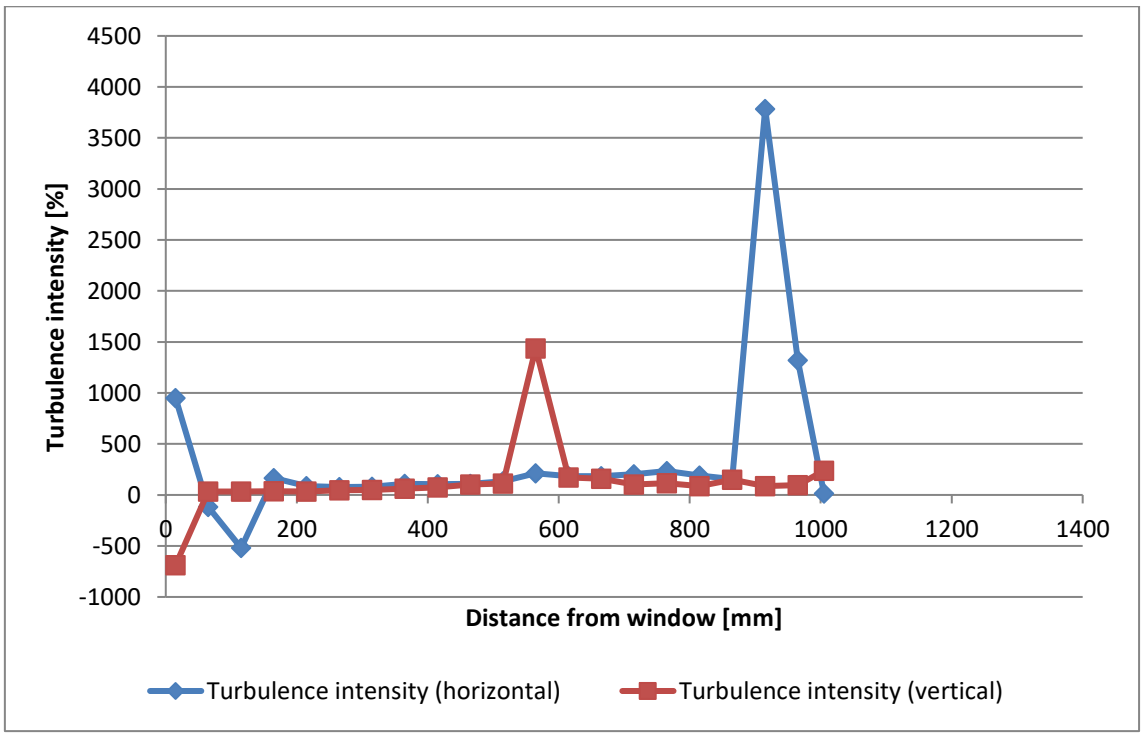

Figure 46 Turbulence intensity across width of HRSG (2nd window from bottom)

12.8.3 3rd window from bottom

Table 23: LDA measurements from 3rd window

Row	X (mm)	Offset from Window (mm)	Count (1)	Count (2)	Data rate (1) (#/s)	Data rate (2) (#/s)	Validation (1) (%)	Validation (2) (%)	Horizontal Velocity	Vertical Velocity	LDA1 RMS (m/s)	LDA4 (2) RMS (m/s)	Turb. Int. Horizontal (%)	Turb. Int. Vertical (%)	Velocity Vector	Vector Angle
1	0	15	2000	2000	184.07	414.27	1.97	2.44	14.78	-39.42	43.95	42.92	297.3613	-108.879	42.0997	-69.4471
2	50	65	2000	2000	145.8	46.4	29.91	4.32	-3.63	-0.38	15.77	43.37	-434.435	-11413.2	3.649836	5.976139
3	100	115	2000	1647	76.09	18.32	96.65	7.6	-2.66	5.92	8.01	40.57	-301.128	685.3041	6.490146	-65.8045
4	150	165	2000	988	54.52	11.07	98.11	85.62	0.5	21.4	7.53	10.39	1506	48.5514	21.40584	88.66156
5	200	215	2000	1418	68.54	15.82	98.59	92.35	3.16	18.89	7.05	8.25	223.1013	43.6739	19.15249	80.50325
6	250	265	2000	2000	52.17	50.77	98.24	95.39	3.78	15.06	7.36	8.37	194.709	55.57769	15.52714	75.91006
7	300	315	2000	1399	138.81	24.02	98.59	92.99	2.27	11.58	6.43	7.18	283.2599	62.00345	11.80039	78.90908
8	350	365	2000	597	26.38	10.21	98.61	95.32	1.65	8.06	6.58	7.19	398.7879	89.20596	8.227156	78.43057
9	400	415	2000	980	37.88	16.42	98.26	91.65	0.95	6.48	6.43	6.19	676.8421	95.52469	6.549267	81.65957
10	450	465	1255	549	13.98	9.31	96.88	91.47	0.32	4.45	6.1	6.33	1906.25	142.2472	4.461491	85.88693
11	500	515	2000	2000	421.61	382.48	98.38	83.99	-0.26	4.62	5.52	6.79	-2123.08	146.9697	4.62731	-86.779
12	550	565	2000	2000	161.24	158.02	97.83	81.99	-2.22	5.34	6.76	6.35	-304.505	118.9139	5.783079	-67.4259
13	600	615	1603	974	17.93	16.33	95.36	87.77	-1.08	3.03	5.18	6.59	-479.63	217.4917	3.216722	-70.3821
14	650	665	2000	1313	74.23	22.44	95.79	90.46	-1.03	4.2	5.2	5.58	-504.854	132.8571	4.324454	-76.2208
15	700	715	1133	871	12.74	14.54	97.38	92.62	-1.95	2.8	5.52	6.18	-283.077	220.7143	3.412111	-55.1455
16	750	765	942	398	10.51	6.92	98.15	87.45	-1.82	4.53	5.22	5.42	-286.813	119.6468	4.881936	-68.1114
17	800	815	189	280	2.22	4.99	97.42	87.37	-2.27	4.14	4.05	5.35	-178.414	129.2271	4.721493	-61.2636
18	850	865	75	163	0.91	2.74	99.14	93.22	-3.46	5.61	3.93	6.53	-113.584	116.3993	6.591184	-58.3355
19	900	915	1490	2000	17.8	69	98.32	93.45	-1.89	7.01	4.88	6.45	-258.201	92.01141	7.260317	-74.911
20	950	965	131	204	1.56	3.61	98.89	83.69	-2.73	8.32	4.63	5.97	-169.597	71.75481	8.756443	-71.834
21	990	1005	2000	2000	69.74	137.12	97.26	80.59	-2.69	9.33	4.7	5.93	-174.721	63.55841	9.710046	-73.9168

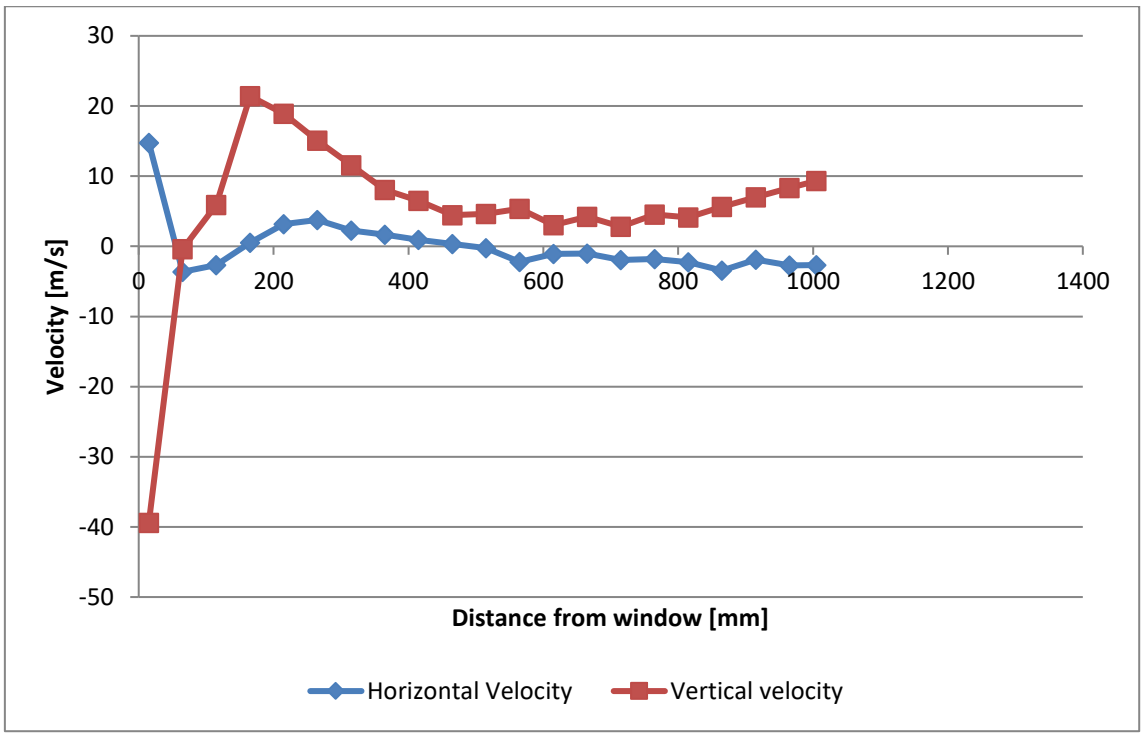

Figure 47 Gas velocities across width of HRSG (3rd window from bottom)

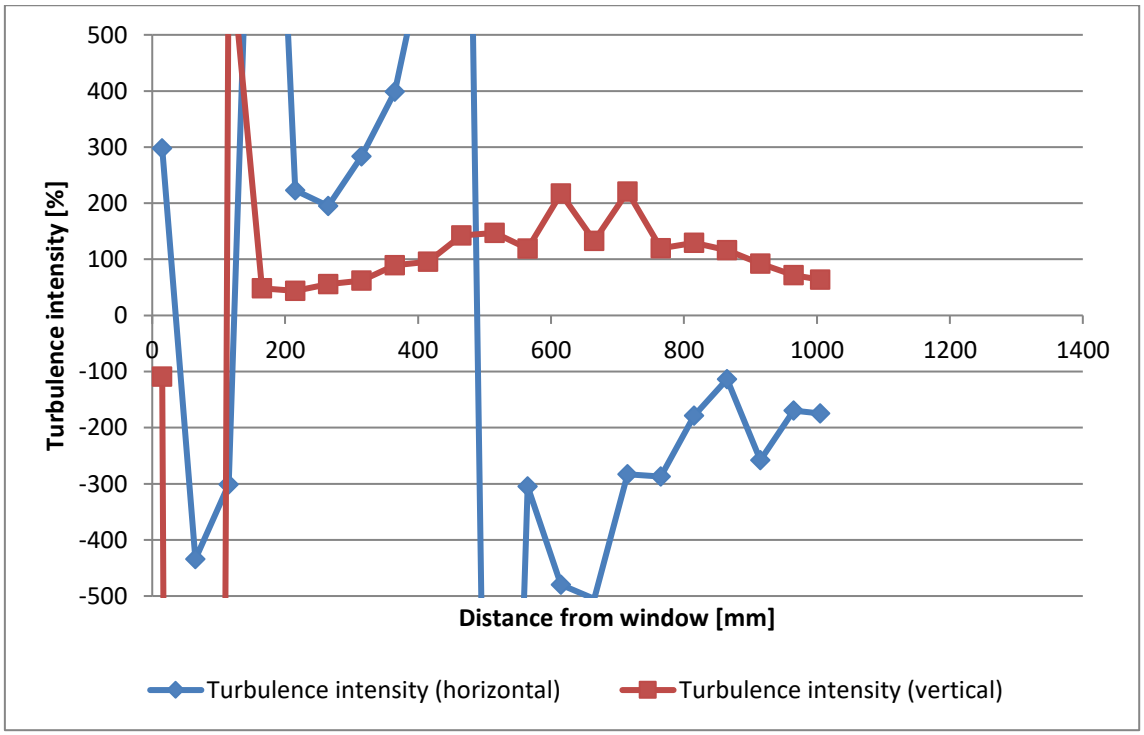

Figure 48 Turbulence intensity across width of HRSG (3rd window from bottom)

12.8.4 4th window from bottom

Table 24: LDA measurements form 4th window

Row	X (mm)	Offset from Window (mm)	Count (1)	Count (2)	Data rate (1) (#/s)	Data rate (2) (#/s)	Validation (1) (%)	Validation (2) (%)	Horizontal Velocity	Vertical Velocity	LDA1 RMS (m/s)	LDA4 (2) RMS (m/s)	Turb. Int. Horizontal (%)	Turb. Int. Vertical (%)	Velocity Vector	Vector Angle
1	0	15	2000	2000	117.91	361.25	95.83	100	13.23	-40.25	48.57	41.9	367.1202	-104.099	42.36857	-71.8045
2	50	65	2000	2000	117.07	743.56	96.18	99.85	-2.54	0.05	6.89	0.76	-271.26	1520	2.540492	-1.12772
3	100	115	2000	2000	109.4	325.62	98.02	99.81	-2.44	0.32	6.43	2.73	-263.525	853.125	2.460894	-7.47156
4	150	165	2000	2000	78.99	177.65	97.79	99.23	-1.22	1.08	6.36	4.79	-521.311	443.5185	1.629356	-41.5167
5	200	215	2000	2000	63.98	145.98	97.82	99.38	0.16	1.22	6.12	5.1	3825	418.0328	1.230447	82.52844
6	250	265	2000	2000	84.8	110.21	98.14	99.43	-0.2	0.66	6.54	3.33	-3270	504.5455	0.689638	-73.1416
7	300	315	2000	2000	110.75	149.02	96.68	97.86	0.04	1.22	6.39	4.35	15975	356.5574	1.220656	88.12212
8	350	365	2000	341	54.64	5.77	96.97	97.83	-1.6	6.86	6.52	8.19	-407.5	119.3878	7.044118	-76.8713
9	400	415	2000	2000	39.51	35.28	97.28	96.19	-2.35	3.15	6.11	7.64	-260	242.5397	3.930013	-53.2759
10	450	465	2000	462	36.99	7.78	96.76	98.58	-2.92	2.55	5.78	6.66	-197.945	261.1765	3.876713	-41.1303
11	500	515	2000	2000	47.52	43.72	97.49	98.46	-3.62	-0.17	6.22	7.16	-171.823	-4211.76	3.62399	2.68871
12	550	565	2000	1337	138.68	22.4	95.97	98.59	-3.95	0.34	5.5	5.52	-139.241	1623.529	3.964606	-4.91966
13	600	615	2000	2000	164.35	152.21	99.12	99.5	-4.29	1.37	6.05	6.4	-141.026	467.1533	4.503443	-17.7107
14	650	665	2000	907	29.7	15.22	97.79	99.5	-4.83	0.44	5.52	4.11	-114.286	934.0909	4.85	-5.20512
15	700	715	2000	2000	230.74	214.22	98.92	99.21	-5.58	2.12	5.88	5.12	-105.376	241.5094	5.969154	-20.8032
16	750	765	2000	536	25.99	9.02	97.74	99.28	-5.03	1.2	4.86	4.73	-96.6203	394.1667	5.17116	-13.4182
17	800	815	2000	357	24.47	5.97	97.63	98.48	-4.41	2.65	4.77	6.52	-108.163	246.0377	5.144959	-31.002
18	850	865	792	210	8.94	3.54	97.73	99.05	-4.14	1.64	4.99	5.75	-120.531	350.6098	4.452999	-21.6103
19	900	915	2000	426	31.03	7.4	97.91	99.21	-4.72	3.24	4.73	6.51	-100.212	200.9259	5.725033	-34.4673
20	950	965	178	115	1.99	1.96	96.46	97.44	-4.7	1.48	4.59	4.6	-97.6596	310.8108	4.927515	-17.4789
21	990	1005	168	134	1.93	2.28	91.47	100	-4.7	0.83	4.73	3.29	-100.638	396.3855	4.772725	-10.0149

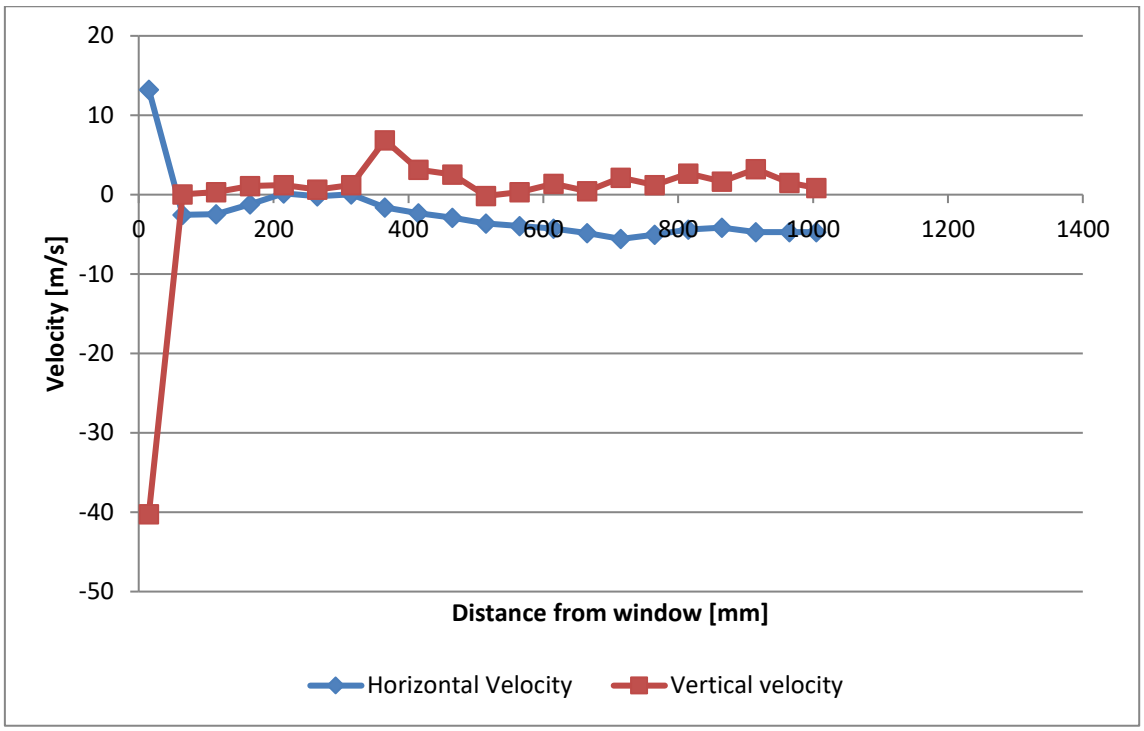

Figure 49 Gas velocities across width of HRSG (4th window from bottom)

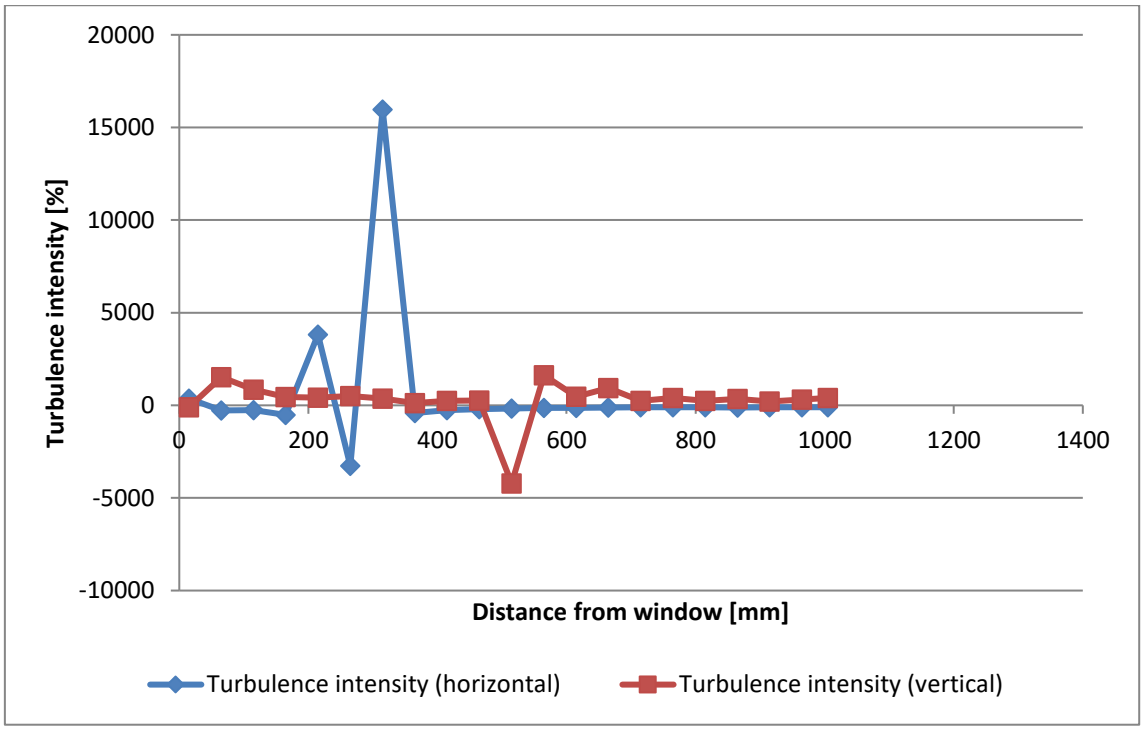

Figure 50 Turbulence intensity across width of HRSG (4th window from bottom)

12.8.5 5th window from bottom

Table 25: LDA measurements from 5th window

Row	X (mm)	Offset from Window (mm)	Count (1)	Count (2)	Data rate (1) (#/s)	Data rate (2) (#/s)	Validation (1) (%)	Validation (2) (%)	Horizontal Velocity	Vertical Velocity	LDA1 RMS (m/s)	LDA4 (2) RMS (m/s)	Turb. Int. Horizontal (%)	Turb. Int. Vertical (%)	Velocity Vector	Vector Angle
1	0	15	2000	2000	727.45	62.52	4.17	1.79	2.82	-5.6	20.54	24.49	728.3688	-437.321	6.26996	-63.2715
2	50	65	2000	932	128.14	15.8	42.01	98.11	-0.86	10.77	11.69	7.67	-1359.3	71.21634	10.80428	94.56546
3	100	115	2000	498	65.88	8.33	29.47	98.51	-1.35	16.76	17.7	8.26	-1311.11	49.28401	16.81428	94.60517
4	150	165	2000	390	71.22	6.54	89.27	99.29	-1.91	15.02	5.46	7.78	-285.864	51.7976	15.14095	97.24705
5	200	215	2000	443	90.3	7.64	96.28	98.58	-2.02	13.53	5.61	8.21	-277.723	60.67997	13.67996	98.49142
6	250	265	2000	1465	281.73	24.55	97.43	99.11	-3.33	11.23	5.61	8.85	-168.468	78.80677	11.71332	106.5165
7	300	315	2000	433	82.56	7.27	96.29	97.13	-0.3	9.71	5.93	7.73	-1976.67	79.60865	9.714633	91.76965
8	350	365	2000	146	32.44	2.49	97.21	98.26	0.41	4.25	6.17	8.83	1504.878	207.7647	4.269731	84.48969
9	400	415	2000	316	82.27	5.34	95.61	97.06	1.44	2.46	6.34	8.23	440.2778	334.5528	2.850474	59.65675
10	450	465	2000	2000	115.64	136.33	96.85	98.29	-1.28	-2.44	7.08	4.25	-553.125	-174.18	2.755358	-117.681
11	500	515	2000	1434	404.28	24.06	95.01	97.85	5.86	-5.43	4.61	6.85	78.66894	-126.151	7.989024	-42.8188
12	550	565	2000	322	44.3	5.46	97.42	99.06	4.56	-5.97	5.68	6.45	124.5614	-108.04	7.51229	-52.6267
13	600	615	2000	275	44.15	4.77	97.76	98.77	5.62	-6.8	5.02	6.04	89.32384	-88.8235	8.821814	-50.4273
14	650	665	2000	365	47.12	6.16	96.68	99.1	5.15	-9.19	5.11	5.67	99.2233	-61.6975	10.53464	-60.7341
15	700	715	2000	693	260.27	11.57	96.29	96.83	6.16	-8.78	5.04	6.41	81.81818	-73.0068	10.72539	-54.9467
16	750	765	1943	281	21.68	4.71	95.47	98.41	6.22	-8.07	5.07	6.21	81.51125	-76.9517	10.18888	-52.3765
17	800	815	2000	1314	36.83	21.99	98.14	98.34	4.87	-5.73	5.64	6.58	115.8111	-114.834	7.51996	-49.6384
18	850	865	2000	404	28.4	7.22	96.62	97.81	5.22	-4.56	5.37	6.9	102.8736	-151.316	6.931234	-41.1393
19	900	915	1692	252	19.08	4.22	96.37	99.22	4.62	-1.67	5.54	6.68	119.9134	-400	4.912566	-19.8735
20	950	965	2000	2000	58.28	62.06	97.04	98.13	7.66	-6.69	5.51	7.76	71.93211	-115.994	10.17014	-41.1329
21	990	1005	1788	280	19.97	4.77	95.6	99.14	2.59	1.74	5.56	6.51	214.6718	374.1379	3.120208	33.89378

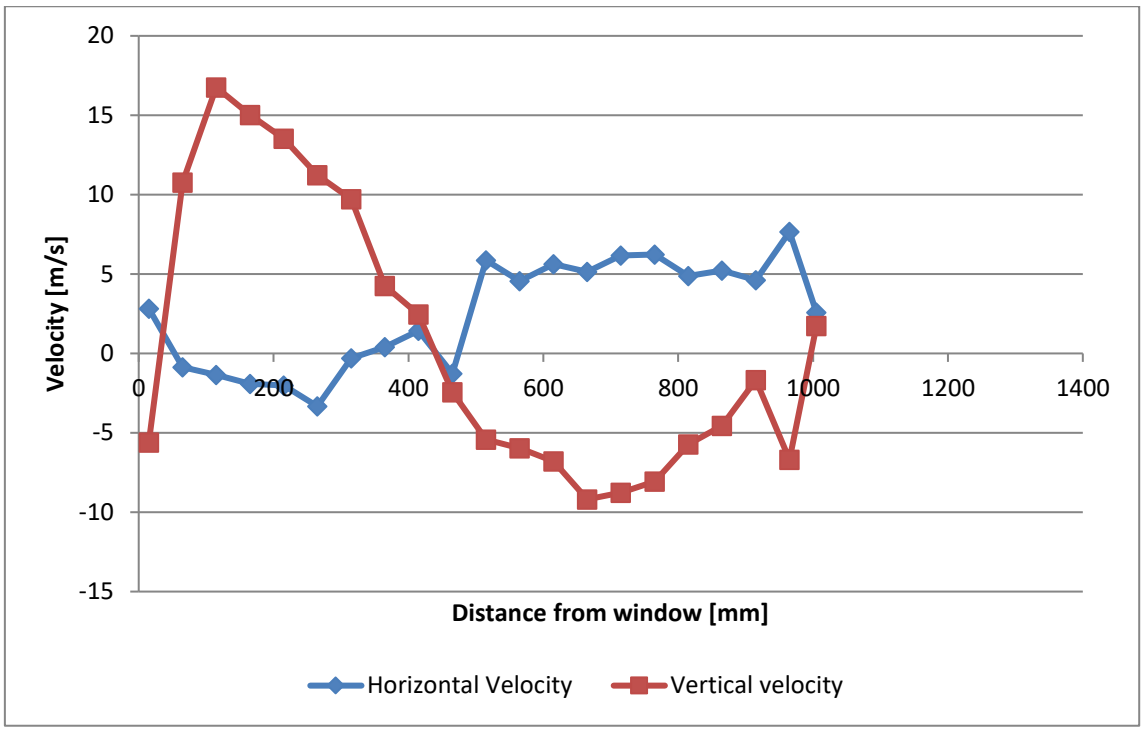

Figure 51 Gas velocities across width of HRSG (5th window from bottom)

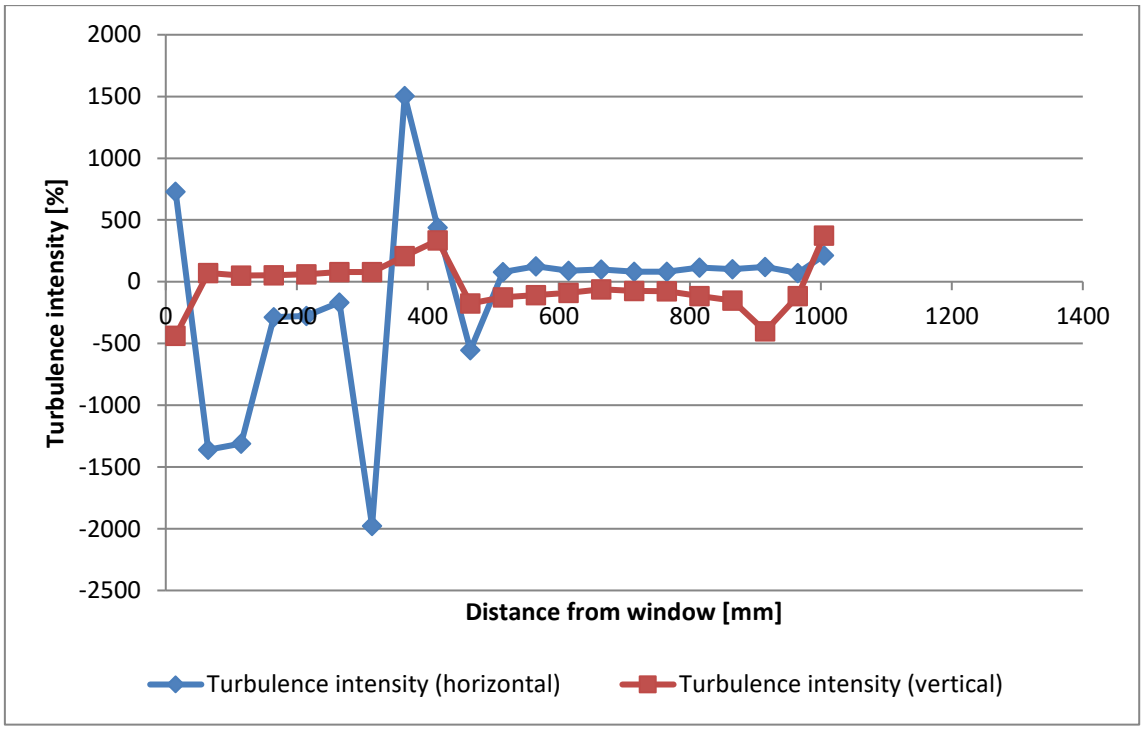

Figure 52 Turbulence intensity across width of HRSG (5th window from bottom)

12.8.6 Velocity Vectors from bottom window.

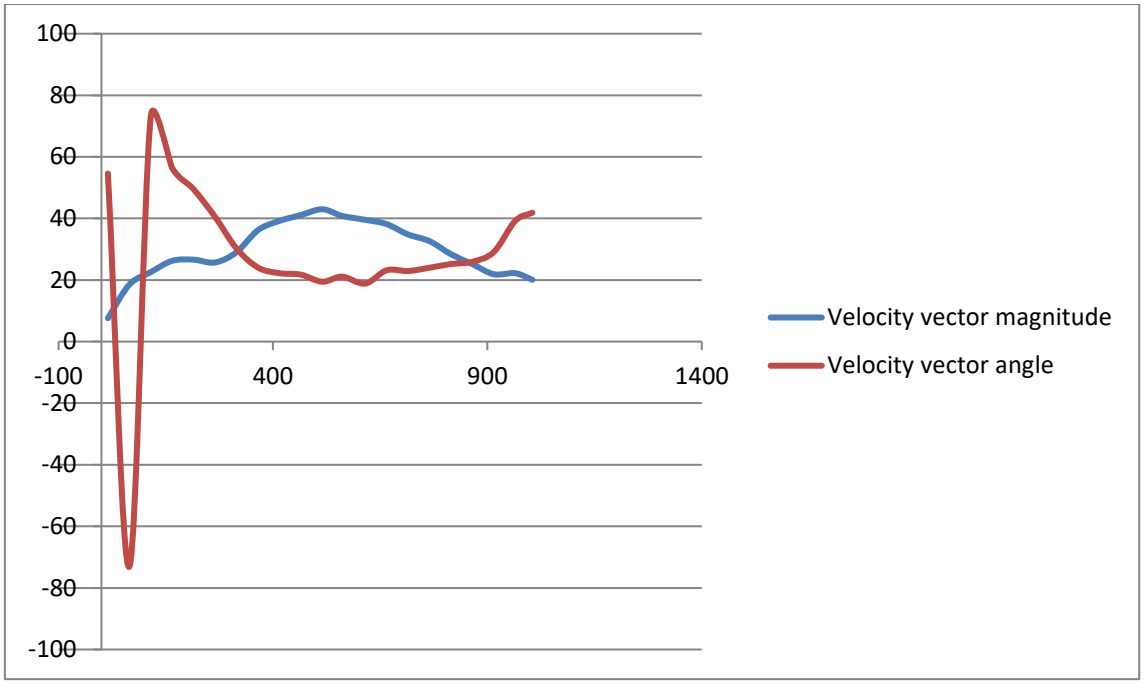

12.8.7 Velocity vectors 2nd from bottom window.

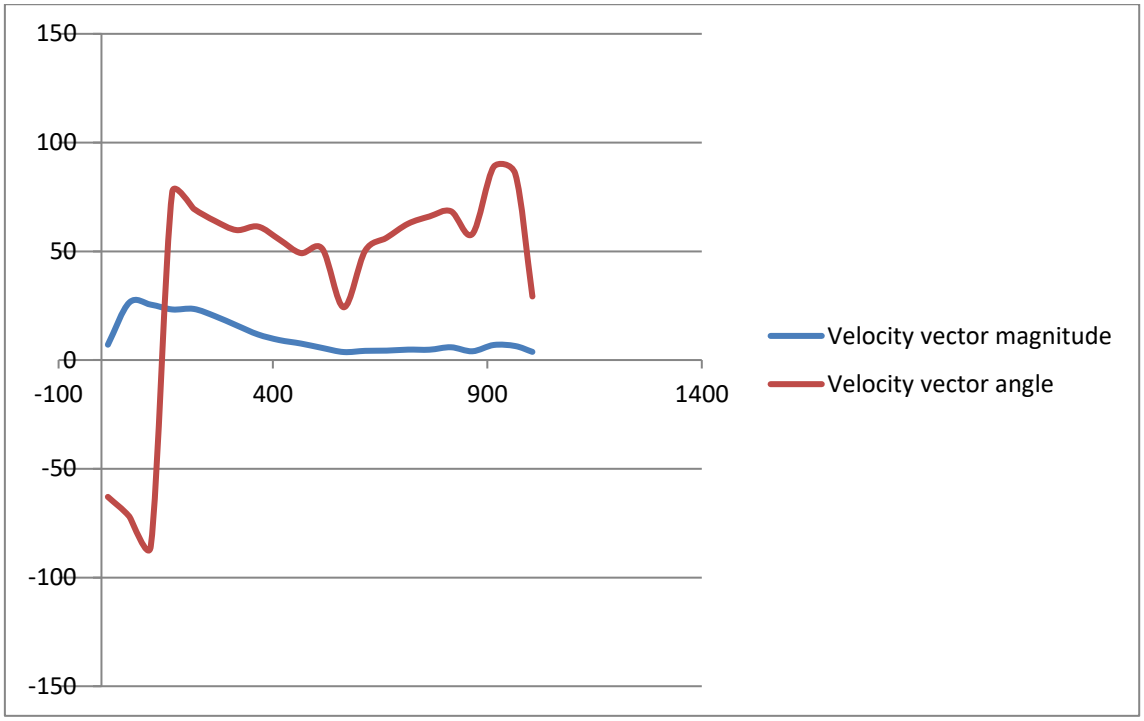

12.8.8 Velocity vectors 3rd window from bottom.

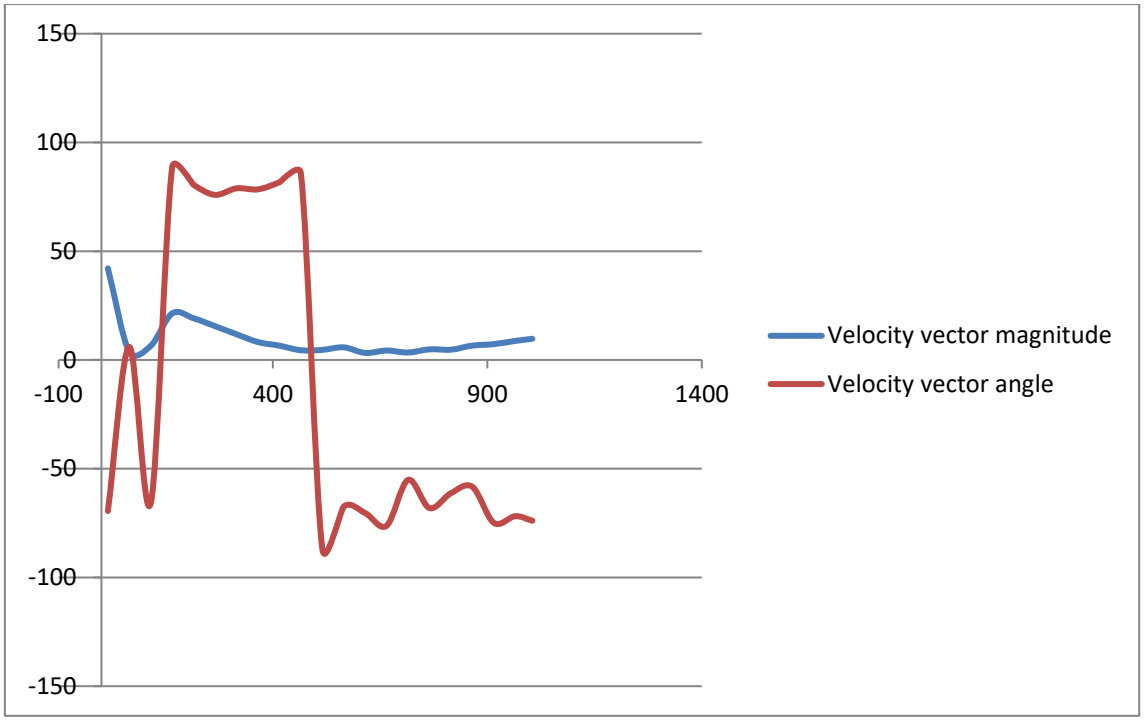

12.8.9 Velocity vectors 4th window from bottom

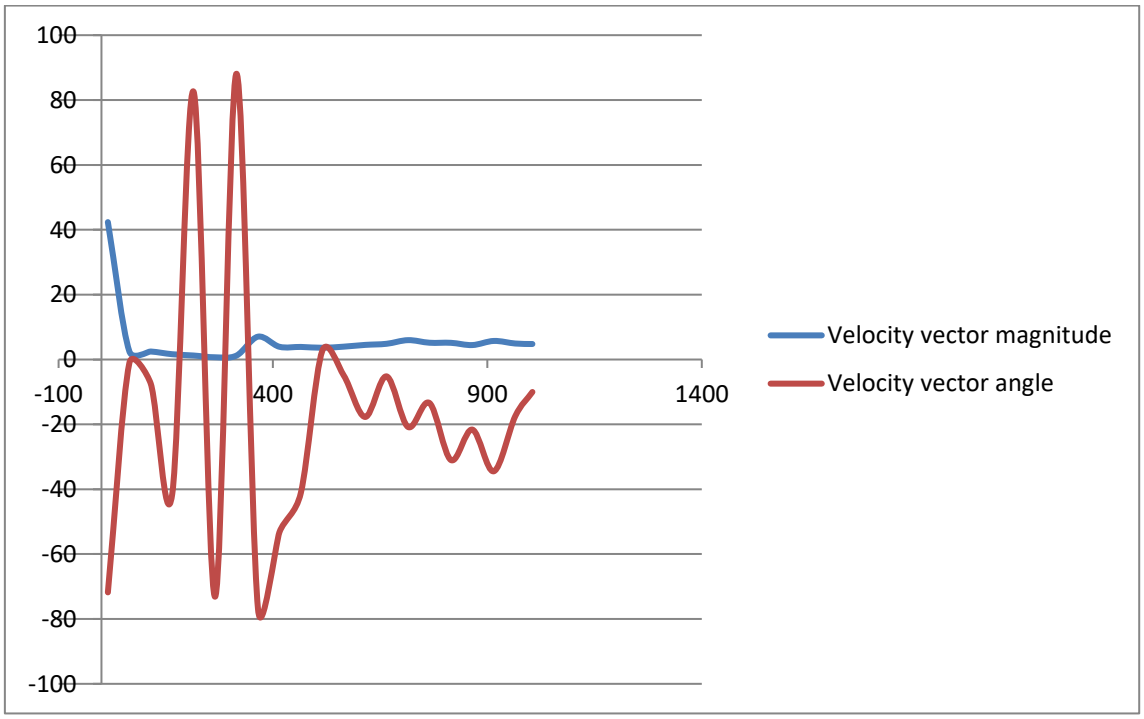

12.8.10 Velocity vectors 5th window from bottom.

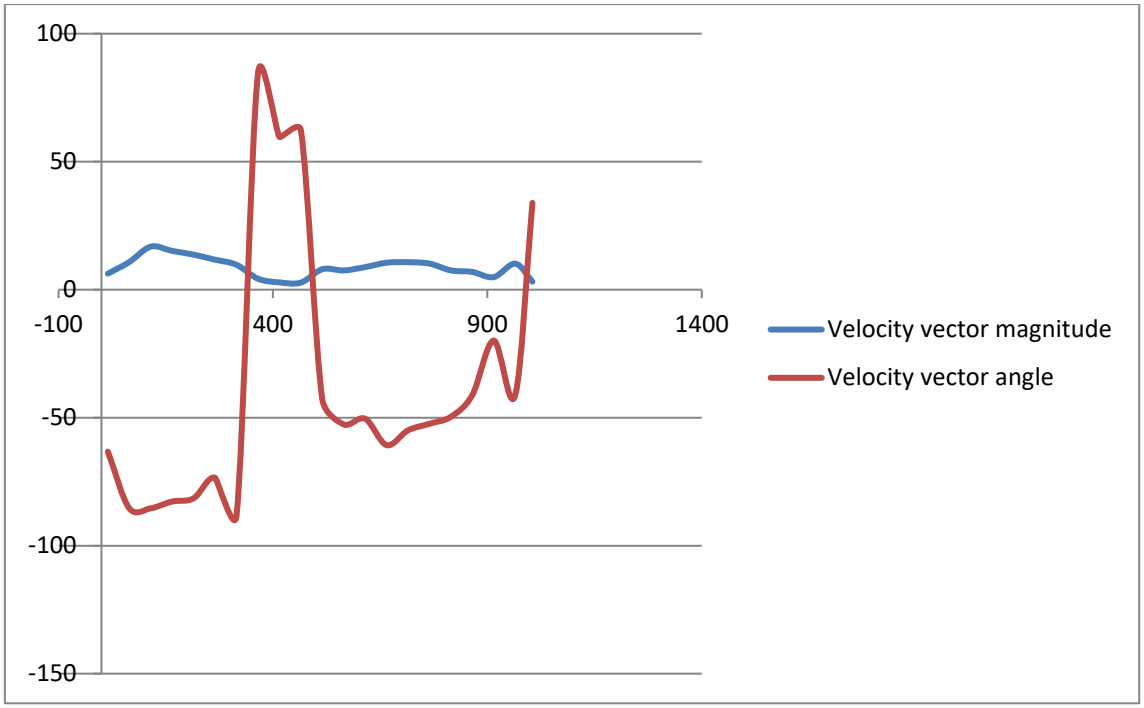

12.9 LDA MEASUREMENTS ACROSS THE 600MM DUCT

The Laser Doppler Anemometer (LDA) optical system used within the duct was a TSI LDA 80mm diameter probe with a 750mm focal length lens. It was positioned on a linear traverse with careful attention to alignment. The optical axis of the LDA was positioned centrally and normal to the window surface aligning the probe volume nominally on the diameter of the cross section. Activating the traverse therefore allows measurements at any point across the diameter of the circular exhaust tube. The set-up was as shown below.

The argon-ion laser and processing optics for the LDA system were positioned in a tent located 5 metres away from the measuring location. This tent helped protect the laser, optics and processing equipment from the environment during the measurement campaign. Optical fibres deliver the laser beam to the LDA emission optics via a transmitter box. Light signals are also captured by the emission optics which transmits the signals via optical fibre to receiving optics located safely back in the tent. This signal is processed by a Dantec BSA-P60 processor and data is collected over the Ethernet network by a PC held located in the control room.

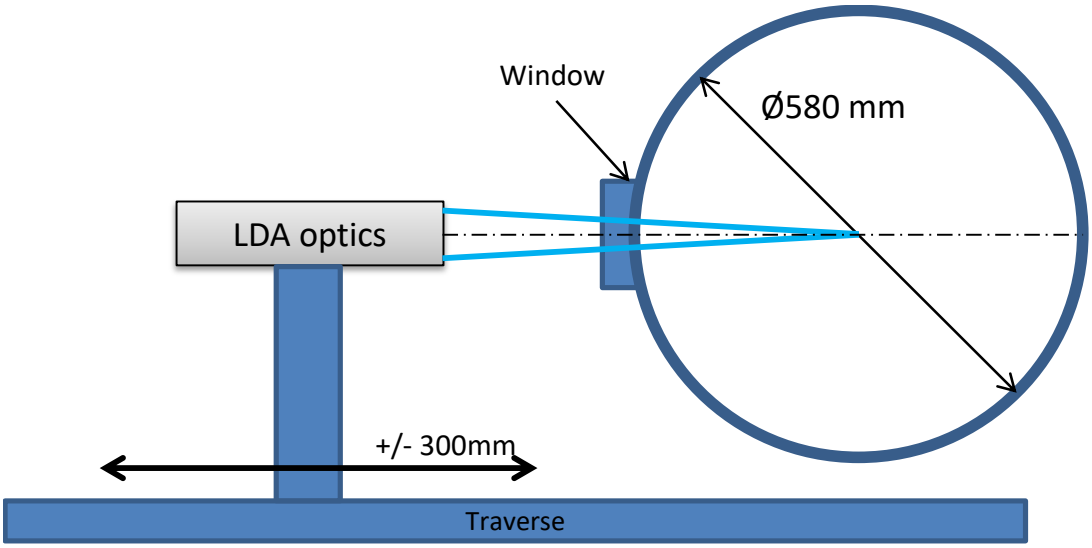

Figure 53: LDA optics configuration

A SCITEK PS-10 solid particle seeder was used to infuse particles into the gas stream. Aluminium oxide powder, with particles 1.0 micron in diameter, was used as these are considered small enough to follow the flow. Dry air was used as a medium to transport the aluminium oxide particles into the gas flow via two rakes. These rakes were positioned in a cross-formation, each spanning the full diameter of the exhaust tube, and were sufficiently upstream (about 9 metres) from the measurement location, so as to allow sufficient distance for flow disturbances caused by the wake of the rakes to die down well upstream of the measurement region. Locating the rakes well upstream of the measurement region also allowed the seeding particles time and distance to disperse more evenly within the tube cross section. The seeding system is shown below.

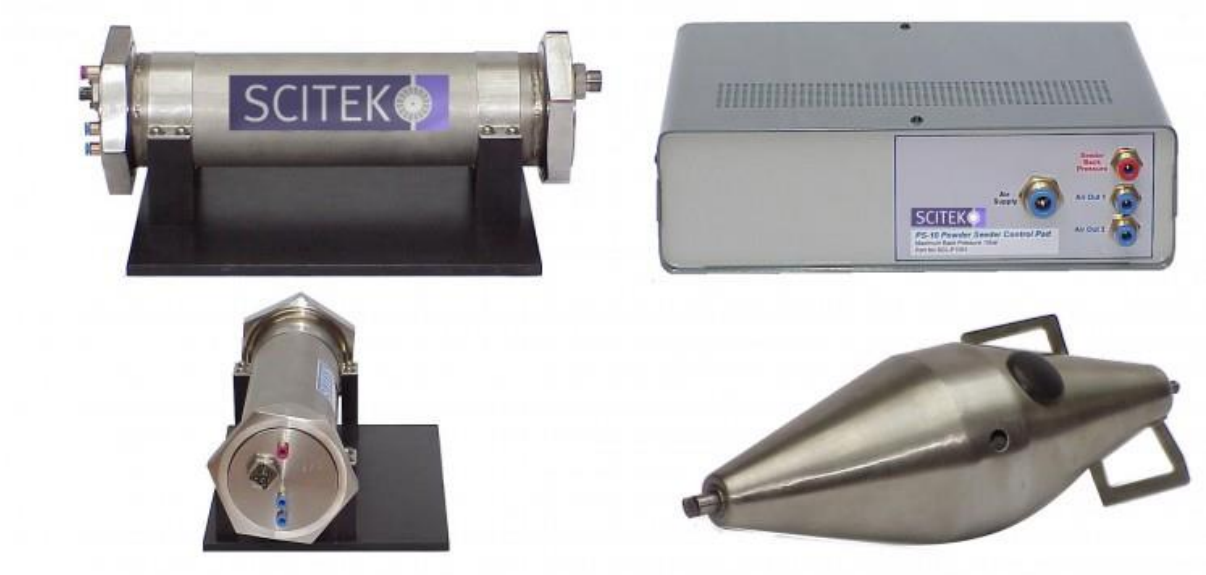

Figure 54: Scitek PS-10 particle seeder

Table 26: LDA measurements across the 600 mm duct

Date of acquisition	X	LDA1-Mean	Axial velocity	LDA4[15] Mean	LDA1 RMS	Axial Turbulence Intensity	LDA4{2) RMS
	[mm]	[m/s]	[m/s]	[m/s]	[m/s]	%	[m/s]
	-300	28.08	28.08	-8.97	24.78	88.2	28.17
	-290	61.74	61.74	-6.6	11.83	19.2	19.46
	-280	73.9	73.9	-23.62	8.46	11.4	19.17
	-270	77.21	77.21	-8.9	7.11	9.2	14.47
	-260	78.22	78.22	7.61	7.95	10.2	27.21
	-250	81.65	81.65	-8.32	14.68	18.0	17.97
	-240	87.63	87.63	-0.09	5.16	5.9	3.79
15/09/16	-220	87.99	87.99	-3.53	4.68	5.3	2.58
	-200	89.85	89.85	#N/A	5.97	6.6	#N/A
	-180	86.91	86.91	1.74	2.91	3.3	1.3
	-160	90.5	90.5	1.23	4.22	4.7	2.71
	-140	85.95	85.95	8.67	11.11	12.9	10.36
	-120	85.89	85.89	1.67	9.32	10.9	2.3
	-100	85.66	85.66	0.82	11.96	14.0	2.16
	-80	77.69	77.69	7.16	22.7	29.2	1
	-60	80.13	80.13	6	14	17.5	0
	-40	77.55	77.55	4.76	24.5	31.6	6.17
	-20	79.72	79.72	#N/A	14.84	18.6	#N/A
	0	81.03	81.03	#N/A	12.13	15.0	#N/A
	20	80.25	80.25	7.88	12.93	16.1	2.6
21/09/16	40	80.61	80.61	10.18	12.93	16.0	1
	60	81.65	81.65	#N/A	9.35	11.5	#N/A
	80	82.37	82.37	7.64	9.23	11.2	0
	100	82.58	82.58	7.22	9.06	11.0	1.33
	120	81.96	81.96	#N/A	14.3	17.4	#N/A
	140						
	160	82.73	82.73	#N/A	12.18	14.7	#N/A
	180	83.13	83.13	#N/A	10.2	12.3	#N/A
	200	79.34	79.34	#N/A	17.28	21.8	#N/A
	220	-72.6	72.6	-3.85	32.62	44.9	0
29/09/16	240	-77.22	77.22	-1.64	37.1	48.0	0
	250	-66.65	66.65	#N/A	46.04	69.1	#N/A
	260	-60.17	60.17	#N/A	45.35	75.4	#N/A
	270	-58.12	58.12	#N/A	44.86	77.2	#N/A
	280	-58.13	58.13	#N/A	45.25	77.8	#N/A